A review of mathematical models for the formation of vascular networks

A Review of Mathematical Models for the Formation of Vascular Networks

M. Scianna*, C.G. Bell†, and L. Preziosi*

Abstract

Two major mechanisms are involved in the formation of blood vasculature: vasculogenesis and angiogenesis. The former term describes the formation of a capillary-like network from either a dispersed or a monolayered population of endothelial cells, reproducible also *in vitro* by specific experimental assays. The latter term describes the sprouting of new vessels from an existing capillary or post-capillary venule. Similar mechanisms are also involved in the formation of the lymphatic system through a process generally called lymphangiogenesis. A number of mathematical approaches have been used to analyse these phenomena. In this article, we review the different types of models, with special emphasis on their ability to reproduce different biological systems and to predict measurable quantities which describe the overall processes. Finally, we highlight the advantages specific to each of the different modelling approaches.

Keywords: continuous model – mechanical model - hybrid models – cellular Potts model – vasculogenesis - angiogenesis -lymphangiogenesis

1 Introduction

Blood vessel formation and development is a multiscale process, caused by the activation of endothelial cells (ECs, the main bricks of the capillary walls) by biochemical stimuli released both by surrounding cells and by ECs themselves. The formation of vascular networks involves two different mechanisms: vasculogenesis and angiogenesis (for a review, see articles [47, 56, 57]). The former process refers to the *de novo* formation of a primitive vascular network, that emerges from directed and autonomous migration, aggregation and organization of the endothelial cells. The latter refers instead to the formation of new vessels from an existing capillary or post-capillary venule. Angiogenic remodelling coordinates with the establishment of blood flow and can occur through sprouting (i.e. by the formation of new branches from the sides of existing capillaries), pruning, resizing of the capillary volume and of the thickness of the capillary wall , or intussusception (i.e. by internal division of the vessel lumen).

*Dip. Scienze Matematiche, Politecnico di Torino, Corso degli Abruzzi 24, 10129, Torino, Italy.

†Mathematical Institute, University of Oxford, 24-29 St Giles', Oxford, OX1 3LB, UK.

In more detail, the process of vasculogenesis starts in the embryo with the assembly of mesoderm-derived precursors of ECs into polygons with well-determined topological characteristics [226], dictated by the principal and paradigmatic function of vasculature: oxygen transport to the tissues. After remodelling, these geometrical properties are more or less maintained in the adult body, where the capillary network, embedded in the tissues and stemmed by the vascular tree, has the same shape as the minimal unit participating in the formation of the vascular network in the embryo [67, 116, 140].

Although angiogenesis intervenes at the embryonic stage to remodel the initial capillary network into a mature and functional vascular bed (comprised of arteries, capillaries, and veins), its main role is played during adult life, when it is involved in many physiological processes, for instance, the vascularization of the ovary and the uterus during the female cycle, of the mammary gland during lactation, and of granulation tissue during wound healing. However, when the equilibrium of its underlying control mechanisms is disrupted, angiogenesis becomes pathological, as in the case of chronic inflammatory diseases like rheumatoid arthritis and psoriasis, vasculopathies like diabetic microangiopathy, degenerative disorders like atherosclerosis and cirrhosis, and tissue injury occurring in ischemia. Indeed, angiogenic progression is also a pivotal transition phase in the development of cancer. By providing nutrition and oxygen, it allows malignant cells to grow and remain viable, and, eventually, to spread metastases through invasion of the circulatory system [57]. Moreover, it is also important in determining the translation of metastases from dormant to aggressive status [56]. The switch to the angiogenic phenotype leads to fast progression, and to a potentially fatal stage, of the disease and represents an important target for therapeutic interventions in most types of malignancies [254].

The understanding of angiogenesis and vasculogenesis is of particular importance in cancer therapy, not only for researching anti-angiogenic therapies, but also for the optimisation of drug delivery to tumour sites. In fact, counter-intuitively, Jain and co-workers [109, 130, 131] have hypothesized that it is important to normalise the vascular network through the restoration of a proper balance of pro-angiogenic and anti-angiogenic factors in order to achieve a better delivery of drugs. Normalization of a usually abnormal tumour vasculature improves perfusion, oxygenation and overall efficacy, and also results in a reduction of tumour interstitial pressure, a further factor which hampers the delivery of drugs to the tumour site.

Recently, there has been increasing interest in controlling the formation of capillary networks in tissue grown *in vitro*. Thus far, the growth of 3D *in vitro* tissues has had limited success due to problems with the diffusion of nutrients inside the scaffold. Even when the tissue growth has been successful (obtained by carefully forcing a flow through the scaffold to assist nutrient delivery during its formation), the absence of an embedded capillary network in the final product causes great difficulty in achieving a successful outcome once the artificial tissue has been implanted into the body; the tissue usually becomes necrotic, due to the lack of a capability to source nutrients. Provision of the scaffold with a ready-made capillary network, or stimulation of its development in the growing tissue, would allow larger 3D tissues to be built and more successful implants to be achieved (see, for instance, [58, 79, 114, 126, 127, 132, 144, 176, 255, 276, 280]). In particular, Stroock and co-workers [303] developed a micro-fluidic device embedded in a tissue-like collagen matrix where ECs can grow on the inner

walls of the micro-channels, thus forming the first capillaries. The 3D matrix surrounding the vessels and the flow through the channels allowed the cells to evolve their structure to a physiological one, and even to form new sprouts; this is very important if the tissue implant grown *in vitro* is to form connections with the existing capillary network in the living host tissue.

Experimental studies performed on the vasculogenic system have revealed the role of many different factors driving the formation of vascular networks, both in physiological and pathological situations. However innumerable other processes, acting at different spatio-temporal scales, remain far from being understood. The complexity of the problem means that it is difficult and expensive to study using solely laboratory-based biological methods, and the support and insight gained by using *in silico* models, which are able to replicate selected features of the experimental system, is vital.

The aim of this review is to present the various different *in silico* approaches used to model the formation of vascular networks, with particular emphasis on their ability to reproduce experimental systems and to predict measurable quantities. Specifically, in Section 2 we focus on vasculogenesis, in Section 3 on angiogenesis and in Section 4 on lymphangiogenesis.

Each section begins with a brief phenomenological description of the underlying biological processes, and proceeds to review the different types of models that have been developed. Continuum models are considered first; these consist of systems of partial differential equations, which can stem from reaction-diffusion or from continuum mechanics conservation laws, when mechanical aspects are important (see Sections 2.2, 3.2, 4). Then we describe cell-based models, e.g. cellular automata and cellular Potts models (see Sections 2.3, 3.4); these models are characterized by a stronger focus on the behaviour of single cells and can be considered as hybrid models, since the concentration fields of the proteins of interests are still treated by reaction-diffusion equations (eventually discretized for integration purposes). A similar hybrid characteristic is also typical of other discrete-continuum models that have been developed for angiogenesis (see Section 3.3). For these models, we distinguish between discretized and discrete models for some cell population still evolving in a continuum environment. In the former case (see Section 3.3.1), the motion of sprout tip cells is governed by rules obtained from the discretization of a suitable partial differential equation. In the latter case (that can be called *discrete-in-continuum models*, see Section 3.3.2), the sprout tip cells move as a point mass in the continuum fields. In both cases, the chemoattractant field, and possibly the substratum, are described through continuous concentrations. In the final part of the angiogenesis section, we discuss models for vessel remodelling and coupling with the outer environment, e.g. tumour growth (see Sections 3.5 and 3.6).

It is useful to remark that we will focus mainly on results obtained in the last ten years. The reader can refer to the excellent review articles [8, 11, 128, 151, 163] for further details on previous contributions. In particular, we will examine in detail some sample models in order to highlight differences between the modelling approaches. Finally, we will compare the different methods, and discuss their advantages and disadvantages.

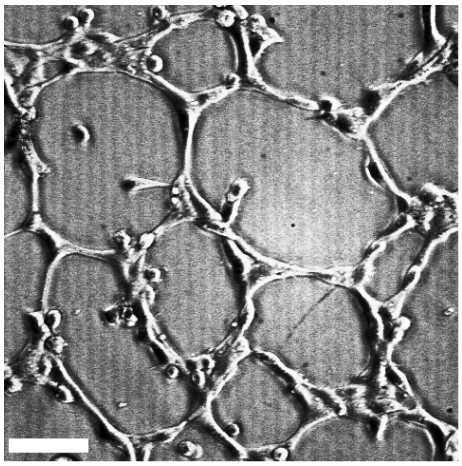

Figure 1: In vitro vasculogenesis.

2 Vasculogenesis

2.1 The Mechanisms of Vasculogenesis

Since vessel formation and reorganization is of fundamental importance, a large number of *in vitro* assays have been proposed to provide a deeper understanding of selected underpinning molecular-scale and cellular-scale events. One of the most well-known is the tubulogenic experiment, which is the laboratory counterpart of *in vivo* vasculogenesis (see Figure 2.1). Tubulogenic assays can be performed using different experimental set-ups, with different substrata and different endothelial cell-lines, as reviewed in [277]. Typical substrata include Matrigel, fibronectin, collagen, fibrin, and semisolid methilcellulose. Typical endothelial cell-lines include human umbilical vein endothelial cells (HUVEC), human dermal microvascular endothelial cells (HDMEC), human capillary endothelial cells (HCEC), human marrow microvascular endothelial cells, bovine aorthic endothelial cells (BAEC), bovine capillary endothelial cells (BCEC), bovine retin endothelial cells (BREC), rat capillary endothelial cells (RCEC), embryonic stem cells (ESC), calf pulmonary aortic endothelial cells (CPAEC), and adrenal capillary endothelial cells (ACEC).

In recent years, an increasing number of tubulogenic assays have been performed with tumour-derived endothelial cell lines (TECs), isolated and cultured from human carcinomas on the basis of membrane markers. This research has been stimulated by experimental investigations demonstrating that tumour blood vessels differ substantially from their "normal" counterpart. They are irregular and dilated, and it is impossible to identify distinct venules, arterioles, and capillaries [77, 101]. Moreover, their blood flow and permeability is altered, and they possess abnormalities in pericytes and in the basement membrane. As well as exhibiting altered genotype, phenotype, and function, TECs are often aneuploid, display chromosomal instability, and express peculiar genes [46, 201, 243]. In addition, TECs avoid senescence *in vitro* and show enhanced proliferation, motility and over-expression of membrane receptors [23, 44, 45, 46, 112]. Therefore, TECs provide a practical model for study-

ing the mechanisms of malignant vascularization, and for testing the efficacy of anti-angiogenic pharmacological therapies and drugs.

In spite of the large variety of laboratory assays mentioned above, they all have features in common. The selected EC population is initially dispersed in a physiological solution and then poured on the top of a specific substrate, which typically favours cell motility and has biochemical characteristics similar to living tissues. The cells sediment by gravity onto the substrate and then move along it, subsequently aggregating and forming patterns. The overall process, which commonly lasts 9-15 hours, consists of the following steps:

1. Cells initially undergo an isotropic motion around their initial position, maintaining a round shape. Then, it seems that they choose a direction, which is correlated with the location of areas characterized by higher cellular densities, and display an independent migration, with a small random component, until they collide with their nearest neighbours (3-6 hours). This motile phenotype is called "cell persistence", and is related to the inertia of a cell caused by the time taken to rearrange and repolarize its cytoskeleton to change its direction of migration [98, 231]. It is interesting that the cells move significantly faster in this phase, and their movement seems to be of the *amoeboid* type (see, for instance, [291, 298]).

2. After collision, ECs form attachments with their neighbours and eventually form a continuous multicellular network, which can be represented as a collection of nodes connected by capillary chords. At this stage of the process, the number of sites at which the cells adhere to the substrate increases, and the ECs acquire an even more elongated shape. The motion of the cells is now of mesenchymal type, and is much slower due to the activation of numerous adhesion sites.

3. The network slowly moves as a whole, and undergoes a slow thinning process, although the structure remains mostly unaltered. During this stabilization phase, mechanical interactions between cells, and also between cells and the substrate, become important.

4. Finally, individual cells fold up to form the lumen of the capillary, resulting in a vascular network, as described in [113, 141].

2.1.1 Activity of chemical morphogens and related intracellular pathways

As detailed in the previous section, it seems to be well-established that the motion of cells in the first phase of patterning is towards regions characterized by higher cell densities. A natural question to ask is how do the cells feel the presence of other cells? What is the mechanism underlying intercellular crosstalk? In this regard, recent research clearly confirms that ECs exchange signals during vasculogenesis by the release and absorption of specific chemical morphogens (such as vascular endothelial growth factor isoforms (VEGF-A), acidic and basic fibroblast growth factors (FGFs), epidermal growth factor (EGF), and transforming growth factor-α and -β (TGF-α and -β), as for instance reviewed in [56, 84, 120]). These angiogenic factors, which are known to induce EC growth, survival, and motility [85, 192], can in fact bind to specific tyrosine

kinase receptors on the cell surface and induce chemotactic motion along their concentration gradient, i.e. towards zones of higher cellular densities.

In order to quantify both the persistent and the chemotactic component in cell motion, a statistical analysis of the cell trajectories was performed in [10, 202, 234, 244], by measuring the displacement between successive turns and the cumulative distance. In particular, Parsa et al. [202] and Serini et al. [244] measured both the angle between two subsequent displacements relative to the same trajectory (which gives a measure of the persistence), and the angle between the cell instantaneous velocity and the VEGF-A concentration gradients at the same point (which gives a measure of the chemotactic behaviour). They confirmed persistence of cell locomotion in time, and observed that cellular migration was indeed in the direction of the gradients of the concentration field.

The autocrine/paracrine growth factors also play a role in determining the dimensions of the final overall network. In particular, different types of morphogens can lead to different mesh sizes, as observed in [229], where mice lacking heparin-binding isoforms of VEGF-A form vascular networks with a larger structure. As discussed below, and proved by different theoretical models [103, 244], this is related to the fact that the typical size of the network is determined by the product of the diffusion constant and the half-life of the chemical factor, which are affected by its molecular weight and therefore specific for each chemical species. In [115], it is clearly shown how elimination of endogenous VEGF-A in ECs plated on Matrigel prevents the formation of networks, even when VEGF-A is added exogenously and homogeneously on the top of the layer of cells. This confirms the importance of endogenous VEGF in the formation of capillary networks.

The diffusive chemical morphogens not only stimulate a chemotactic response from the ECs, but also activate a series of calcium-dependent cascades. These cascades regulate the phenotypical behaviour of cells, in particular motility, which is in turn influenced by cell-to-cell contact. This means that the morphogens also play an essential role in the stabilization of the capillary network. Molecules of selected growth factors initiate a series of intracellular cascades, which results in the indirect production of second messengers (such as arachidonic acid (AA) and nitric oxide (NO)). These messengers bind to sites on the cell plasmamembrane, open cation channels, and allow the influx of extracellular calcium into the cytosol, as characterized in [87, 88, 89, 177, 182]. This process, also called non-capacitive (or non-store-operated) calcium entry (NCCE or NSOCE), causes localized and peripheral restricted accumulations of the calcium ion [271], which regulates important biophysical properties of vascular cells, such as their elasticity, migratory capacity, and adhesive strength [31, 180, 183, 184].

2.1.2 Effect of cell density

Several experimental approaches clearly show that, over a defined range of densities of seeded cells (say from 100 to 200 cells mm^{-2}), the resulting network is characterized by typical inter-capillary distances (i.e. mean diameter of cellular lacunae) extending from 50 to 300 μm. These dimensions are ideal for optimal metabolic exchange (determined by the diffusivity of the oxygen): a coarser net would cause necrosis of the tissues in the central region, whereas a finer net would be useless (see [67, 116]). Indeed, as observed *in vivo* in [95], the vascular

mesh does not develop properly for cell densities outside this range. To clarify this phenomenon, Serini and co-workers [244] performed specific experiments, in which they varied the number of seeded cells, and used methods of statistical mechanics to quantitatively characterize the resulting patterns [103, 68]. They observed that there is a transition between a phase in which dynamics generates several disconnected structures (i.e. below a critical value ~ 100 cells/mm^2), to a phase in which a single connected structure appears. This process is an example of percolative transition and is studied in detail in [68].

A detailed analysis of the topological parameters characterizing the network (such as average branch length, number of branches, number of nodes, or capillary-like structure area) was performed in [202]. The same article also devotes particular attention to the evolution of the shapes of single ECs. They characterize cell behaviour in five phases dominated by cell aggregation, spreading, elongation, plexus stabilization, and plexus reorganization.

When too many cells are seeded, another transition, called Swiss-cheese transition, is observed. This is the formation of regions without cells, called lacunae, in a confluent layer of undifferentiated ECs that do not form a proper network [191, 244].

2.1.3 Interaction between cells and ECM

The topological properties of the capillary network are strictly regulated also by the content of matrix proteins in the substrate, which control cell attachment to the gel surface. Experimental observations have shown that lacunae form in the zones deprived of ECM molecules [274]. Indeed, in [277], the authors noticed that the formation of cellular holes was accompanied by a degradation of fibrin gels in the substrate. They measured the fibrin degradation products present in the culture medium and found an increase after 10 hours of seeding HUVECs. The same group has also performed some experiments, where they changed the fibrin concentration in a substratum of 1 mm thickness with a confluent population of HUVECs (i.e. with a density ≈ 1500 cells/mm^2). As the fibrin concentration was increased from 0.5 mg/mL to 8 mg/mL, the number of formed lacunae strongly decreased, but without any increase in size. In particular, a structured capillary mesh, with a typical chord length of $550 \pm 50\mu$m, only formed for lower fibrin concentrations. At higher concentrations, the ensemble of cells persisted as a continuous carpet without any holes. These results suggested that fibrinolysis leads to cell apoptosis and detachment from the surface, eventually culminating in the formation of functional lacunae. The same researchers have repeated the experiments using BRECs. In this case, a higher fibrin concentration (≈ 8 mg/mL) was necessary to form an organized capillary network, with a mean chord length of 400μm. This is consistent with the fact that BRECs have a high fibrinolytic activity. Hence, at lower concentrations, the matrix gel is degraded too quickly and the cells were not able to adhere at all. For this reason, some experiments were performed adding protease inhibitors (aprotin up to a concentration of 1 μg/mL); this decreased the degradation and allowed the formation of capillary-like structures. However, if the fibrin degradation was completely inhibited, the capillary network no longer formed.

The interaction between cells and the ECM during tubulogenesis has been the subject of many experiments. In [284, 285, 286], the authors seeded different

types of cells (BAECs, cells of the murine Leydig cell line TM3, human fibroblasts, human smooth muscle cells, and murine PYS-2 cells) on gelled basement membrane matrices (BBMs), which were characterized by a constant thickness of 1 mm and a variable rigidity, and regulated by selected amounts of gelled native type I collagen. They found that, with 0.6mg/mL collagen, BAEC and TM3 cells formed capillary networks in 24 hours, whereas, at 2mg/mL collagen, cells were flattened, spread, and unorganised. In addition, they used a set-up in which the substratum was distributed in a wedge-shape substratum, with its thickness increasing from 10 μm to 500 μm over a length of 17 mm, or from 10 μm to 400 μm over a length of 4 mm. The experiments showed that the length of the chords is positively correlated with the thickness of the substrate. Probably, on a very thin substrate, a capillary structure would not form at all.

2.2 Continuum models of vasculogenesis

The first mathematical models aimed at describing vasculogenesis were developed in the eighties by Murray and co-workers [185, 186, 187, 197]; these were then followed by a series of papers, [161, 162, 188, 189, 190, 191, 274], which are reviewed in more detail in [11, 163]. These mechanics-based models assume that the mechanism driving the formation of the vascular network and its morphological characteristics is the pulling action of the ECs on the extracellular matrix (ECM).

If we denote the density of endothelial cells by ρ_c, the density of the ECM by m, and the displacement of the extracellular matrix with respect to its stress-free configuration by $\mathbf{u}_m$, then the structure of the model is the following:

$$\frac{\partial \rho_c}{\partial t} + \nabla \cdot \mathbf{J}_c = 0\,, \tag{2.1}$$

$$\frac{\partial m}{\partial t} + \nabla \cdot (m\mathbf{v}_m) = 0, \tag{2.2}$$

$$\nabla \cdot (\mathbb{T}_c + \mathbb{T}_m) + \mathbf{F} = \mathbf{0}\,, \tag{2.3}$$

where $\mathbf{v}_m = d\mathbf{u}_m/dt$ is the ECM velocity, $\mathbf{J}_c$ is the cellular flux, and $\mathbf{F}$ is the force due to the interaction between the ECM and the Petri-dish. Eqs. (2.1) and (2.2) model conservation of the cell and ECM densities, while Eq. (2.3) is a force balance for the whole system: the mixture of cells and the ECM. The term $\mathbb{T}_c$ accounts for the forces internal to the system due to cell traction, and $\mathbb{T}_m$ for the viscoelastic response of the ECM.

In [161], a growth term, $\Gamma_c = \gamma_c \rho_c$, was included in the right-hand side of equation (2.1) to describe cell proliferation, but was subsequently neglected in the stability analysis and in the simulation. In [274], an additional decay term, $\Delta = -\delta_m \rho_c (1 - \rho_c) m$, was included in the right-hand side of equation (2.2) to account for ECM cleavage by the ECs, which is assumed to play a role in the formation of lacunae.

Motivated by the experimental evidence described in Section 2.1.1, which shows the importance of chemical cues, especially during the first phase of vascular development, a different mathematical model was proposed in [12, 103, 244] based on the following assumptions:

1. ECs neither duplicate nor die during the process;

2. ECs communicate via the release and absorption of molecules of a soluble growth factor, which acts as a chemoattractant and can reasonably be identified with VEGF-A;

3. ECs show persistence in their motion;

4. ECs are slowed down by friction due to interaction with the fixed substratum;

5. Closely packed ECs mechanically respond to avoid overcrowding.

The resulting mathematical model for the density of cells, ρ_c, their velocity, $\mathbf{v}_c$, and the concentration of chemoattractant, c, is then given by:

$$\frac{\partial \rho_c}{\partial t} + \nabla \cdot (\rho_c \mathbf{v}_c) = 0\,, \tag{2.4}$$

$$\frac{\partial c}{\partial t} = D\nabla^2 c + \alpha \rho_c - \frac{c}{\tau}\,, \tag{2.5}$$

$$\rho_c \left(\frac{\partial \mathbf{v}_c}{\partial t} + \mathbf{v}_c \cdot \nabla \mathbf{v}_c \right) = \nabla \cdot \mathbb{T}_c + \mathbf{F}_{chem} + \mathbf{F}_{cm}\,. \tag{2.6}$$

Eq. (2.4) describes mass conservation and corresponds to the first assumption.

Eq. (2.5) is a reaction-diffusion (RD) equation for the chemical factor, which is produced at a rate α and degrades with a half life τ. The diffusion coefficient, D, can be estimated from available data for molecular radii [178, 288] by using the Stokes–Einstein relation $D = k_{\mathrm{B}}T/\left(6\pi\eta r_{\mathrm{H}}\right)$, where k_{B} is the Boltzmann constant, T the temperature, η the solvent viscosity, and r_{H} the hydrodynamic radius of the molecule [213]. In the case of VEGF-A, this gives $D \sim 10^{-7}\,\mathrm{cm}^2\,\mathrm{s}^{-1}$. The half life of VEGF-A was measured in [244] using a radioactive tracer, giving a value of $\tau = 64 \pm 7\,\mathrm{min}$.

Equation (2.6) assumes that the governing equation for cell motion can be obtained on the basis of a suitable force balance. Although the second term in the left-hand side of the momentum equation is reminiscent of an inertial term (which is negligible in most biological phenomena), it should be interpreted as a term which models *cell persistence*, i.e. the resistance of cells to changes in their direction. The terms on the right-hand side represent the possible causes of a change in cell directional motion. These include the fundamental chemotactic body force:

$$\mathbf{F}_{chem} = \rho_c \beta(c) \nabla c\,, \tag{2.7}$$

where $\beta(c)$ measures the intensity of the cell response, which can include saturation effects, e.g.

$$\beta(c) = \frac{\beta}{1 + sc}\,, \qquad \text{or} \qquad \beta(c) = \beta \left(1 - \frac{c}{c_0}\right)_+ . \tag{2.8}$$

Here

$$f_+ = \begin{cases} f & \text{if } f > 0\,; \\ 0 & \text{otherwise}\,; \end{cases} \tag{2.9}$$

is the positive part of f and the parameters s and c_0 regulate the saturation of the chemotactic response. The linear dependence of the force on ρ_c corresponds to the assumption that each cell experiences a similar chemotactic action, so that the momentum balance in integral form depends on the number of cells in the control volume and the related local equation on the local density. The drag force $\mathbf{F}_{cm} = -\epsilon\rho_c\mathbf{v}_c$ was taken to be proportional to the velocity with respect to the substratum (assumed rigid in (2.6)), and proportional to the cell density for the same reasons as above. Possible generalizations of the cell-ECM interaction force could include the mechanisms of integrin attachment and detachment, as recently done in [214].

Finally, the partial stress tensor, $\mathbb{T}_c$, measures the response of the ensemble of cells to deformations. Several constitutive equations can be formulated, but unfortunately very little experimental data is available on the mechanical characteristics of cell populations in similar environmental conditions. It can be argued that because the cytosol is a watery solution containing many long proteins contained in a viscoelastic membrane, the ensemble of cells might behave as a viscoelastic material. However, even if one wants to consider such an effect, the characteristic times of the viscoelastic behaviour are much smaller than those related to cell motion (minutes with respect to hours), so that viscoelasticity probably plays a secondary role in the process of vascular network formation. On the other hand, plasticity should probably be taken into account to describe the breaking of cell-to-cell adhesion bonds [13, 214].

In the absence of experimental evidence, the simplest constitutive equation possible,

$$\mathbb{T}_c = -p(\rho_c)\mathbb{I}\,, \tag{2.10}$$

is considered in [12, 103, 244]; this choice of stress tensor corresponds to modelling the cells as an inviscid fluid. This assumption implies, for instance, that the ensemble of cells cannot sustain shear, which, of course, is not true.

Equation (2.6) then reduces to:

$$\frac{\partial\mathbf{v}_c}{\partial t} + \mathbf{v}_c\cdot\nabla\mathbf{v}_c = -\frac{1}{\rho_c}\nabla p(\rho_c) + \beta(c)\nabla c - \epsilon\mathbf{v}_c\,. \tag{2.11}$$

The model, (2.4), (2.5) and (2.11), can be linked to classical models in particular instances. For example, if both the pressure and the persistence terms are neglected in (2.11) then the cells will immediately adjust to the limit velocity, and this leads to classical chemotactic models (see, for instance, [121, 198]), for which blow-up in finite time is possible. If the pressure term is retained, one has instead the model studied in [139], in which the blow-up of the solution is prevented by imposing suitable conditions on the pressure term, e.g. convexity. Using a Chapman-Eskog expansion, Filbet et al. [86] deduced the above model (2.4–2.6) as a hydrodynamic limit of a kinetic velocity-jump process.

The main feature of the model can be understood most simply by neglecting pressure, and assuming for the moment that diffusion is a faster process than pattern formation, so that the time derivative in the diffusion equation, (2.5), can be neglected as a first approximation. Then, if we solve formally the quasi-stationary diffusion equation for c and substitute the solution into the persistence equation, (2.6), we can write (for $p = \epsilon = 0$):

$$\frac{\partial\mathbf{v}_c}{\partial t} + \mathbf{v}_c\cdot\nabla\mathbf{v}_c = \frac{\alpha\beta}{D}\,\nabla\left[\left(\frac{1}{\ell^2} - \nabla^2\right)^{-1}\rho_c\right]\,. \tag{2.12}$$

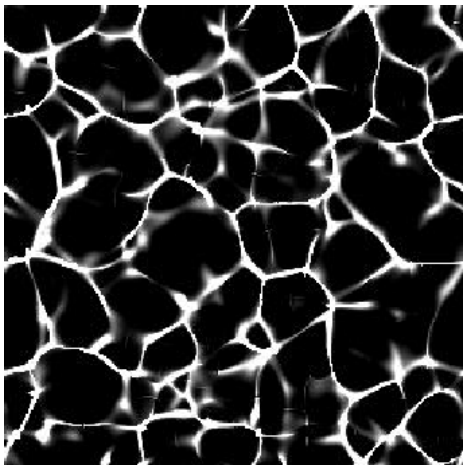

Figure 2: Network structure obtained with the vasculogenesis continuous model (2.4, 2.5, 2.11).

The appearance in the dynamical equations of the characteristic length,

$$\ell := \sqrt{D\tau}\,, \tag{2.13}$$

suggests that the dynamics could favour patterns characterised by this length-scale. Indeed, if we rewrite the right-hand side of (2.12) in Fourier space as

$$\frac{\alpha\beta}{D}\,\frac{\mathrm{i}\mathbf{k}}{k^2+\ell^{-2}}\,\rho_{c\mathbf{k}}\,,$$

we observe that the operator $\mathrm{i}\mathbf{k}/\left(k^2+\ell^{-2}\right)$ acts as a filter, which selects the Fourier components of ρ_c having wavenumbers of order $1/\ell$ and damps the components with higher and smaller wavenumbers. Experimental measurements of the parameters gives $\ell \sim 100\,\mu$m, which is in good agreement with experimental data.

It appears, then, that the process of network formation is initially driven by the following mechanism. Density inhomogeneities are translated in a landscape of concentration of VEGF-A, where details with scale smaller than ℓ fade away. The cells move by chemotaxis toward the ridges of the concentration landscape, enhancing even further the relevant scale, and eventually this produces a network structure characterised by a length-scale of order ℓ. In this way, the model provides a direct link between the range of intercellular interactions and the dimensions of the network structure, which is a physiologically relevant feature of real vascular networks. The results of a simulation are shown in Figure 2. As expected, a change in the diffusion of the chemical factors leads to a change in the typical size of the network, in agreement with the observation that larger effective diffusivities lead to vascular networks with a larger mesh [229].

A detailed analysis of the dependence of the topological characteristics of the network structure on the density of seeded cells has been performed in [103, 244]. They observed the percolative and Swiss-cheese transitions described in Section 2.1.2, with fractal dimensions consistent with the experimental measurements.

2.2.1 Exogenous control of vasculogenesis

A generalization of the models in the previous section to include multiple species of chemical factors, characterized by different physical properties and biological actions (e.g. attraction and repulsion), has been considered in [142]. Interest in this type of model is motivated by the possibility of using exogenous chemoattractants and chemorepellents to stimulate the formation of vascular networks for tissue engineering purposes. These exogenous chemoattractants and chemorepellents are impregnated into suitable gel structures, which form the substrate onto which the ECs are subsequently placed.

Denoting the concentrations of exogenous chemoattractant and chemorepellent by c_a and c_r respectively, the model in [142] can be written as:

$$\frac{\partial \rho_c}{\partial t} + \nabla \cdot (\rho_c \mathbf{v}_c) = 0\,, \tag{2.14}$$

$$\frac{\partial \mathbf{v}_c}{\partial t} + \mathbf{v}_c \cdot \nabla \mathbf{v}_c = -\frac{1}{\rho_c}\nabla p(\rho_c) - \epsilon \mathbf{v}_c + \beta(c)\nabla c + \beta_a(c_a)\nabla c_a - \beta_r(c_r)\nabla c_r\,, \tag{2.15}$$

$$D\nabla^2 c - \frac{c}{\tau} + \alpha \rho_c = 0\,, \tag{2.16}$$

$$D_a \nabla^2 c_a - \frac{c_a}{\tau_a} + \pi_a(t) H_a(\mathbf{x}) = 0\,, \tag{2.17}$$

$$D_r \nabla^2 c_r - \frac{c_r}{\tau_r} + \pi_r(t) H_r(\mathbf{x}) = 0\,, \tag{2.18}$$

where the time derivatives of the concentrations have been neglected since the characteristic diffusion time-scales are much smaller than the one characterizing cell motion. The functions H_a and H_r define where the exogenous chemicals are physically placed, while their release is determined by π_a and π_r. For the sake of simplicity, it is assumed that π_a and π_r are constant, which assumption is valid if the release time is much larger than the time of formation of the network, i.e. of the order of ten hours. Of course in some particular cases it may be possible to integrate analytically (2.17) and/or (2.18), so that the resulting solution can be directly substituted in (2.15).

In the same way as before, the new RD equations (2.17) and (2.18) are characterised by two more natural length-scales, $\ell_a = \sqrt{D_a \tau_a}$ and $\ell_r = \sqrt{D_r \tau_r}$, related to the ranges of action of the exogenous chemoattractant and chemorepellent, respectively. Within these ranges, the effect of the exogenous chemical factors strongly influence the structure of the network. However, outside these ranges endogenous chemotaxis governs the formation of a more isotropic network. An example is shown in Figure 3, where a thin stripe of chemorepellent has been placed down the middle of the figure.

Generally speaking, it was found that chemorepellents are more effective in driving the formation of vascular networks than chemoattractants. From a morphological point of view, chemoattractants induce the formation of capillaries within their range of action, and these capilliaries tend to run perpendicularly to the source of chemoattractant; on the other hand, chemorepellents induce the formation of capillaries which tend to run parallel to the source of chemorepellent, and are situated at a distance from the source of the order of magnitude of the range of action, as shown in Figure 3.

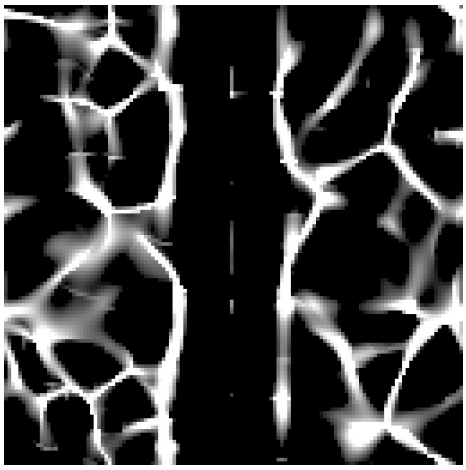

Figure 3: Vasculogenesis simulation in presence of a thin stripe of chemorepellent obtained by the model (2.14–(2.18).

2.2.2 Substratum interactions

From the phenomenological description given in Section 2.1, it is clear that in the second phase of vascular network formation, the mechanical interaction of the cells with the substratum and its mechanical properties themselves become important. Since these features cannot be described by the model (3.4, 3.5, 3.11) proposed above, Tosin et al. [273] extended it to include these mechanical processes. They still assumed only endogenous chemotaxis, although the generalization to exogenous chemical factors is straightforward. Although inertial effects can be certainly neglected, inclusion of the non-rigidity of the substratum into the model requires an extra force balance equation that can be written as:

$$\nabla \cdot \mathbb{T}_m - \mathbf{F}_{cm} + \mathbf{F}_{ext} = \mathbf{0}\,. \tag{2.19}$$

Here, $\mathbf{F}_{ext}$ is the anchoring force of the substratum to the Petri dish, which can be taken to be proportional to the displacement $\mathbf{u}_m$ of the substratum:

$$\mathbf{F}_{ext} = -\frac{s}{h}\mathbf{u}_m\,, \tag{2.20}$$

where h is the substratum thickness.

The other interaction force, $\mathbf{F}_{cm}$, due to cell-ECM interaction is the one present in the persistence equation (2.6), but with the opposite sign here as it is an internal force between the two constituents. However, in this case, the deformability of the substratum requires the definition of this force to take into account the relative motion of the cells with respect to the ECM. In this respect, Tosin et al. [273] assumed that it includes both an elastic and a viscous contribution. During the ameboid motion, the interaction force acting on the cells is of viscous type. This implies a weak interaction between the cells and the substratum (characterised by a quick removal of bonds and formation of new bonds), and a corresponding weak deformation of the substratum, so that the interaction force is modelled as:

$$\mathbf{F}_{visc} = -\epsilon\rho_c(\mathbf{v}_c - \mathbf{v}_m)\,, \tag{2.21}$$

where $\mathbf{v}_m = d\mathbf{u}_m/dt$.

The elastic contribution takes into account the fact that, after some time, cells attach themselves to the substratum and form stronger focal adhesion bonds. One can then assume that, if the cell anchors in $\mathbf{u}_m$ and then moves to $\mathbf{u}_c$, then the elastic force is proportional to $\mathbf{u}_m - \mathbf{u}_c$. This change of behaviour characterises the transition between the phase dominated by chemotaxis and that dominated by mechanics. In other words, this force is absent in the initial ameboid motion and starts when the motion becomes of mesenchymal type, i.e. when cells start attaching more strongly to the adhesion molecules of the substratum. In [273], it was assumed that there exists a characteristic time, t_{th}, needed to anchor to the adhesion sites on the substratum; this characterises the transition between a purely ameboid phase and a mesenchymal phase, so that:

$$\mathbf{F}_{elast} = -\kappa\rho_c\,(\mathbf{u}_c - \mathbf{u}_m)\,H(t - t_{th})\,, \tag{2.22}$$

where κ is the anchoring rigidity and H is the Heaviside function.

Another interesting hypothesis is that the ameboid motion stops whenever cells come into contact, so that the strongly reduced velocity permits a better link with the adhesion molecules of the substratum. This phenomenon could be included in the previous model by assuming that

$$\mathbf{F}_{elast} = -\kappa(\rho_c)\rho_c\,(\mathbf{u}_c - \mathbf{u}_m)\,,$$

and taking $\kappa(\rho_c)$ to vanish below a given value ρ_{th} of cell density, e.g. $\kappa(\rho_c) = \kappa H(\rho_c - \rho_{th})$. This mechanism is consistent with the one involving intercellular calcium dynamics described in Section 2.3.

Tosin et al. [273] also included a further modification to the model, which is consistent with the above-cited calcium dynamics. Since the release of endogenous VEGF is assumed to decrease as a consequence of cell-to-cell contact (in agreement with the activation of inhibiting calcium-related pathways described in Section 2.1.1 and modelled in Section 2.3), they assumed that the production of VEGF is density-dependent, so that:

$$\alpha(\rho_c) = \frac{\hat{\alpha}_c\rho_c}{1 + \eta\rho_c^2}\,.$$

To conclude, since the terms (2.21) and (2.22) must be found with the opposite sign in the persistence equation for the cells, but the term in (2.20) must not (because it does not act on the cells), the final model can be written as:

$$\begin{cases} \dfrac{\partial\rho_c}{\partial t} + \nabla\cdot(\rho_c\mathbf{v}_c) = 0\,, \\ \dfrac{\partial c}{\partial t} = D\nabla^2 c + \dfrac{\hat{\alpha}_c\rho_c}{1+\eta\rho_c^2} - \dfrac{c}{\tau}\,, \\ \dfrac{\partial\mathbf{v}_c}{\partial t} + \mathbf{v}_c\cdot\nabla\mathbf{v}_c = -\dfrac{1}{\rho_c}\nabla p(\rho_c) + \beta(c)\nabla c \\ \qquad\qquad - \epsilon(\mathbf{v}_c - \mathbf{v}_m) - \kappa(\rho_c)\,(\mathbf{u}_c - \mathbf{u}_m)\,, \\ -\dfrac{E}{2(1+\nu)}\nabla^2\mathbf{u}_m - \dfrac{E}{2(1-\nu)}\nabla(\nabla\cdot\mathbf{u}_m) \\ \qquad\qquad + \epsilon(\mathbf{v}_c - \mathbf{v}_m) + \kappa(\rho_c)\,(\mathbf{u}_c - \mathbf{u}_m) - \dfrac{s}{h}\mathbf{u}_m = \mathbf{0}\,. \end{cases}$$

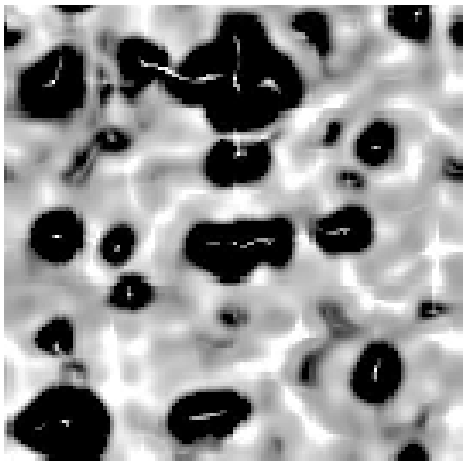

Figure 4: Vasculogenesis simulation by the model (2.23) in presence of a stiff substratum.

The effect of mechanical stretching obtained in the simulation is comparable to what is observed *in vitro*, namely that, by pulling on the extracellular matrix, the cells deform the substratum. However, if the substratum is too rigid or if cell adhesion is too strong, then it is very hard for the cells to form a chord. In the limit of very stiff substrata, then the morphogenic process leads to the formation of lacunae rather than chords, as shown in Figure 4. The mechanical interactions seem also to play an important role in guaranteeing the stability of the network.

2.3 Cellular Potts Models of Vasculogenesis

Due to the spatial scales involved, cell-based models are particularly suited to capture and describe mechanisms and dynamics at the cellular level. In addition, they allow more flexibility to include sub-cellular phenomena of interest (e.g. adhesion mechanisms and activation of protein pathways). One such methodology is the cellular Potts model (CPM), which has been widely applied to study vasculogenesis. This is a lattice-based Monte Carlo technique, which follows an energy minimization philosophy [106, 107, 108, 111, 164].

In order to model vasculogenic assays CPMs use bi-dimensional lattices (i.e. regular numerical repeated graphs). Each grid site $\mathbf{x} \in \Omega \subset \mathbb{R}^2$ is labelled by an integer number, $\sigma(\mathbf{x})$. Using the typical terminology adopted in CPM models, a neighbour of site $\mathbf{x}$ is identified by $\mathbf{x}'$, while its overall neighbourhood is identified by:

$$\Omega_{\mathbf{x}}^{'} = \{\mathbf{x}' \in \Omega : \mathbf{x}' \text{ is a neighbour of } \mathbf{x}\}.$$

Sub-domains of contiguous sites with identical spin σ form discrete objects, which are characterized by an object type, $\tau(\sigma)$.

In classical CPMs of tubulogenesis, each object identified by its spin σ represents an entire and undifferentiated cell of type $\tau = C$. The experimental matrix substrate (e.g. Matrigel), on which the EC population resides, is commonly modelled as a generalized object $\sigma = 0$ of type $\tau = M$, and is assumed

to be static, passive and homogeneously distributed throughout the simulation domain, forming no large-scale structures. Connections (links) between neighbouring lattice sites of unlike index $\sigma(\mathbf{x}) \neq \sigma(\mathbf{x}')$ represent cell membranes.

As in all applications of CPMs, the EC culture gradually and iteratively evolves to reduce a pattern effective energy, described by a Hamiltonian, H. The functional H contains a variable number of terms, consisting of cell attributes (e.g. volume, surface), true energies (e.g. cell-cell adhesions), and terms mimicking energies (e.g. response to external chemical stimuli). Its local gradient is the "force" acting on any point of the simulation domain. The energy minimization core algorithm is a modified Metropolis method for Monte Carlo dynamics. It is able to capture the natural exploratory behaviour of biological individuals, via thermal membrane fluctuations and biased extensions and retractions of their membranes, with a preference for displacements which reduce the local effective energy of the configuration. To mimic cytoskeletally-driven pseudopod extensions and retractions, a lattice site, $\mathbf{x}_{source}$, is selected at random and assigns its state ($\sigma(\mathbf{x}_{source})$) to one of its unlike neighbours, $\mathbf{x}_{target} \in \Omega'_{\mathbf{x}_{source}}$, which has also been randomly selected. The Hamiltonian of the system is computed before and after the proposed update, and the change is accepted with a Boltzmann probability function:

$$P(\sigma(\mathbf{x}_{source}) \rightarrow \sigma(\mathbf{x}_{target})) = \begin{cases} e^{-\Delta H/T} & \Delta H > 0\,; \\ 1 & \Delta H \leq 0\,, \end{cases} \tag{2.23}$$

where $\Delta H = H_{after\ spin\ flip} - H_{before\ spin\ flip}$ is the net energy difference, and T is an effective Boltzmann temperature which is constant for the whole system in classic CPMs, representing the idea of a generic and homogeneous "culture motility" [170, 171, 172, 173, 174, 236]. A total of n proposed updates, where n is the number of sites of the domain Ω, constitutes a Monte Carlo Step (MCS), which is the basic iteration and the unit of time used in the model.

As a more detailed illustration, let us consider the Hamiltonian functional used by the authors in reference [173]; this contains three terms, which control the shape of the ECs, their homotypic (i.e. cell-to-cell) and heterotypic (i.e. cell-ECM) adhesive interactions, and their chemotactic response:

$$H = H_{adhesion} + H_{shape} + H_{chemical}. \tag{2.24}$$

The first term, $H_{adhesion}$, phenomenologically implements the general extension of Steinberg's differential adhesion hypothesis (DAH) [111, 250, 251]:

$$H_{adhesion} = \sum_{\mathbf{x}\in\Omega, \mathbf{x}'\in\Omega'_{\mathbf{x}}} J_{\tau(\sigma(\mathbf{x})),\tau(\sigma(\mathbf{x}'))}(1 - \delta_{\sigma(\mathbf{x}),\sigma(\mathbf{x}')}), \tag{2.25}$$

where $\mathbf{x}$, $\mathbf{x}'$ represent two neighbouring lattice sites, $\delta_{x,y}$ is the Kronecker delta, and the J's are cell-cell ($J_{C,C}$) or cell-matrix ($J_{C,M}$) binding energies per unit area. They are assumed to be constant in time and homogeneous in space.

The next term, H_{shape}, imposes a geometrical constraint on ECs. It is written in the following elastic-like form, which increases as the cells deviate from a designated target area A_σ, under the hypothesis that cells do not grow or divide during patterning:

$$H_{shape} = H_{area} = \lambda_C^{area} \sum_{\sigma} (a_\sigma - A_C)^2. \tag{2.26}$$

Here a_σ is the current area of cell σ, and λ_C^{area} is an energy penalty (a *Potts coefficient*), which represents the cells' resistance to compression.

The final term, $H_{chemical}$, describes the biased walk of ECs up gradients of VEGF. The authors in [233] assume that the velocity of the drift depends both on the gradient strength and on the absolute concentration of the chemical, so that the resulting effective-energy change at each copy attempt reads:

$$\Delta H_{chemical} = -(1 - \delta_{\sigma(\mathbf{x}_{source}),0})\mu^{ch} \left[\frac{c(\mathbf{x}_{target})}{1 + s\ c(\mathbf{x}_{target})} - \frac{c(\mathbf{x}_{source})}{1 + s\ c(\mathbf{x}_{source})} \right]. \tag{2.27}$$

The chemotaxis coefficient is given by $\mu^{ch} = \mu^{ch}_{C,M} \gg 0$ at cell-ECM interfaces, and $\mu^{ch} = \mu^{ch}_{C,C} = 0$ at cell-cell interfaces, respectively. This ensures that chemotactic extensions occur only at cell-ECM interfaces, and reflects the VE-cadherins suppression of pseudopods (contact-inhibition of chemotaxis). Finally, the factor $(1-\delta_{\sigma(\mathbf{x}_{source}),0})$ (where 0 represents the extracellular medium) is used to implement a pseudopod-extension-only chemotaxis, where only extending pseudopods at the cell-ECM interface respond to the chemoattractant.

Chemoattractant diffusion and degradation is described macroscopically, using an RD equation analogous to Eq. (2.5) in the models presented above [103, 244]:

$$\frac{\partial c}{\partial t} = D\nabla^2 c + \alpha(1 - \delta_{\sigma(\mathbf{x}),0}) - \frac{1}{\tau}\delta_{\sigma(\mathbf{x}),0} c(\mathbf{x}, t)\,. \tag{2.28}$$

Here α is the secretion rate from inside the cells, *tau* the half life in the ECM (i.e. due to proteolytic enzymes or by binding to ECM components), and D the diffusion constant in the ECM. The co-presence of a continuum description for the chemical factors and a lattice-based description for the cell behaviour gives a hybrid characteristic to all CPMs proposed in the literature to describe vasculogenesis and angiogenesis.

Although the value for D in (2.28) is taken to be smaller than that set for VEGF-A165 in [103], and as a result steeper gradients are formed in the concentration, capillary formation is still observed.

This very interesting hybrid model demonstrates that the definition of a single set of cell behaviours, i.e. contact-inhibited chemotaxis to an autocrine-secreted chemoattractant, can consistently reproduce the formation of a capillary network, which is in good agreement with the related *in vitro* experiments, performed with cultures of mouse allantois. The simulations performed also indicate that the pattern emerges over a wide range of cell-cell adhesions and that it is widely independent of cell shape. Moreover, the authors successfully apply the same model to reproduce capillary sprouting from an initially round island of ECs, suggesting common underlying driving mechanisms. In particular, their results show that no sprouting occurs at too low cell motilities T if the pseudopods respond to the chemoattractant only during extension, and it is necessary to implement an extension-retraction chemotaxis (i.e. by dropping the related factor in Eq. (2.27)). In contrast, for higher motilities, vascular

branching develops with both mechanisms, the process being slower in the case of extension-only chemotaxis.

In [173] the authors also investigate how sprouting depends on the chemotactic strength, $\mu_{C,M}$. In particular, they find a critical value separating sprouting from non-sprouting clusters. At intermediate values of the parameter, most vascular cords are two cells wide, while at high values the cords become longer and thinner (i.e. only one cell wide). For even higher chemotactic responses, the cells intercalate, moving to the peaks of the chemical gradient. Finally, in order to compare with the model in [103], the authors perform simulations varying the diffusion length of the chemoattractant. In agreement with the continuum approach, they observed that longer diffusion lengths produce thicker cords with larger inter-cord spaces. At the extremes, the clusters do not sprout well when the VEGF diffusion length approaches the EC-cluster diameter, whereas they dissociate if the diffusion length is shorter than the diameter of single cells.

In [172], the same group starts from the experimental observation that ECs dramatically change shape in the second phase of vasculogenesis after cell aggregation. In response to growth factors, intracellular-store-based calcium entry remodels the actin cytoskeleton of ECs, and changes their shape from rounded to elongated and bipolar [81] (see also the description in [202]). Such a cell-polarized shape is essential for blood-vessel development. In fact, it causes anisotropic cell migration, which produces rapid inter-cellular connections resulting in a fine network, and a sideways movement, which is fundamental for pattern coarsening and stabilization. Therefore, they add an energetic constraint on cell-length to the Hamiltonian (2.24):

$$H_{length} = \lambda_C^{length} \sum_{\sigma} (l_\sigma - L_\sigma)^2, \tag{2.29}$$

where l_σ is the length of cell along its longest axis, L_σ its target length, and λ_C^{length} the relative Potts coefficient. In particular, the length of a cell is derived from the largest eigenvalue of the inertia tensor, with the assumption that the cell is approximately an ellipse. However, since the length constraint may cause a cell to split into disconnected patches, the authors also introduce a connectivity constraint, which reflects the physical continuity and cohesion of the cell. The rest of this model is analogous to that previously presented, except that, in this case, the authors no longer consider a saturation behaviour of the cell chemical response (i.e. they impose $s = 0$ in Eq. (2.27)), and they implement an increased extensibility chemotactive response, without contact inhibition (i.e. $\mu^{ch} = \mu^{ch}_{C,M} = \mu^{ch}_{C,C} \gg 0$ in the same equation (2.27)). Interestingly, although these assumptions are slightly different, a standard vasculogenesis process is consistently reproduced, with a final structure resembling a capillary plexus, where cords of cells enclose lacunae of homogeneous dimensions. In this article, the authors also analyse the kinetics of the patterning, finding that the number of branch points and lacunae initially drops quickly, with non-exponential dynamics, and then slowly stabilizes, resulting in the typical equilibrium size of the network. Some simulations then show that reducing the target cell length below a critical value (or dropping the length constraint) inhibits the formation of the network. Interestingly, by varying the number of simulated cells, these authors find both a percolative and a Swiss-cheese transition analogous to [103].

A more detailed CPM was developed in [138] to reproduce an *in vivo* vasculogenic process during embryonic development, where endothelial precursor cells of mesodermal origin, known as angioblasts, assemble into a characteristic network pattern. In particular, the authors assume that VEGF is not autocrinally produced by the angioblasts, but by the ECM. The EC precursors instead secrete non-diffusive matrix components, able to bind and immobilize the signalling agent in close proximity to the cell. The authors propose the following system of differential equations for the concentrations of free soluble (c_f) and bound (c_b) VEGF, and for ECM molecules (m):

$$\begin{cases} \dfrac{\partial c_f}{\partial t} = D\nabla^2 c_f + \gamma_f - \kappa c_f m - \dfrac{c_f}{\tau}, \\ \dfrac{\partial c_b}{\partial t} = \kappa c_f m, \\ \dfrac{\partial m}{\partial t} = \gamma_m \delta_{\sigma(\mathbf{x}),0} - \delta c_f m. \end{cases} \tag{2.30}$$

Here γ_f ithe constant rate of VEGF production, γ_m is the production rate of ECM molecules by cells, and $\kappa c_f m$ is a second-order mass action term with effective kinetic rate κ.

The system Hamiltonian used in such a model is the same as in Eq. (2.24). It takes into account geometrical constraints for the angioblasts; homotypic and heterotypic interactions; and the chemical response, which distinguishes between chemotactic cues created by both bound and soluble VEGF:

$$\Delta H_{chemical} = -\mu_b^{ch}(c_b(\mathbf{x}_{target}) - c_b(\mathbf{x}_{source})) - \mu_f^{ch}(c_f(\mathbf{x}_{target}) - c_f(\mathbf{x}_{source})). \tag{2.31}$$

In particular, the ECM-bound VEGF is assumed to provide stronger chemical signalling than its freely diffusing forms, as observed in [66, 229], by setting $\mu_b^{ch} > \mu_f^{ch}$.

As demonstrated by a morphometric analysis, this model is able to produce polygonal cellular patterns that accurately resemble the *in vivo* early vascular bed in quail embryos, recorded by confocal microscopy. The simulated networks show a high degree of similarity with respect to a broad spectrum of morphological descriptors, including lacunae number/sizes/shapes, network and interface lengths, cord widths, degree distribution and fractal properties. As observed by the authors themselves, fine-grained spatial cues for chemotactic cell migration can be generated without postulating unrealistically low VEGF diffusion rates [172, 173]. Furthermore, the stability of the network structures increases over time, instead of collapsing after a transient time, as in previous models [103, 172]. Another interesting feature of this work is that cell elongation does not need to be postulated *a priori*, as in [172], as the angioblasts polarize as a natural consequence of chemotaxis towards matrix-bound VEGF. Moreover, a set of simulations reveals two time-scales characterizing the pattern dynamics: in the early stages, a fully connected network forms, whereas, over longer time-scales, it increases in the overall surface area, ensuring an efficient distribution of nutrients and waste removal.

All of the CPMs described above have neglected the evolution of intracellular dynamics that underlie cell phenotypic behaviour. In [238] an extension

of CPMs in this direction takes into account specific agonist-induced calcium-dependent pathways that are important to describe the final stabilization phase of the vasculogenic process. In this approach the modelling environment is characterized by a constant flux of information from finer to coarser levels, i.e. the kinetics of the molecular sub-cellular networks strongly determine cell mesoscopic properties and behaviour.

Instead of "normal" ECs, the model specifically describes tumour-derived endothelial cells (TECs) with their related parameters and protein cascades. Referring to [239, 240] for more details, each cell is defined as a compartmentalized unit η, composed of two subregions which, in turn, are standard CPM objects σ: the cell nucleus, a central more or less round cluster, of type $\tau = N$, and the surrounding cytosol of type $\tau = C$. This is obviously a more realistic representation, which allows a more detailed reproduction of cell morphological changes during capillary formation. The TEC population as usual resides in a homogeneous matrix, a generalized substrate $\sigma = 0$ of type $\tau = M$.

The Hamiltonian of the system is set to be:

$$H = H_{adhesion} + H_{shape} + H_{chemotaxis} + H_{persistence}. \tag{2.32}$$

The term $H_{adhesion} = H^{int}_{adhesion} + H^{ext}_{adhesion}$ is similar to the one in Eq. (2.25), but contains different contributions to describe the generalized contact between subunits belonging to the same cell, or the effective adhesion between membranes of different cells:

$$\begin{aligned} H_{adhesion} = \sum_{\substack{\mathbf{x}\in\Omega \\ \mathbf{x}'\in\Omega'_{\mathbf{x}}}} & \left[J^{int}_{C,N}\delta_{\eta(\sigma(\mathbf{x})),\eta(\sigma(\mathbf{x}'))}(1-\delta_{\eta(\sigma(\mathbf{x})),\eta(\sigma(\mathbf{x}'))}) \right. \\ & \left. + J^{ext}_{C,C}(1-\delta_{\sigma(\mathbf{x}),\sigma(\mathbf{x}')})(1-\delta_{\eta(\sigma(\mathbf{x})),\eta(\sigma(\mathbf{x}'))}) \right]. \end{aligned} \tag{2.33}$$

Here $J^{int}_{C,N} \in \mathbb{R}^-$ is a constant high tension which prevents the cells from fragmenting, whereas $J^{ext}_{C,C}$ represents the local adhesive strength between cells $\eta(\sigma(\mathbf{x}))$ and $\eta(\sigma(\mathbf{x}'))$, whose value will be discussed below.

The geometrical attributes of cell subunits are modelled by:

$$\begin{aligned} H_{shape} &= H_{area} + H_{perimeter} \\ &= \sum_{\eta,\sigma} \left[\lambda^{area}_{\eta,\sigma} \left(\frac{a_{\eta,\sigma} - A_{\tau(\sigma)}}{a_{\eta,\sigma}} \right)^2 + \lambda^{per}_{\eta,\sigma} \left(\frac{p_{\eta,\sigma} - P_{\tau(\sigma)}}{p_{\eta,\sigma}} \right)^2 \right], \end{aligned} \tag{2.34}$$

where $a_{\eta,\sigma}$ and $p_{\eta,\sigma}$ are the actual dimensions of the compartments, and $A_{\tau(\sigma)}$ and $P_{\tau(\sigma)}$ their target values, which correspond to the typical dimensions of the nucleus and the cytosol of a TEC in a quiescent state. With respect to the standard formulation (2.26), the form of (2.34) allows finite energetic contributions, as well as a blow-up in the case of $a_{\eta,\sigma}, p_{\eta,\sigma} \to 0$, which means that an infinite energy is needed to shrink a cell to a point. The parameters $\lambda^{area}_{\eta,\sigma}$ and $\lambda^{per}_{\eta,\sigma}$ are energy penalties referring to the mechanical moduli of the cell compartments. Assuming that TECs do not grow during patterning, $\lambda^{area}_{\eta,\sigma}$ is kept high for any η and for σ such that $\tau(\sigma) = C, N$. Moreover, the rigidity of the nucleus is implemented by a high $\lambda^{per}_{\eta,\sigma}$ for any η and for σ such that $\tau(\sigma) = N$. Finally, the elasticity of the cytosolic region, evaluated by $\lambda^{per}_{\eta,\sigma}$ for any η and for $\sigma : \tau(\sigma) = C$, is enhanced by calcium ions, which facilitate cytoskeletal reorganization, as stated below in Eq. (2.38).

The term, $H_{chemotaxis}$, implements an extension-only chemotactic term similar to the one present in [173]:

$$\Delta H_{chemotaxis} = \mu_{\eta}^{ch} \left[Q(\mathbf{x}_{target}) - Q(\mathbf{x}_{source}) \right] , \tag{2.35}$$

where $\mathbf{x}_{source}$ is a cytosolic site of cell η, and $\mathbf{x}_{target}$ is one of its neighbouring medium sites. The quantity, $Q(\mathbf{x}, t)$, evaluates the local extracellular level of VEGF (see Eq. (2.39)) sensed by the moving cell membrane site, and is given by:

$$Q(\mathbf{x}, t) = \sum_{\mathbf{x}' \in \Omega'_{\mathbf{x}}} c(\mathbf{x}', t) ,$$

where $\mathbf{x} \in \{\mathbf{x}_{source}, \mathbf{x}_{target}\}$ and $\mathbf{x}'$ is a medium first-nearest neighbour of $\mathbf{x}$. The local chemical response of cell η is measured by μ_{η}^{ch}, which is set to null at cell-cell interfaces to describe a contact-inhibited chemotaxis.

Finally, $H_{persistence}$ explicitly models the persistent motion characteristic of vascular cells:

$$H_{persistence} = \sum_{\eta} \mu_{\eta}^{pers} |\mathbf{v}_{\eta}(t) - \mathbf{v}_{\eta}(t - \Delta t)|^2, \tag{2.36}$$

where $\mathbf{v}_{\eta}$ is the instantaneous velocity of the center of mass of cell η, and $\Delta t = 1$ MCS. The coefficient μ_{η}^{pers} controls the cell persistence time and is given by:

$$\mu_{\eta}^{pers} = \mu_{pers,0} \left(\frac{l_{\eta}}{L_0} - 1 \right) , \tag{2.37}$$

where $l_{\eta}(t)$ is the current measure of the long axis of cell η (measured as in [172]), and L_0 is the initial cell diameter. Relation (2.37) describes the fact that, after analogous chemical stimulations, elongated vascular cells have been observed to have a longer persistent movement than round cells [125].

In [237], a more realistic interface between the microscopic intracellular level and the mesoscopic phenomenological cell scale is achieved by the use of a nested modelling philosophy, where the biophysical properties of the ECs vary as a function of their molecular state, and in particular of their internal calcium level, Ca. Specifically,

$$\begin{cases} J_{C,C}^{ext} = J_0 \ \exp\left(-j \widetilde{Ca}(\mathbf{x}, t) \widetilde{Ca}(\mathbf{x}', t) \right) , \\ \mu_{\eta}^{ch} = \mu_0^{ch} \widetilde{Ca}(\mathbf{x}, t) , \\ \lambda_{\eta,C}^{per} = \lambda_0^{per} e^{-k \widetilde{Ca}_{\eta}(t)} , \end{cases} \tag{2.38}$$

where

$$\widetilde{Ca}(\mathbf{x}, t) = \frac{1}{Ca_0} Ca(\mathbf{x}, t) - 1 , \qquad \text{and} \qquad \widetilde{Ca}_{\eta}(t) = \frac{1}{a_{\eta}(t) Ca_0} \sum_{\mathbf{x} \in \eta} Ca(\mathbf{x}, t) - 1 .$$

These relations mimic the biological fact that the local concentration of calcium ions enhances the avidity of both the local cadherins (either with quantitative changes in their expression or with the activation of the already exposed molecules) and of VEGF surface receptors (whose activity mediates the cell

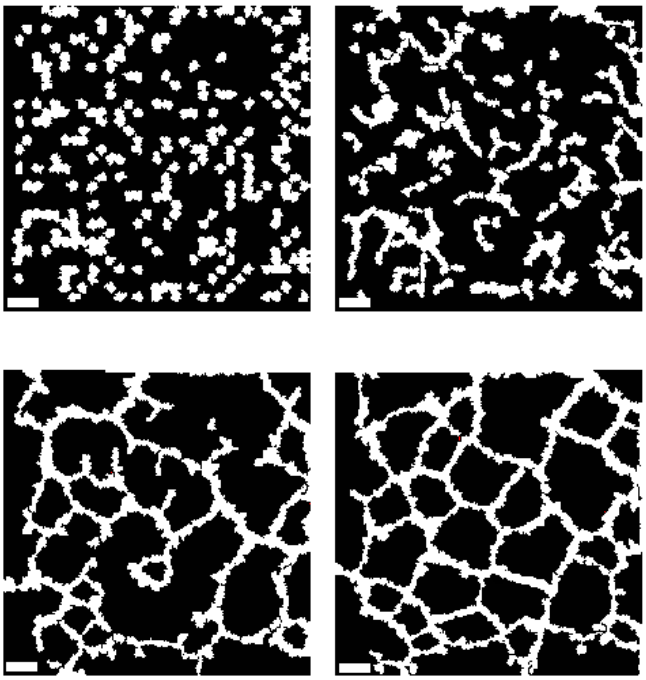

Figure 5: Temporal evolution of the network structure obtained using the cellular Potts model for TEC vasculogenesis ($t = 0, 4, 8, 12\,h$. Scale bar=50 μm).

chemotactic force). Moreover, the overall intracellular level of the ion promotes continuous and dramatic actin-myosin interactions, resulting in increments in cell elasticity, i.e. in quick changes of cell morphology. Also the motility coefficient T in (2.23) is taken to be an increasing function of the normalized calcium level in the cell $\widetilde{Ca}_\eta(t)$.

The constitutive laws summarized in (2.38) represent a step forward with respect to the classical CPMs presented so far. In fact,

- Each vascular cell-type features distinct biophysical properties, which are inherited from its internal molecular state;
- The adhesiveness and the chemotactic strength are no longer homogeneous over the entire cell membrane, but vary locally, revealing the role of microscopic inhomogeneities;
- Cell mesoscopic characteristics are no longer constant over time, but constantly adapt during the process, as a consequence of continuous internal and external stimuli.

The agonist-induced intracellular pathways are modelled by a system of RD equations, based on the following set of assumptions:

1. VEGF is autocrinally released by TECs, and diffuses and degrades throughout the extracellular environment;

2. Single molecules of morphogen are sequestered by the cells (via their surface tyrosine kinase receptors), and initiate a sequence of reactions culminating in the production of arachidonic acid (AA) and nitric oxide (NO) in the sub plasmamembrane regions [136, 177, 179, 271];

3. NO production is also triggered within the cell cytosol by AA itself;

4. NO and AA open related and independent calcium channels in the cell plasmamembrane, leading to extracellular calcium entry [87, 88, 177, 179, 271, 289];

5. Calcium ions, which also enhance the intracellular production rate of both AA and NO [179], are reversibly buffered to proteins such as calmodulin or to mitochondria [27, 31, 137], and then extruded back from the cell by plasmamembrane calcium ATPase and Ca^{2+}-Na^{+} exchangers [110, 124, 278].

Then, the extracellular evolution of VEGF (always denoted by c) is controlled by:

$$\frac{\partial c}{\partial t} = D\nabla^2 c - \frac{c}{\tau} - B(c) + S\,, \tag{2.39}$$

where $S = S(\mathbf{x}, t)$ describes the autocrine secretion of the growth factor from cells' membrane at a constant rate. VEGF binding and uptake by tumour-derived ECs is defined by the function $B(c)$, which is proportional to the local concentration of the ion and is limited to a maximum rate related to the number of membrane receptors.

For each cell η, the current local levels of AA and NO (i.e. at site $\mathbf{x}$: $\tau(\sigma(\mathbf{x})) = C, N$) are defined, respectively, as $a(\mathbf{x}, t)$ and $n(\mathbf{x}, t)$, and are controlled by the following RD equations [181, 238, 237]:

$$\frac{\partial a}{\partial t} = D_a\nabla^2 a - \frac{a}{\tau_a} + \gamma_a R(B(c)) + \tilde{\gamma}_a Ca\,, \tag{2.40}$$

$$\frac{\partial n}{\partial t} = D_n\nabla^2 n - \frac{n}{\tau_n} + \gamma_n R(B(c)) + \tilde{\gamma}_n \frac{Ca}{s_n + Ca}\,\frac{a}{s_a + a}\,. \tag{2.41}$$

The third terms in Eqs. (2.40) and (2.41) describe the production rates of AA and NO at the cells' membrane, which are proportional to the quantity of sequestrated VEGF molecules (i.e. B is defined as in (2.39)). The last term in Eq. (2.40) implements the calcium-dependent feedback mechanism in AA bio-synthesis, while the analogous term in Eq. (2.41) accounts for the double regulation of NO production (both AA- and Ca-mediated).

For each cell η, the intracellular concentration of calcium is controlled by the following RD problem:

$$\begin{cases} \dfrac{\partial Ca}{\partial t} = K_{buff} D_{ca}\nabla^2 Ca, & \text{in } \eta; \\ \mathbf{n}\cdot\nabla Ca = k_{Ca}(Ca - \widehat{Ca})_+ \dfrac{k_a a}{q_a + a} + \dfrac{k_n n}{q_n + n}, & \text{at the boundary of } \eta, \end{cases} \tag{2.42}$$

where the scaling factor $K_{buff} < 1$ models the activity of intracellular endogenous buffers, which decreases the intracellular diffusion of calcium.

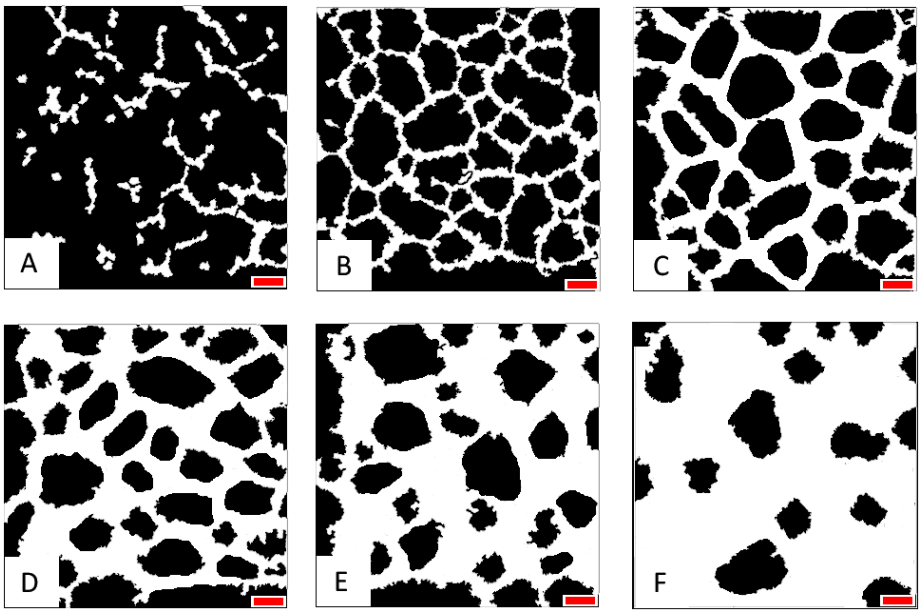

Figure 6: Dependence of the CPM model for TEC vasculogenesis on the density of seeded cells ($n = 50, 150, 200, 300, 400, 500$. Scale bar=50 μm).

As shown in Figure 5, the resulting model is able to describe a TEC tubulogenic assay, with a number of parameters which are under control and biologically significant. Indeed, it indicates a close dependence of the topology of the structure on cell density, similar to that observed in [103, 172] for normal ECs (see Figure 6).

The effect of activation/inactivation of calcium dynamics is depicted in Figure 7. In particular, calcium-related networks are up-regulated during the migration phase and switch off upon reaching confluence, leading to a decrease in motility.

The connection of the cell-based models with the sub-cellular chemical machinery allows virtual testing of specific and biologically reasonable anti-angiogenic

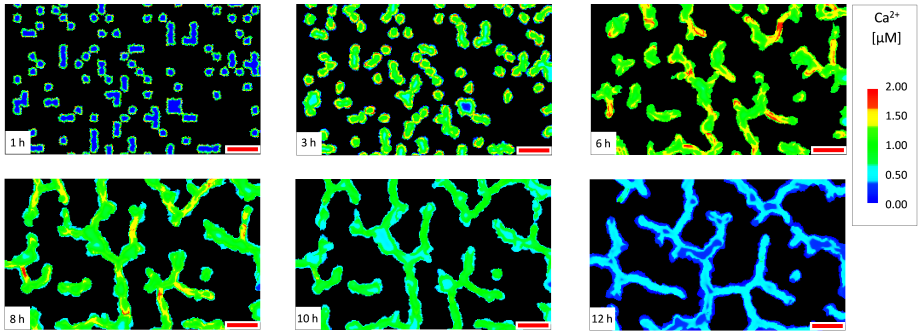

Figure 7: Temporal evolution of calcium within ECs involved in tubule formation.

OPTIMAL POTENTIAL THERAPIES				
BIOLOGICAL MECHANISM	**MODEL PARAMETER**	**EFFICIENCY**	**EXISTING COMPOUND**	**TOTAL TUBULE LENGTH (μm)**
VEGF UPTAKE	β_V	+++	sorafenib, sunitinib, vatalanib	
VEGF DEGRADATION	λ_V	+++		
CALCIUM ENTRY	F_{AA}, F_{NO}	+++	CAI	
AA PRODUCTION	v_{AA}, c_{AA}	+	AACOCF3	
NO PRODUCTION	$v_{Ca\text{-}AA}$, v_{NO}	+	L-NAME, L-NMMA	
CYTOSKELETAL REMODELING	μ_{pers}	+++	phalloidin	
PERSISTENCE	μ_{in}	+++		
CHEMOTAXIS	μ_{ch}	+++		
ADHESION	$J^{ext}(C,C)$	+++	anti-VE-cadherin antibodies	
CONTROL				

Figure 8: Potential anti-angiogenic therapies. Each line represents a possible strategy to inhibit VEGF-induced tubulogenesis. The related modified parameters are displayed in the second column. The third column gives an idea of the efficiency of the proposed solutions: +++ means a reduction in total tubule length with respect to the physiological value larger than 66%, ++ in the range 50% – 66%, and + in the range 33% – 50%. The last column reports the relative average values (mean over 10 simulations, error bars show standard deviation).

strategies, which produce an abnormal capillary-like bed. As reviewed in Figure 8, the proposed model confirms the efficiency of current therapies, which focus on the abrogation of VEGF activity or on interference with the calcium machinery, and can suggest novel and interesting cancer therapies, e.g. blocking the mechanisms of cytoskeletal remodelling and inter-cellular adhesion, or inhibiting the chemotactic and persistent component of cell motion. Indeed, all of the proposed solutions emerge from biologically reasonable variations in model parameters or assumptions.

The basic assumption introduced by Szabo et al. [262] is that the ECs behave actively and prefer to adhere to other elongated ECs, rather than remaining in the middle of the aggregate. Such a preferential adhesion mechanism is sufficient for the formation, and the subsequent stabilization of branches. Indeed, this mechanism would also explain the formation of multicellular long segments in cultures growing in standard conditions on solid substrates, which are therefore not subjected to chemical or mechanical stimuli.

The Hamiltonian used in this work accounts only for the standard terms describing the cell morphological changes (see Eq. (4.4)) and the intercellular adhesion (see Eq. (4.3)). In particular, there is only a constraint on cell area (this implies that cells are allowed to significantly remodel), the cell-medium

contact strength is normalised to 1, while the cell-cell adhesiveness is a variable parameter.

The proposed preferential attraction to elongated cells is formulated by adding a new inherently asymmetric term in the Boltzmann transition function (4.1). In more detail, the authors first define a measure of the anisotropy of each cell σ, with

$$\theta_\sigma = \left(\frac{a_\sigma}{b_\sigma}\right)^{1/2} - 1\,, \tag{2.43}$$

where $a_\sigma \geq b_\sigma$ are the two eigenvalues of its inertia tensor. Then, they represent the tendency of the cell to be adjacent to polarized individuals as:

$$\begin{aligned} &W(\sigma(\mathbf{x}_{source}) \to \sigma(\mathbf{x}_{target})) \\ &= \lambda^{asym}\left[\delta_{\tau(\sigma(\mathbf{x}_{source})),C} - \delta_{\tau(\sigma(\mathbf{x}_{target})),C}\right]\sum \theta_{\sigma(\mathbf{x})}, \end{aligned} \tag{2.44}$$

where $\delta = 1$ if σ is a cell (i.e. $\tau(\sigma(\mathbf{x})) = C$) and 0 elsewhere, thus ensuring that only cells (and not the medium) exhibit this preference. The summation is taken over only those neighbour sites of $\mathbf{x}_{target}$ that belong to cells other than $\sigma(\mathbf{x}_{source})$ and $\sigma(\mathbf{x}_{target})$. Eq. (2.44) also implies that the strength of attraction depends only on the contact target.

The resulting probability function provided by the authors in the same work is given by:

$$P(\sigma(\mathbf{x}_{source}) \to \sigma(\mathbf{x}_{target})) = \min\left\{1, e^{-\Delta H + W}\right\}. \tag{2.45}$$

Here the Boltzmann temperature T is set equal to 1, and the term W can be interpreted as the asymmetric extension of the standard adhesion term (4.3). It is useful to notice that (2.45) is an asymmetric transitional probability and that it can no longer satisfy a balance condition, so that the dynamics of the system can not be interpreted as the relaxation of an energy functional to a thermal equilibrium.

In the simulations, after an initial bud appears, the constituting elongated cells attract other individuals (that isotropic cell-cell adhesion alone would keep within the aggregate) so that the segment continues to extend. This influx of additional cells helps to stabilize the extending sprout. The sprouts, which are able to connect pairs of islands, are structured further, whereas the others degenerate, as the overall system reaches a stationary state where surface-tension-driven coarsening is balanced by the formation of new sprouts. In contrast with [103, 244], the characteristic dimensions of the final pattern depend on the cell density. Specific sets of simulations show that a connected network of sprouts occurs only for λ^{asym} greater than the isotropic intercellular adhesive strength. Moreover, for a fixed value of λ^{asym}, increments in the cell-cell adhesiveness result in coarser structures. This CPM differs from those in [170, 172, 174] by the fact that the polarization of ECs is not imposed by a specific rule in the Hamiltonian, but arises from the asymmetric correction of the Boltzmann probability.

The basic assumption that the emergence of vascular sprouts is driven by cell preferential attraction to stretched elongated individuals is developed by the same authors in a different type of model [261]. Here, the motility of cells is described as a persistent diffusion process, where the velocity of each individual

k, represented as a point particle, satisfies a Langevin equation:

$$\frac{d\mathbf{v}_k}{dt} = -\frac{\mathbf{v}_k}{\tau} + \sqrt{D}\xi_k + \mathbf{M}_k, \tag{2.46}$$

where τ is the persistent time of motion, D a diffusion parameter which depends on cell type, and ξ_k an uncorrelated white noise. The term $\mathbf{M}_k$ is a deterministic bias which represents the interaction of cell k with the local environment, i.e.,

$$\mathbf{M}_k = \sum_j \frac{\mathbf{x}_j - \mathbf{x}_k}{|\mathbf{x}_j - \mathbf{x}_k|} \left[f_1(|\mathbf{x}_j - \mathbf{x}_k|) + w_j f_2(|\mathbf{x}_j - \mathbf{x}_k|) \right], \tag{2.47}$$

where the summation is taken over the Voronoi neighbours of $\mathbf{x}_k$. The function f_1 is an intercellular repulsion, which ensures cell impenetrability, and f_2 is an intercellular attraction. The cell preferential adhesion to anisotropic structures (which, in the absence of an explicit representation of cell shape, are inferred from the overall particle configuration) is implemented by a specific construction of the weights w_j:

$$w_k = \frac{1}{n_k} \sum_{j:|\mathbf{x}_j - \mathbf{x}_k| < R} \left| \exp(2i\varphi_{jk}) \right|, \tag{2.48}$$

where the sum is taken over all the n_k cells within a circle of radius R around k, and φ_{jk} represents the angle between the vector $(\mathbf{x}_j - \mathbf{x}_k)$ and a reference direction. Indeed, $w = 0$ for particles in an isotropic environment and $w = 1$ for particles in a highly elongated, linear configuration.

The resulting simulations show that, at sufficiently high density of random-sited cells, a network pattern emerges both by sprouting of new branches and by coarsening of adjacent cords. Moreover, the authors conclude that the characteristic pattern size is almost independent of the initial cell density, which instead determines the connectivity of the mesh, with a percolative transition as in [103, 237].

3 Angiogenesis

3.1 Mechanisms of Angiogenesis

Although angiogenesis is a physiological process occurring in many different circumstances (for instance, in wound healing, ovary and uterus vascularization during the female cycle, and mammary gland vascularization during lactation), the majority of the literature on angiogenesis focuses on tumour-induced angiogenesis, one of the most dangerous pathological aspects. In fact, one of the crucial milestones in tumour development is the so-called angiogenic switch, when the tumour gains the ability to trigger the formation of its own vascular network by the secretion of angiogenic factors.

As expected angiogenesis has many similarities with vasculogenesis, although its origin is very different. In the case of angiogenesis, the new vessels sprout from existing capillaries and post-capillary venules. Angiogenesis is regulated by precise genetic programmes and is strongly influenced by many chemical factors (generally called tumour angiogenic factors (TAF)) and the subsequent activation of even more related pathways. Some of the proteins involved are vascular endothelial growth factor (VEGF), transforming growth factor β (TGF-β), basic

fibroblast growth factor (bFGF), hypoxic growth factor (HIF), platelet-derived growth factor (PDGF), metallo-proteinases (MMPs), and angiopoietins (Ang-1 and Ang-2). In addition, several cell populations (such as macrophages, pericytes, and smooth muscle cells) influence the process through e.g. inflammation and vessel maturation. All of these contributing features render the process very complex, and the interested reader can find more information for instance in references [16, 47, 56, 57, 163, 203, 227]. In particular, an in-depth and very useful phenomenological description having in mind the following modelling step is given in [16, 163]. Although the reader can refer to these reviews for more details, we summarize the main stages of angiogenesis below.

The first stage of angiogenesis is characterized by changes in the shape of the ECs covering the walls of the blood vessel, by the loosening of the adhesive connection between cells, and by the reduction of vascular tonus. This induces an increase in the permeability of the blood vessel, which in turn results in an increase in both the availability of nutrients and the interstitial pressure.

The following stage consists of the production of proteolytic enzymes (serine-proteins, iron-proteins) which degrade the basal lamina and the extracellular matrix surrounding the capillary, thus facilitating cellular movement. Then the ECs are able to proliferate and to migrate chemotactically towards the place where it is necessary to create a new vascular network. In this phase it is possible to distinguish between tip cells leading the way through the ECM and stalk cells forming in the rear of the lumen of the new capillary. During growth, capillaries may undergo *branching* or they can merge to form loops when two capillaries encounter each other, a process called *anastomosis*. From these branches and loops more sprouts may form. Indeed, the whole process may repeat several times resulting in a capillary network through which blood may circulate.

The stage of differentiation is characterized by the exit of ECs from the cellular cycle and by their capacity to survive in sub-optimal conditions and to build themselves primitive capillary structures, not yet physiologically active.

Finally, in the maturation stage, the newborn vessel is completed by the formation of new perivascular ECM and by the arrival of pericytes and sometimes of flat muscle cells. During this phase a major role is played by angiopoietins (Ang-1, Ang-2), which results in the development of the simple endothelial tubes into a more elaborate vascular tree composed of several cell types. The angiopoietins contribute to the maintenance of vessel integrity through the establishment of appropriate cell-cell and cell-matrix connections.

After the formation of the vascular network, a reorganization process commences, influenced by the blood flow. This involves the loss of some physiologically useless capillaries, the adaptation of the size of the lumen, and the remodelling of the extracellular matrix.

Angiogenesis can also be simulated *in vitro* [17, 94], where clusters of ECs, cultivated in an extracellular matrix gel, are able to migrate, to proliferate and to build structures similar to capillaries.

For sake of completeness, we mention a further process leading to vessel formation called atherogenesis, which is triggered by the occlusion of an artery. In order to avoid the possible formation of ischemic tissues, the pre-existing arteriolar connections enlarge to become true collateral arteries. By bypassing the site of occlusion, they have the ability to markedly grow and increase their lumen, thus providing enhanced perfusion to regions near the occlusion. The formation of these collateral arteries is not simply a process of passive dilata-

tion, but of active proliferation and remodelling. However, no mathematical modelling has been devoted to this process.

3.2 Continuum Models of Angiogenesis

The article by Deakin [75] represents the first attempt to model angiogenesis as a result of the migratory response of ECs to angiogenic factors leading to the formation of capillary loops. Approximately a decade later, several continuum models followed. Generally speaking these models consist of a set of advection-reaction-diffusion equations for the cell densities, ρ_i, and the concentrations of chemicals, c_j, in the form:

$$\frac{\partial \rho_i}{\partial t} + \nabla \cdot (\rho_i \mathbf{v}_i) = \nabla \cdot (K_i \nabla \rho_i) + \Gamma_i - \Delta_i \,, \quad i = 1, \ldots, N \,, \tag{3.1}$$

$$\frac{\partial c_j}{\partial t} + \nabla \cdot (c_j \mathbf{w}_j) = \nabla \cdot (D_j \nabla c_j) + P_j - L_j \,, \quad j = 1, \ldots, M \,. \tag{3.2}$$

Here the advection velocities $\mathbf{v}_i$ and $\mathbf{w}_j$, the growth terms Γ_i, the death terms Δ_i, the production terms P_j, and the decay terms L_j in general depend on all the cell densities and concentrations of chemical factors. In many cases, the advection velocities are directed towards the source of the angiogenic stimulus or towards hypoxic regions via a chemotactic term, or towards regions with a higher concentration of ECM or matrix-bound proteins, via a haptotactic term, i.e. :

$$\mathbf{v}_i = \sum_{i=1}^{M} \chi_i(c_i) \nabla c_i \,.$$

One family of articles on modelling angiogenesis is based on the idea originally proposed by Balding and McElwain [22], who distinguished between the density of tip cells, ρ_t, and of stalk cells, ρ_s (also named capillary sprouts). The former are sensitive to VEGF, while the latter follow by duplication. This mechanism is modelled in one-dimension by postulating the presence of a so-called *snail-trail* term in the equations, so that if the tip cells are subject to an advective flux

$$J_{snail} = -K_c \frac{\partial \rho_t}{\partial x} + \rho_t \chi(c) \frac{\partial c}{\partial x} \,,$$

then there is a growth term in the equation for the density of stalk cells given by $-J_{snail}$. The model then writes as:

$$\frac{\partial \rho_t}{\partial t} = -\frac{\partial J_{snail}}{\partial x} + \gamma_{cs} c \rho_s - \delta_{ts} \rho_t \rho_s \,, \tag{3.3}$$

$$\frac{\partial \rho_s}{\partial t} = -J_{snail} - \delta_s \rho_s \,, \tag{3.4}$$

and they are then coupled to an RD equation for the tumour angiogenic factor. We remark that ρ_t and ρ_s do not have the same units.

We also observe that only tip cells are allowed to proliferate in these equations; this corresponds to the experimental observation that EC proliferation occurs mainly near the tip of the vasculature and is rather infrequent in the main body of the growing vasculature. The death term describes the anastomosis of tip cells when they encounter other stalk cells.

The general three-dimensional model of this type that can be found in the literature can be summarized as:

$$\frac{\partial \rho_t}{\partial t} + \nabla \cdot \mathbf{J}_{snail} = \Gamma_{branch} - \Delta_{anast}\,, \tag{3.5}$$

$$\frac{\partial \rho_s}{\partial t} = K_s \nabla^2 \rho_s + |\mathbf{J}_{snail}| + \Gamma_s - \delta_s \rho_s\,, \tag{3.6}$$

where

$$\mathbf{J}_{snail} = -K_c \nabla \rho_t + \rho_t \chi(c) \nabla c\,, \tag{3.7}$$

and

$$\Gamma_{branch} = \gamma_{cs} c \rho_s + \gamma_{ct} c \rho_t\,,$$

$$\Delta_{anast} = \delta_{ts} \rho_t \rho_s + \delta_{tt} \rho_t^2\,,$$

$$\Gamma_s = \gamma_s \left(1 - \frac{\rho_s}{\rho_{s0}}\right) \rho_s\,.$$

The terms in Δ_{anast} describe respectively tip-to-stalk and tip-to-tip anastomosis. In specific cases, some of the terms can be neglected. For instance, in [50, 102, 207, 208], $\gamma_{ct} = \delta_s = 0$, which corresponds to the assumptions that tip cells are generated only by the duplication of stalk cells and that there is no death of stalk cells. We must also mention that the model parameters need to be carefully calibrated, and that in three-dimensional situations there is some ambiguity in properly defining the snail-trail term in (3.5) and (3.6).

3.2.1 Wound-Healing Angiogenesis

Although the original model by Balding and McElwain [22] was developed to investigate corneal angiogenesis, the same concept was used ten years later to model wound-healing-induced angiogenesis (see, for instance, [48, 49, 50, 102, 207, 208]). In this section, we focus on the main modifications introduced by different authors and on some models that have been recently used as a basis for more complex models.

In [207], the diffusion coefficient of stalk cells, K_s, is assumed to depend linearly on the concentration of tip cells. This choice has been probably done in order to describe a higher random motility near the tip of the vessels. In addition, the growth term in the equation for the stalk cells has been omitted. The authors perform a boundary layer analysis and investigate a travelling wave solution.

The model in [208] is more complex, as it consists of six equations for the densities of tip cells, stalk cells, fibroblasts, and extracellular matrix, and for the concentrations of oxygen and an angiogenic factor. In addition, the snail-trail term in (3.5, 3.6) is modified to become:

$$\mathbf{J}_{snail} = -K_c m \rho_t^n \nabla \rho_t + \chi(c) m \rho_t \nabla c\,, \tag{3.8}$$

so that the motility coefficient increases with the amount m of ECM. On choosing $n > 0$, the equation for the tip cells becomes a degenerate parabolic equation, which gives rise to solutions with compact support (if the initial condition has

compact support). The governing equations for the densitities of fibroblasts, f, and ECM, m, include a similar snail-trail term:

$$\frac{\partial f}{\partial t} + \nabla \cdot \mathbf{J}_f = \gamma_f \left(1 - \frac{f}{f_0}\right) f \,, \tag{3.9}$$

$$\frac{\partial m}{\partial t} = K_m \nabla \cdot (f \nabla \rho_s) + |\mathbf{J}_f| + \gamma_m \left(1 - \frac{m}{m_0}\right) f \,, \tag{3.10}$$

where $\mathbf{J}_f$ is given by:

$$\mathbf{J}_f = -K_f f^n \nabla f + f m \chi_f(c) \nabla c \,.$$

We remark that the growth term for the fibroblast density is a logistic term, whilst the growth term for the ECM density models production by the fibroblasts up to a saturation value.

Working in spherical coordinates, the authors in [50] modify the model in [207] both by omitting the diffusion and the growth term in (3.6) and by introducing a snail-trail velocity rather than a flux:

$$\mathbf{v}_{snail} = -K_c \nabla \rho_t + \chi(c) \nabla c \,. \tag{3.11}$$

The term in (3.11) is substituted into the mass balance equation and gives rise again to a degenerate parabolic equation. The relation between $\mathbf{v}_{snail}$ and $\mathbf{J}_{snail}$ in (3.5) is simply given by $\mathbf{J}_{snail} = \rho_t \mathbf{v}_{snail}$.

Based on the work of [207], Flegg et al. [90] recently proposed a model of hyperbaric oxygen therapies to assist the healing of chronic wounds, and in particular diabetic foot ulcers (see also [270] for a review of the biology of the problem). Their one-dimensional model describes the evolution of the densities of both tip and stalk cells and the concentration of oxygen c_o, and defines the snail-trail velocity as:

$$v_{snail} = -\chi \frac{\partial c_o}{\partial x} \,,$$

so that cells tend to move towards hypoxic regions. The model is written as:

$$\frac{\partial \rho_t}{\partial t} + \frac{\partial \rho_t v_{snail}}{\partial x} = \gamma_{tc} \rho_s H(c_o - c_L) H(c_H - c_o) - \delta_t \rho_t \,, \tag{3.12}$$

$$\frac{\partial \rho_s}{\partial t} = \rho_t v_{snail} + \gamma_s \rho_s \left(1 - \frac{\rho_s}{\rho_{s0}}\right) \,, \tag{3.13}$$

$$\frac{\partial c_o}{\partial t} = \frac{\partial^2 c_o}{\partial x^2} + \pi_s \rho_s (1 + \delta_{ON}(t)) - \frac{d_{cs} c_o \rho_s}{\rho_{s0}} - d_c c_o \,. \tag{3.14}$$

On the right-hand side of (3.12), the first term describes the proliferation of tip cells only for $c_o \in [c_L, c_H]$, while the last term describes their natural death (anastomosis is more realistically accounted for in a following paper [91]). On the right-hand side of (3.14), the second term describes the increase in the oxygen supply with the vessel density, the third term the oxygen uptake by the vessels themselves, and the last the natural decay of oxygen, which can also be due to oxygen consumption by the cells in the environment. The term $\delta_{ON}(t)$ (which is equal to 0 or 1 depending on whether the therapy is off or on) accounts for the fact that the level of oxygen in the wound substantially increases during hyperbaric oxygen therapies.

In [91], the model was then extended in the spirit of [208] to include the effect of angiogenic factors, fibroblasts, and ECM.

Both models supported the importance of intermittency in healing chronic wounds, while therapies using normobaric oxygen were ineffective. They also indicated that patients with a poor arterial supply of oxygen, or with a high consumption of oxygen by the wound tissue, may not respond adequately to hyperbaric oxygen therapies.

The work by Gaffney et al. [102] modifies the snail-trail concept by assuming that tip and stalk cells move with proportional flux terms. Specifically, they took:

$$J_{snail} = -K_t \frac{\partial \rho_t}{\partial x} - K_s \rho_t \frac{\partial \rho_s}{\partial x}\,, \tag{3.15}$$

and postulated the following minimal model:

$$\frac{\partial \rho_t}{\partial t} = -\frac{\partial J_{snail}}{\partial x} + \gamma_t \rho_t - \delta_{ts}\rho_t\rho_s - \delta_{tt}\rho_t^2\,, \tag{3.16}$$

$$\frac{\partial \rho_s}{\partial t} = -k\frac{\partial J_{snail}}{\partial x} + \gamma_s \rho_t \rho_s \left(1 - \frac{\rho_s}{\rho_0}\right) + \gamma_s' \rho_s \left(1 - \frac{\rho_s}{\rho_0'}\right) + \beta(\delta_{ts}\rho_t\rho_s + \delta_{tt}\rho_t^2)\,, \tag{3.17}$$

where there is no chemical factor triggering angiogenesis. The last two terms in both equations describe the transformation of tip cells into stalk cells due to anastomosis as a result of the encounter of a tip cell with a capillary or another tip cell respectively. In addition, in (3.16), the first reaction term describes vessel branching, whereas in (3.17), it is a logistic growth term, which also considers the effect of the presence of tip cells.

Following the same idea, but with the proportionality constant also proportional to ρ_s, Schugart et al. [235] develop a much more complex model with seven equations describing the evolution of capillary tips, stalk cells, fibroblasts, inflammatory cells (e.g. macrophages and neutrophils), ECM, oxygen, and angiogenic factor. The model is characterized by two snail-trail-like coupling terms, one involving tip and stalk cells (notice the sign difference in the chemotactic term):

$$\mathbf{J}^t_{snail} = -K_t \nabla \rho_t + \chi_c \frac{m}{m_0} \rho_t H(\rho_{t0} - \rho_t) \nabla c\,,$$

and the other involving fibroblasts and ECM:

$$\mathbf{J}^f_{snail} = -K_f \nabla f + \chi_f f H(f_0 - f) \nabla c\,.$$

Another difference with respect to (3.16) is the fact that the snail-trail term is introduced into the equations for the capillary sprouts and for the ECM as an advection term based on the observation that mass balance (and not the material derivative as written in [235]) implies that equations have the form of (2.4). Finally, inflammatory cells move chemotactically towards hypoxic regions and standard RD equations hold for the chemical factors.

Hence the governing equations can be written as:

$$\begin{cases} \dfrac{\partial \rho_t}{\partial t} = -\nabla \cdot \mathbf{J}^t_{snail} + (\gamma_{cs} c \rho_s + \gamma_{ct} c \rho_t) H(\rho_{t0} - \rho_t) - (\delta_{st} \rho_s + \delta_{tt} \rho_t) \rho_t \,, \\ \dfrac{\partial \rho_s}{\partial t} = K_s \nabla^2 \rho_s - \nabla \cdot (k_s \rho_s \mathbf{J}^t_{snail}) + \gamma_s G_b(c_o) \rho_s \left(1 - \dfrac{\rho_s}{\rho_{s0}}\right) , \\ \dfrac{\partial f}{\partial t} = -\nabla \cdot \mathbf{J}^f_{snail} + \gamma_f G_f(c_o) f \left(1 - \dfrac{f}{f_0}\right) , \\ \dfrac{\partial m}{\partial t} = K_m \nabla^2 m - \nabla \cdot (k_m m \mathbf{J}^f_{snail}) + \gamma_m m \left(1 - \dfrac{m}{m_0}\right) , \\ \dfrac{\partial \rho_i}{\partial t} = K_i \nabla^2 \rho_i + \nabla \cdot [\chi_i \rho_i H(\rho_{i0} - \rho_i) \nabla c_o] - \delta_i \rho_i \,, \\ \dfrac{\partial c}{\partial t} = D_c \nabla^2 c + \gamma_c G_c(c_o) \rho_i - (\delta_{ct} \rho_t + \delta_{cs} \rho_s + \delta_c) c \,, \\ \dfrac{\partial c_o}{\partial t} = D_o \nabla^2 c_o + \gamma_o G_o(c_o) \rho_s - (\delta_{of} f + \delta_{oi} \rho_i) c_o \,, \end{cases} \tag{3.18}$$

The contribution due to macrophage-derived growth factors (MDGF) is considered by Maggelakis [155, 156], who proposed a model where the capillary density grows according to an ODE with a logistic term and a growth coefficient proportional to the concentration of MDGF. Of course, due to the absence of any advection or diffusion term, such a model requires that capillary cells are present everywhere in the wound.

By suitably merging the models by Maggelakis [155, 156] (for the coupling with MDGF), by Gaffney et al. [102] (for angiogenesis), and by Holmes and Sleeman [123] (for the coupling of angiogenesis and ECM contraction due to the action of ECs), Javierre and coworkers present models in a series of recent papers [281, 282, 283], which attempt to couple wound-healing angiogenesis with re-epithelialization, whilst also taking into account visco-elastic effects related to wound contraction. As in [123], the mechanochemical model is based on the work by Murray and coworkers [185, 186, 187], which is the same basis for their vasculogenesis models discussed in Section 2.2 and in more detail in references [11, 163]. The densities of ECM, fibroblasts, epithelial cells and capillaries, and the concentrations of oxygen, VEGF, and epithelial growth factor (EGF), are described through advection-reaction-diffusion equations similar to those in (3.2) with the feature that all the advective velocities are equal to that of the ECM. This simplifying assumption, known as the *constrained mixture hypothesis* in mixture theory, has the questionable implication that all chemical factors are transported by the ECM, as though they were bound to the ECM. However, the presence of diffusion terms does allow molecules to move randomly relative to the ECM.

A similar approach is used by Valero et al. [279], who deduce a model for the concentrations of oxygen and MDGF, and the densities of fibroblasts and capillaries. It is assumed that the density of the ECM is proportional to the density of capillaries, which determines the deformation of the ECM through an Ogden constitutive equation. Also in this case a constrained mixture hypothesis is enforced, but it is not completely clear how the deformation is computed.

Xue et al. [300] also developed a mechanochemical model coupled with an-

giogenesis to describe wound healing. Working in radial symmetry, they treat the ECM as a compressible viscoelastic fluid, but then they use the constitutive equation for an incompressible Maxwell fluid. The rest of the model is similar to [235] (see Eq. (3.18)), except for minor terms and except for the fact that the chemotactic behaviour of fibroblasts is triggered by the action of growth factors like PDGF-A and TGF-β, rather than by VEGF directly. These factors are produced by macrophages that evolve according to an equation similar to that for the fibroblasts.

3.2.2 Tumour-Induced Angiogenesis

Snail-trail models very similar to (3.5) and (3.6) were also proposed by Byrne and Chaplain [48, 49] for the scenario in which the formation of the vascular network is stimulated by the production of VEGF by a tumour. On the other hand, Chaplain and coworkers (see, for instance, [61, 63, 196]) have also proposed several models based on RD equations for ECs, fibronectin, and TAF, characterized by the presence of chemotaxis and haptotaxis terms, so that in (3.1)

$$\mathbf{v}_c = \chi_c(c)\nabla c + \chi_f \nabla f\,,$$

where f is the density of fibronectin.

In the same framework as described in detail in [163], much more detailed models were developed by Levine, Sleeman and coworkers [145, 146, 147, 148], which take into account many more cell populations, chemical factors, and their related receptors and receptor complexes. For instance, macrophages, pericytes, and anti-angiogenic agents were added into the model in [146]. In the latest development of this series of articles, Plank et al. [212] develop a reinforced random walk model to study the action of angiopoietins (Ang-1 and Ang-2) on angiogenesis. Capillaries are distinguished as mature or immature. The stabilising and destabilising effects of Ang-1 and Ang-2, respectively, are taken into account through their influence on the motility coefficient. Ang-1 (c_{a_1}) stabilises vessels by decreasing the motility coefficient, whereas Ang-2 (c_{a_2}) destabilises vessels by increasing the motility coefficient, which allows the ECs to move more freely, and to respond chemotactically and possibly haptotactically. This concept is quantified by defining the diffusion coefficient as:

$$K_c(c_{a_1}, c_{a_2}) = k\frac{(1+\alpha_2 c_{a_2})^{n_2}}{(1+\alpha_1 c_{a_1})^{n_1}}\,.$$

Angiopoietin also influences the chemotactic coefficients and the proliferation of immature ECs, that activates only if the ratio of c_{a_2}/c_{a_1} is above a threshold value. Among other things, the model supported the conjecture that Ang-2 is a critical regulator of angiogenic activity. The absence of Ang-2 allows Ang-1 to maintain vessels in the quiescent state, while expression of Ang-2 allows either angiogenic outgrowth, or vessel regression, depending on the presence or absence of VEGF.

As a final example of a continuum model aimed at describing tumour-induced angiogenesis, we recall reference [123], in which the growth of capillaries is coupled to ECM contraction, as already mentioned in the previous section.

Generally speaking, however, all of the continuum models described in the previous section and above do not allow the morphology of the capillary net-

works to be captured, which is very much at variance with the vasculogenesis models discussed in Section 2.2.

An exception is the model by Travasso et al. [275] that describes the formation of capillaries through an order parameter ϕ. The capillaries are identified by the regions where $\phi > 0$, i.e. $\rho_s = \phi_+$. The model can then be written as follows:

$$\frac{\partial \phi}{\partial t} = K\left[\nabla^2(\phi^3 - \phi) - \epsilon\nabla^4\phi\right] + \gamma_s \min\{c, c_{max}\}\phi_+ \,, \tag{3.19}$$

$$\frac{\partial c}{\partial t} = \nabla \cdot (D\nabla c) - \delta_c \phi_+ c + \gamma_c(\omega) \,, \tag{3.20}$$

where ϵ is related to the width of the capillary wall, δ_c is the uptake coefficient of TAF from ECs, and a source of TAF, $\gamma_c(\omega)$, from hypoxic cells is randomly placed at a certain distance from the pre-existing vessel, until oxygen is properly delivered to them by the newly formed capillary vessels. The term in the Laplacian in (3.19) destabilizes solutions with small densities, giving rise to a backward heat equation term, that is however stabilized by the bi-Laplacian. This results in an aggregation-like mechanism, well-known in phase-field theory, and sometimes denoted as *spinoidal decomposition*, that can be found in other tumour growth models (see, for instance, [64, 297]).

The differentiation of stalk cells into tip cells occurs only at large values of both TAF and ϕ. The tip cells will chemotactically move (only if the chemical gradient is above a threshold G_{min}) according to:

$$\mathbf{v} = \chi \min\{|\nabla c|, G_{max}\} H(|\nabla c| - G_{min}) \frac{\nabla c}{|\nabla c|} \,, \tag{3.21}$$

where χ is their chemotactic response and G_{max} is a saturation coefficient.

A cell-cell contact-dependent mechanism (for instance through the Notch pathway) prevents the activation of two neighbouring cells. This rule is implemented by allowing the activation only of those cells whose centre is at a given distance from the centres of already existing tip individuals. Indeed, when one of the activation conditions is no longer satisfied, a differentiated EC returns to the stalk cell state.

Finally, to merge tip cell and capillary dynamics, the order parameter inside the tip cell, denoted by ϕ_c, is defined by the following ratio:

$$\phi_c = \frac{\gamma_s \min\{c, c_{max}\} \pi R_c}{2|\mathbf{v}|} \,, \tag{3.22}$$

which is determined by the excess cell density by proliferation that occurs as the tip cell moves chemotactically in the tissue per unit time ($\gamma_s \min\{c, c_{max}\}\pi R_c^2$) divided by the area that the cell sweeps per unit time ($2R_c|\mathbf{v}|\phi_c$). Here R_c is the estimated radius of an EC.

The final result is a branching structure, similar to a vascular tree, directed towards the chemotactic source. Anastomosis is also present. Focussing on the dependence of the vessel tree structure on the underlying parameters, it is observed that:

- For low values of the chemotactic response χ, the vessels are thick and not so ramified. The reason for this is that, the slower the tip cells move,

the more time the stalk cells behind have to proliferate and to consume angiogenic factors. The subsequently reduced concentration of angiogenic factors becomes insufficient to induce further branching.

- For low values of the proliferation rate of stalk cells γ_s, the emerging vessels are thin and without ramifications, whereas at high proliferation rates, they are thick and have many branches, which may merge laterally to form even thicker vessels. Since physiologically the capillaries have a definite range of radii, these outcomes suggest that the parameters related to chemotaxis and proliferation must be properly balanced.

- An increase in TAF production from the hypoxic cells, γ_c, enhances vessel branching while leaving vessel diameter unchanged. For too low values of γ_c, the vessel network cannot even form.

Finally, the authors simulate the role played by the MMPs produced by the hypoxic cells. By cleaving the ECM, MMPs free heparin-binding angiogenic factors, thus influencing the structure of the vessel network. At low values of MMP activity, few vessels develop in the direction of hypoxic regions, while higher values lead instead to a straighter and thinner vessel phenotype.

3.3 Discrete and Discretized Models in Continuum Fields

3.3.1 Tumour-Induced Angiogenesis

An idea proposed by Anderson and Chaplain [14, 59, 60] represented a breakthrough in modelling realistic vascular structures. Their idea consisted essentially of the following. Instead of using reinforced random walk methods to obtain a continuum model from a discrete one, it is useful to retain the discrete feature for the capillary sprout tips, following their random path in a cubic lattice towards the tumour, or even to go back to a discrete and stochastic version of a continuum model to capture the cell-scale structures (see also [16] for a review). In order to distinguish this type of model from cell-based models that also possess hybrid characteristics, following the spirit of the titles of the articles [14, 73, 169] this type of hybrid models can be denoted as *discrete-continuum models*, or as *discretized models*. In fact, in them, cells are described as discrete entities moving according to laws obtained by a discretization of suitable continuum models under the influence of chemical fields and substrata described as a continuum, which are then possibly discretized.

Focussing on the ECs at the sprout-tips, where there is no proliferation in the absence of branching, the basic model is written as:

$$\frac{\partial \rho_t}{\partial t} + \nabla \cdot \left[\left(\frac{\chi}{1+sc} \nabla c + w_f \nabla f \right) \rho_t \right] = K \nabla^2 \rho_t \,, \tag{3.23}$$

$$\frac{\partial c}{\partial t} = -\delta_c \rho_t c \,, \tag{3.24}$$

$$\frac{\partial f}{\partial t} = \gamma \rho_t - \delta_f \rho_t f \,, \tag{3.25}$$

where δ_c is the uptake coefficient from tip cells, δ_f is the degradation of fibronectin by tip cells, and γ is the production rate of fibronectin by the cells.

Therefore, the TAF secreted by the tumour diffuses into the surrounding tissue and sets up the initial concentration gradient between the tumour and any pre-existing vasculature, which is responsible for the directionality in the formation of the new capillaries. Then, ECs uptake TAF, while its diffusion is neglected.

In [14], this continuum model is simulated, but, as mentioned above, the main idea consists of using the resulting coefficients of the five-point stencil of the standard central finite-difference scheme to generate the probabilities of movement of an individual cell in response to the chemoattractant gradients superimposed to an isotropic random walk.

Working in two-dimensions, if P_0 depends on both the probability of the cell of being stationary and on the probability of cells of moving from the node $\{i, j\}$ to one of its neighbours, P_1 is related to the probability of new cells coming from the node to the right, and similarly for the others, one can write:

$$\rho_{j,k}^{i+1} = P_0\rho_{j,k}^i + P_1\rho_{j+1,k}^i + P_2\rho_{j-1,k}^i + P_3\rho_{j,k+1}^i + P_4\rho_{j,k-1}^i\,, \quad (3.26)$$

$$c_{j,k}^{i+1} = \left(1 - \Delta t\delta_c\rho_{j,k}^i\right) c_{j,k}^i\,, \quad (3.27)$$

$$f_{j,k}^{i+1} = \left(1 - \Delta t\delta_f\rho_{j,k}^i\right) f_{j,k}^i + \Delta t\gamma\rho_{j,k}^i\,, \quad (3.28)$$

where, for sake of brevity, we have re-written ρ_c as ρ and, for instance,

$$\begin{aligned} P_0 &= 1 - \frac{4\Delta tK}{\Delta x^2} \\ &\quad + \frac{\Delta t}{4\Delta x^2}\,\frac{s\chi}{(1+sc_{j,k}^i)^2}\left[(c_{j+1,k}^i - c_{j-1,k}^i)^2 + (c_{j,k+1}^i + c_{j,k-1}^i)^2\right] \\ &\quad - \frac{\Delta t}{\Delta x^2}\left[\frac{\chi}{1+sc_{j,k}^i}\left(c_{j+1,k}^i + c_{j-1,k}^i + c_{j,k+1}^i + c_{j,k-1}^i - 4c_{j,k}^i\right)\right. \\ &\qquad \left. + w_f\left(f_{j+1,k}^i + f_{j-1,k}^i + f_{j,k+1}^i + f_{j,k-1}^i - 4f_{j,k}^i\right)\right], \\ P_1 &= \frac{\Delta tK}{\Delta x^2} - \frac{\Delta t}{4\Delta x^2}\left[\frac{\chi}{1+sc_{j,k}^i}(c_{j+1,k}^i - c_{j-1,k}^i) + w_f(f_{j+1,k}^i - f_{j-1,k}^i)\right]. \end{aligned}$$

In particular, if there is no chemical gradient, the situation is isotropic and the probabilities $P_1, \ldots, P_4$ of moving in any direction are equal. Even in this case, the extraction of a random number will decide whether the tip cell will stay still or will move to a particular neighbouring node rather than another. On the other hand, in presence of a chemical gradient the random walk becomes biased, because the cell has a higher probability of moving up the gradients of chemical factors.

The main merit of the discretized set-up is that it allows phenomena like branching and anastomosis, and their dependence on sub-cellular mechanisms, to be more properly described, which is difficult to do using a model based on partial differential equations. With regards to branching, the authors assumed that the density of ECs necessary to allow capillary branching is inversely proportional to the distance from the tumour and proportional to the concentration

of TAF. However, further ramification can only happen a minimal distance from the previous branching point, and, of course, there must be enough space in the discretized grid to allow the formation of a new capillary. This assumption is consistent with the observation that the distance between successive branches along the capillaries decreases as the tumour is approached. This phenomenon is called the *brush border effect* and is well-described by the model and the simulation.

Regarding anastomosis, when a capillary tip meets another capillary during their motion, then they merge to form a loop. If two sprout tips meet, then only one of the original sprouts continues to grow. In the simulation presented, particular attention is given to the importance of branching and anastomosis in order to get a realistic network (see the 3D animation available at the web site www.maths.dundee.ac.uk/šanderso/3d/index.html). Some qualitative properties of the full continuum model focusing on the distribution of tip cells can be found in [15, 246], and logistic growth of cells is included in [74].

Different models were developed by Sleeman and coworkers [210, 211, 247] using a similar approach. In particular, Plank and Sleeman [210] added the effect of a proteolytic enzyme of the ECM (say, MMPs) and of angiostatin, an anti-angiogenic factor, which is assumed to act as an MMP-inhibitor. The protease is produced by ECs stimulated to move by the presence of VEGF. When the density of fibronectin falls below a certain threshold level, the basement membrane has been sufficiently degraded to allow ECs to move into the ECM. They assumed that while VEGF and protease have a chemotactic action, haptotaxis has the effect of attracting cells to regions of low fibronectin concentration, in contrast to the model by Chaplain and Anderson (see Eq.(3.23)).

In [301] Eqs.(3.23–3.25) are modified by introducing a discrete scheme based on a nine-point stencil of the finite difference scheme, and assuming with little biological justification a dependence of vessel motility on the distance from the center of the tumour.

In [211] a circular random walk model is applied to (3.23–3.25) in order to make cell motion independent of the lattice, and the resulting network is compared in detail with that obtained using the cubic lattice. Simulations are also generalized to the model proposed in [210], which mainly focusses on the effect of angiostatin.

3.3.2 Discrete Models in Continuum Field

Similarly to [211], the core of the models described below consists of tracking the trajectory of sprout tips moving as a point mass in a continuum substratum under the influence of a continuum field of chemoattractant. For this reason, such models can be denoted as *discrete-in-continuum models*. For instance, in Sun et al. [256, 257, 258] the capillaries are traced out by the trajectory of the tip cells, which move subject to both chemotaxis and haptotaxis. The evolution of fibronectin is again given by (3.25), whilst, using a different approach to equation (3.24), the chemoattractant is constantly produced outside the capillaries and is absorbed by them, as well as decaying naturally. Specifically, the motion of tip cells is described in [257] by:

$$\mathbf{v} = k(c)\frac{\mathbf{u}}{|\mathbf{u}|}\,, \qquad \text{where} \quad \mathbf{u} = \mathbb{K}(\chi\nabla c + w_f\nabla f)\,, \tag{3.29}$$

where $\mathbb{K}$ is a tensor which accounts for the anisotropy of the extracellular matrix. Branching occurs when sprouts are older than a threshold branching age, under the assumption that new sprouts must mature before being able to branch. In addition, sprouting requires a strong deviation in the direction of the velocity.

As usual, anastomosis occurs when a sprout tip meets another sprout tip or a sprout. After a tip-to-sprout anastomosis, the tip cell forms part of the loop, and will no longer undergo sprouting. On the other hand, tip-to-tip anastomosis might either lead to the disappearance of both tips in the case of a *head-on-head* encounter, or to the survival of one tip cell only in the case of a *shoulder-on-shoulder* encounter. From the simulations, it appears that capillaries tend to fill the space but to avoid anastomosis, probably because when the capillaries approach each other the VEGF field pulls capillary tip cells aside, so that they move along parallel directions.

A similar approach is used by Milde et al. [175], who describe the motion of capillary sprout tips using the following expression:

$$\frac{d\mathbf{v}}{dt} + \lambda \mathbf{v} = \eta \mathbb{K} \left(\frac{\chi}{1 + sc} \nabla c + w_f \nabla f_b \right) , \tag{3.30}$$

rather than (3.29), which can be however obtained in the strongly damped limit. The terms η and $\mathbb{K}$ both depend on the density m of the ECM. In particular, η has a bimodal behaviour (as shown for instance in the experiments in [80, 200], and by the models in [241, 242]) and is given by:

$$\eta(m) = \eta_0 (m_0 + m)(M - m) \qquad \text{with} \quad m_0 < M \, .$$

The tensor $\mathbb{K}$ is given by:

$$\mathbb{K}(m) = (1 - \beta m)\mathbb{I} + \beta m \mathbb{D} \, ,$$

where $\mathbb{D}$ is an orientation tensor that can be related to the microscopic direction of ECM fibres and can be obtained through digital tensor imaging (see [65, 121]).

The last term in (3.30) describes haptotaxis and depends on the density, f_b, of bound fibronectin (which is cleaved by sprout tips that produce MMPs). A distinction is also made between cleaved, soluble, and bound VEGF. Bound VEGF is also cleaved by MMPs, and the soluble and cleaved forms (which could be merged in a single equation) are absorbed by the capillaries. Chemotaxis is caused by all forms.

Branching occurs where the local curvature of the trajectory of tip cells exceeds a threshold level. A sample result of the simulations is displayed in Figure 9.

The three-dimensional model proposed by Das et al. [73] can be divided into two distinct, but communicating, modules: a stochastic and a deterministic one. The former is a lattice model based on Markov processes, where at any time each lattice point can be occupied either by a cell, by ECM, or remain empty. Cells can be quiescent, proliferating, migrating, or apoptotic, and transitions between the states are described by transition probabilities. Transitions to a state of migration or proliferation go through a series of sub-states, the number of which is determined by the persistence time and the progression through the cell-cycle. Apoptotic cells leave the grid site empty.

Every grid site occupied by the ECM is associated with a *field* describing the concentrations of VEGF and MMPs, and with the stiffness of the ECM.

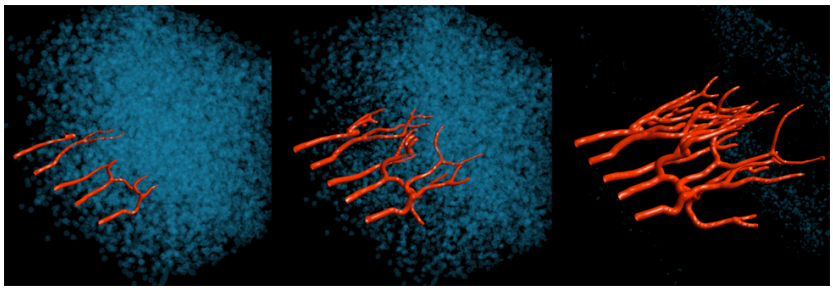

Figure 9: Growth of a capillary network according to the model in [175]. The figure on the right shows only the vascular tree. Figure courtesy of F. Milde and P. Koumoutsakos.

Intercellular communication occurs only via the *field*, and the related local and global concentrations change the cell transition probabilities.

The deterministic component of the model is composed of the advection-reaction-diffusion equations that govern the evolution of VEGF (in its soluble, ECM-bound, and receptor-bound forms), MMPs, matrix-binding sites available for binding to MMPs, and cleaved matrix. In contrast to previous models, this model also includes transport of both soluble VEGF and MMPs by the interstitial fluid. However, this contribution is then neglected in the simulations.

The authors also employ a further set of rules for cell evolution, which include:

1. The direction of cell migration is stochastic and biased towards the lattice point occupied by the ECM with the highest concentration of chemoattractants and MMP;

2. A cell can only migrate into a lattice position occupied by ECM, but can divide into either empty space or ECM;

3. Cells are allowed to divide both at the cell monolayer where sprouts stem from and in the stalks of the capillaries;

4. After division, the daughter cells occupy the ECM lattice position with the highest concentration of MMP, since it causes local degradation of ECM;

5. A migrating or dividing cell releases MMPs into all the adjacent elements with an amount that depends on the state of the cell itself;

6. VEGF is both released and consumed by the cells according to their state.

In all simulations, cells are initially seeded as a monolayer and a VEGF gradient is established. New sprouts are allowed to be initiated for the first 4 hours only, to mimick the fact that when the first sprouts appear, they inhibit further sprouting nearby.

In the extreme scenario when almost all of the cells are in a state of migration, many individuals are seen to protrude far into the ECM. In the opposite scenario when most of the cells are proliferating, the entire monolayer starts to expand and forms large clusters. Furthermore, it is observed that sprout formation is

inhibited when the probability of cells remaining in the quiescent state is higher. However, several branches develop in all the intermediate cases. It is interesting that the length of the growing sprouts is positively correlated to a decrease in the proliferation rate of the ECs and/or to an increment in the probabilities that they remain quiescent or migrate. In these cases, fewer sprouts are initiated, but they grow longer. On the contrary, a higher rate of cell mitosis gives rise to network-like short capillary structures.

Another set of simulations indicates that the formation of a large number of continuous sprouts requires a balance between migration and quiescence, which can be interpreted as a balance between effective capillary induction and stabilization. Moreover, the model predicts that the ratio between proliferation and quiescence should be increased in order to increase the number of continuous sprouts when compared with isolated migrating cells. Finally, the authors indicate the range of probabilities within which the formation of branched sprouts occurs, and they demonstrate, in close comparison with experimental assays, the crucial role played by the VEGF machinery in new vessel formation.

Other developments, targeted at better numerical implementations and visualization techniques, can be found in references [149, 150, 223, 224, 265, 266, 287], in which very realistic vascular structures are presented. In particular, [149, 223] focus on angiogenesis in skeletal muscles.

3.3.3 Corneal and Retinal Angiogenesis

The cornea is particularly suited to visualize the processes of formation of vascular networks, since it is transparent and initially avascular. In addition, it is particularly easy to implant a fragment of a solid tumour or a polymer bead containing TAF, and to observe vessel sprouting from the nearby limbal vessels. Indeed, Balding and McElwain [22] mentioned above took inspiration for their model from experiments performed on the cornea.

Harrington et al. [117] proposed a contiuum-based discrete model of corneal angiogenesis, which is a development of a previous model by Tong et al. [272]. Their model is characterized by the diffusion and uptake of both a tumour angiogenic factor and an inhibitor. Proliferation of the ECs forming the capillaries is possible if the concentration of TAF is above a given threshold and the concentration of inhibitor is below another threshold. The evolution of the capillaries is described at a discrete level, with rules determining the direction of vessel growth; this is influenced by the previous capillary direction and by the concentration gradients of the tumour angiogenic factor and the inhibitory factor. Sprouting of vessels from the limbal vessel, and branching, also depend on the concentrations of the growth factors. However, little branching occurs and vessels tend to merge while progressing toward the source of TAF.

Jackson and Zheng [129] also propose a model for corneal angiogenesis, in which a system of PDEs governs the evolution of VEGF, Angiopoietin-1 and -2, and EC mass and maturation. The discrete aspect of the model is that each individual EC is located in a point of discretized space, and is assigned a time-dependent cell mass and a maturity level. A sprout is then formed of an array of discrete points. The shape of the sprout is also influenced by the distribution and alignment of ECM fibres.

Retinal angiogenesis also received some attention in the early years of angiogensis modelling, in particular the RD approach proposed by Maggelakis

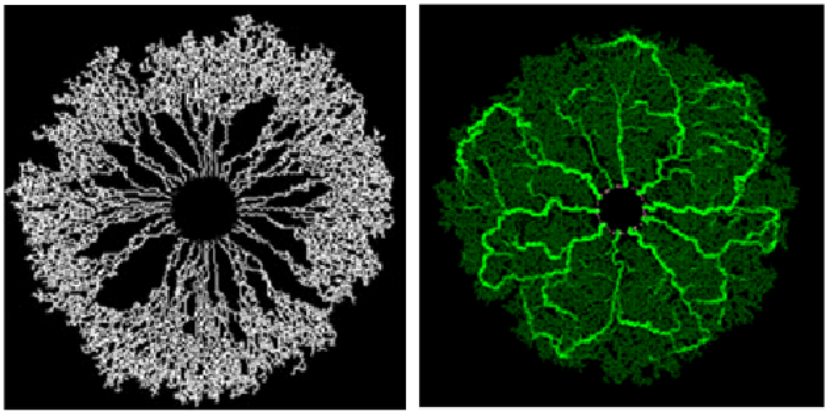

Figure 10: Retinal angiogenesis as described in ref. [169, 290]. On the left the vessel structure and on the right the dimensions of the vessel radii after remodelling. Figure courtesy of M. Chaplain.

and Savakis [157, 158]. In general, the models aim to show possible causes of pathological angiogenesis in the retina that can impair vision and even lead to blindness in some cases. This pathology, for instance, may affect diabetic people and premature children, who are prone to be affected by proliferative retinopathy.

More recently, Aubert et al. [20] focussed on the *ab initio* development of the retinal vascular plexus (see references [100, 104] for a review of the process), and they deduced a continuum model very similar to that proposed by Gaffney et al. [102] for wound healing, with an additional chemotactic contribution to the *snail-trail* term (3.15).

In the same article, a further extension of the model is proposed to account for the presence of astrocytes and PDGF-A. Astrocytes emerge from the optic nerve region before the formation of the vascular plexus, and start migrating across the inner surface of the retina under the chemotactic action of PDGF-A. The coupling of the dynamics of the astrocytes and of the capillary tip cells occurs through the assumption that the production of VEGF is proportional to the density of astrocytes.

As already discussed in Section 3.2.2, the continuum model above is unable to generate vascular networks. However, a more realistic discretized (or discrete-continuum) model is presented in [169, 290] (see Figure 10). It employs the procedure explained in Section 3.3.1 to account for the effect of PDGF-A and astrocytes, and it includes the following additional features:

- A haptotactic term due to the action of a protein bound to the underlying plexus of retinal ganglion cells, which form at an earlier stage of development;
- The activity of matrix degrading enzymes produced by astrocyte and endothelial tip cells, that reduce the local concentration of two different matrix-bound proteins secreted by astrocytes themselves.

Using the models describing blood flow through vascular networks and vessel remodelling that will be discussed in Section 3.5 (see, for instance, [166, 167,

252, 253]), they also studied the subsequent adaptation of the vascular network in response to blood flow.

Capasso and coauthors [54, 55] instead use a family of stochastic processes to describe the cells forming the vessel network. The network of vessels is modelled as the union of the trajectories traced out by tip cells, which evolve according to a system of Langevin-like stochastic differential equations. Branching is modelled by the birth of new tip cells according to a stochastic point process. Both the stochastic differential equations and the branching process are coupled with RD equations describing the evolution of the underlying relevant chemical fields, such as nutrients and tumor angiogenic factors. As the authors clearly state, their main aim is not to propose a new model, but to investigate the role of randomness and the relationship between the different qualitative behaviours obtained by using the fully stochastic model, the deterministic continuum model (that can obtained though suitable limiting procedures), and the hybrid model (in which the parameters of the stochastic model are dependent on the deterministic approximation of the underlying fields (parameter homogenization)). The outcomes can be summarized as:

1. The continuum model cannot capture the vascular structure at all;

2. The hybrid model may lead to realistic vascular structures only if parameter homogenization is applied after a sufficiently large time, so that the laws of large numbers are applicable.

In more detail, three different cell types are considered in [55]: mural cells, type-2 cells and dead cells. Mural cells are mature cells that supply a protein which, as we shall see below, affects the motion of tip cells (the authors call this protein a nutrient). When the concentration of these cells is low, they duplicate and generate type-2 cells. The mural cells barely move and may die. Type-2 cells are either tip cells or stalk cells in the neighbourhood of tip cells. They can proliferate and die. In addition to Brownian motion, their movement is regulated by repulsive chemotaxis with respect to the motility protein produced by mural cells, and attractive chemotaxis with respect to VEGF. When the concentration of type-2 cells is high, they convert themselves into mural cells.

3.4 Cell-Based Models of Angiogenesis

The first CPM for tumour-induced angiogenesis was developed by Bauer et al. [25]. As in other CPMs (see Section 2.3), the basic Hamiltonian is formed by three terms that regulate, respectively, the shape of all cell types (see Eq. (4.4)), the mutual adhesive interactions (see Eq. (4.3)), and the chemotactic movement of the activated ECs (see Eq. (4.5), in this case without contact inhibition and saturation, i.e. $s = 0$).

With respect to vasculogenesis models, however, angiogenesis models require cell duplication, so when the parental EC doubles its volume (which is possible since the Potts coefficient λ^{area} is set very low) and has gone through a defined time span (corresponding to the duration of the cell cycle), it undergoes mitosis. Then the authors differentiate between tip and stalk ECs, and only the latter are allowed to proliferate.

The tumour-secreted pro-angiogenic factor is assumed to diffuse throughout the stroma, where it decays and is taken up by ECs. The morphogen satisfies a

partial differential equation of type (4.17), where $B(c) = \min\{c, c_{max}\}$ is again limited by a threshold value and S is the constant amount of chemical supplied at the boundary of the domain where the tumour is supposed to be localized. Simulations start with the tumour and a single EC on opposite sides of the domain. The space in-between represents the stroma and is composed of ECM fibers, (almost fixed) tissue specific cells and generic interstitial fluid, and is penetrated by the vascular sprouts.

The model is extended in [26] to highlight the effect of ECM topography on vascular morphogenesis and the mechanisms that control cell shape and orientation, sprout extension speeds, and sprout morphology. It is found that both the ECM density and the connectivity and orientation of the fibre network influence the speed and morphology of sprout extension. The density and heterogeneity of the ECM fibres also affect capillary branching. The model predicts an optimal density for capillary network formation and shows that maximal sprout extension speeds are achieved within a density range similar to the density of collagen found in the cornea.

The authors also evaluate the effects of MMPs produced by the tip cell on the velocity of the sprouts, and demonstrate that degradation promotes sprouting at high densities, but has an inhibitory effect at lower densities.

A cellular Potts model, with very similar inputs to the one above for the Hamiltonian and the diffusion equation for VEGF, is at the basis of a parallel-computational search for novel potential anti-angiogenic strategies for anti-cancer therapies, as presented in [159]. However, in this case, the Hamiltonian also accounts for haptotaxis through an energetic contribution analogous to the classical linear chemotactic term (4.4):

$$\Delta H_{haptotaxis} = -\mu^{hapto}(m(\mathbf{x}_{target}) - m(\mathbf{x}_{source}))\,, \tag{3.31}$$

where m is the local level of matrix proteins. The gradient is created by the fact that, as they migrate, tip ECs cleave ECM in their surroundings at a constant rate (as in Anderson and Chaplain's model [14]). Eventually, when the quantity of proteins within a fibre drops below a given threshold, the fibre disappears.

As a biologically relevant outcome of the model, the authors evaluate the level of oxygen in the tissue and, in particular, within the tumour mass. The oxygen profile is described by an RD equation similar to (4.17), where the term B now measures the absorption of oxygen by the tumour cells. This absorption is limited to a maximum rate, which is realistic since the capacity of the cells to absorb oxygen saturates at a limit value determined by the maximum rate of reaction on their membranes. The term S accounts for the amount of oxygen secreted only by the sprouts that form loops, since only such vessels will be capable of maturing and carrying blood flow.

The resulting simulations display emergent processes such as the growth and development of single sprouts, and their subsequent anastomosis. Moreover, parallel-computational implementations, which cover a large range of parameter values, allow the Pareto-optimal anti-angiogenic strategy to be identified, which results in a reduction in the amount of oxygen supplied to the tumour mass of approximately 50%. In particular, possible strategies include:

- The disruption of the machinery of the angiogenic factor;
- The inhibition of the ability of the ECs to degrade ECM components;

- Inducing an increase in adhesiveness between the ECs themselves and the stromal cells.

Interestingly, the authors also quantify the cost of each biomedical strategy, starting with the following assumptions:

1. Currently available treatments have a low cost;
2. Treatments with the potential to become available in the foreseeable future have a medium cost;
3. Treatments that are forecast to be difficult to develop with current technologies have a high cost.

In the review article [72], the authors examine the critical features of some of the CPMs described above. Firstly, they discuss these assumptions made in the angiogenic models presented in [25, 159]:

1. The stalk cells are only passively dragged by the motile tip individuals;
2. The overall structure is stabilized by intercellular adhesive interactions.

They argue that these assumptions could not account for full multicellular sprouting. In fact, such a structure, which is stabilized by surface tension only, would be prone to Plateau-Rayleigh instability, eventually resulting in its break-up. In order to overcome this issue, the authors suggest that both tip and stalk cells should be allowed to actively migrate in response to gradients of external growth factor. The same review also contests that the CPMs, which reproduce *in vitro* vessel-sprouting from spheroids of ECs based on the activity of an autocrine chemoattractant (i.e. [171, 173]), require further assumptions to allow an aggregation of cells to establish a branched structure. Gradients in the concentration of chemoattractant induce an instability in the surface of the overall colony, which results in the initial extension of sprouts. However, it is the finite compressibility of the cells between such primary branches (i.e. their ability to resist compression) that provokes the outer individuals to migrate further. The authors also argue that the proposed autocrine morphogens (i.e. VEGF isoforms) are unlikely to be the effective regulator of the spouting process, and are rather simply a contributing factor. According to the authors, the concentration of the autocrine VEGF molecules is too small when compared with the amount already present in the ECM microenvironment. Finally, they emphasise that the patterns produced in the standard chemotactic models of vasculogenesis arise from a gradual coarsening of short, dispersed EC segments, rather than from a real sprouting mechanism, i.e. the extension of long EC segments.

In reference [263], the same group extends the model proposed in [262] to demonstrate that longer multicellular sprouts cannot be fully explained by the sole presence of a preferential cell-cell adhesion, but require both the differentiation of a single tip cell and an active polarization-dependent motility of stalk cells. In their previous approach, the motion of cells is mainly governed by surface-adhesive energies, both isotropic and asymmetric. This results in the following features:

- The movement of the sprout edge is not sufficiently persistent;
- The bodies of the previously formed sprouts move sideways;

- The speed of expansion diminishes over time.

The authors employ the same Hamiltonian functional, but with an additional two terms included in the asymmetric correction of the Boltzmann probability (2.44). These terms implement the effect of the polarization of a cell, both on its self-protrusion and on its membrane dynamics. The first term writes:

$$W_2(\sigma(\mathbf{x}_{source}) \to \sigma(\mathbf{x}_{target})) = \lambda^{pol} \sum_{\sigma} \frac{\mathbf{p}_\sigma}{|\mathbf{p}_\sigma|} \cdot (\mathbf{x}_{target} - \mathbf{x}_{source}), \tag{3.32}$$

where λ^{pol} is the Potts parameter describing the relative importance of the directional component in cell migration, and $\mathbf{p}_\sigma$ is the polarity vector of the individual σ, which is updated as follows (by considering spontaneous decay and reinforcement due to displacement):

$$\Delta\mathbf{p}_\sigma = -\frac{\mathbf{p}_\sigma}{\tau_\sigma} + \Delta\mathbf{x}_\sigma^{CM}. \tag{3.33}$$

Here τ_σ is a characteristic memory length of the polarization vector, and $\Delta\mathbf{x}_\sigma^{CM}$ is the displacement of the centre of mass of the cell due to the proposed spin update. The second term dealing with membrane dynamics is based on the assumption that membrane dynamics in a polarized cell are more pronounced at the leading edge, and inhibited at the sides and trailing surfaces.

It is useful to note that, in this model, the authors establish a feedback loop involving the explicit polarization of the ECs and their movement, whereas in references [237, 238], the elongation of a vascular individual is the result of the remodelling of their cytosolic region in response to a chemotactic-induced migration (facilitated by the stiffness of the nucleus), which directly affects their velocity through the persistence term in (4.14).

In [263], all the model simulations start with a compact aggregation of cells, in which a leader tip cell is distinguished by a higher value of T_σ. The other parameter values are the same for both the leader and the stalk individuals. Specific sets of realizations show that only the full model yields sprouting dynamics comparable to experimental observations. The tip cell pulls the initially passive stalk individuals, and forms a primary branch. The stalk cells then become elongated and attract further individuals, allowing the growing sprout to stabilize and to further elongate. The persistence time of the leading cell determines the shape of the sprout and the speed of elongation. The absence of a differentiated leader cell results instead in the formation of transient sprouts consisting of elongated stalk cells, whose shape is completely determined by the values of the intercellular adhesion parameters. On the contrary, the activity of tip cells is unable to sustain continuous cell recruitment to the sprout by isotropic cell-cell adhesion alone.

Another cellular automaton model was proposed by Markus et al. [165], who focused more on the mechanisms underlying isotropic morphogenesis, including dichotomous and lateral branching, blind vessel ends, and closed loops due to anastosmosis, lateral inhibition of an autocatalytic morphogen, as well as a genetic switch that differentiates tissue into substrate-depleting vessels.

Addison-Smith et al. [3] focus on a different issue related to tumour-induced angiogenesis, namely the mechanisms of sprout formation. In the previous models, the initial site of the sprout on the existing capillary was either given *a priori*

or determined stochastically. In [3], the authors have developed instead a simple mathematical model to determine the probable locations of sprouts and the relative distance between them.

In [30], a hierarchical agent-based model analyzes the role played by the notch-mediated selection of tip cells in the early stage of angiogenesis, i.e. when an immature network of sprouts develops from an existing vessel. In particular, the authors study the feedback loop that links VEGF-A tip cell induction with delta-like 4 (Dll4)/notch-mediated lateral inhibition. They identify VEGF-A concentration, VEGF-A gradients and filopodia extension as further critical parameters in determining the robustness of tip/stalk patterning (also called *salt-and-pepper patterning*).

The model domain is a 3D grid, which is initiated with a single hollow, cylindrical capillary. This parent vessel is comprised of several ECs, described by a given set of lattice sites. There is one cell per vessel cross section, with no auto-cellular junction.

The model simulations show that gradients in VEGF affect the selection rate of EC agents. In a uniform VEGF field, curled filopodia grow in random directions, whereas in the presence of a linear VEGF gradient, they are long and well-directed. The overall VEGF concentration is observed to affect the number of tip cells. A low level of VEGF is not sufficient to induce differentiation of tip individuals, whereas an intermediate level is able to generate the classic salt-and-pepper pattern. Higher levels of VEGF eventually result in a synchronous oscillation, when the ECs are all either tip or stalk at the same time. Normal patterning can be also obtained when the expression level of Dll4 lies within a specific range. When Dll4 is under-expressed, i.e. there is little lateral inhibition, this gives rise to an excess number of tip cells, whereas, when Dll4 is over-expressed, abnormal oscillations occur. Finally, the authors use a phase-plane analysis to establish the relationship between the three selected system behaviours, i.e. no response, no tip cell inhibition, and normal salt-and-pepper.

3.5 Vessel Remodelling

The natural evolution of angiogenesis models similar to that proposed in [60] was to include blood flow in the capillary network, the consequent vessel remodelling [166, 167, 252, 253], and also the recruitment of pericytes [168] that lead to vessel maturation. One of the main aims of these developments is to use the outcome of the vascular network model to study drug perfusion. For instance, it is found that a rather irregular and highly connected network leads to poor blood flow to a tumour, and therefore poor drug delivery.

In these models, the capillary network is treated as a series of small straight tubes in which blood flows according to fully developed Poiseuille flow. The flow, Q, in each capillary is related to the pressure drop, ΔP, between the ends of the tube by the classical expression:

$$Q = \frac{\pi R^4 \Delta P}{8 \mu_{app} L} \,, \tag{3.34}$$

where R and L are respectively the radius and the length of the capillary branch, and μ_{app} is the apparent (or effective) blood viscosity. In fact, as is well known, blood is a complex biphasic mixture of cells and plasma, and certainly possesses

viscoelastic characteristics. The overall impact of the different constituents on the mechanical properties of the blood as a whole depends on the width of the capillary in a very complex manner. Pries and Secomb [216] attempted to resolve the complexity of this problem by proposing the following experimental fit for the apparent (or effective) viscosity of blood:

$$\mu_{app}(R, H_D) = \mu_{plasma}\left[1 + (\mu_{0.45}(R) - 1) f(H_D) g(R)\right] g(R)\,, \tag{3.35}$$

where H_D is the discharge hematocrit (normally $H_D = 0.45$) and

$$f(H_D) = \frac{(1 - H_D)^n - 1}{(1 - 0.45)^n - 1}\,, \tag{3.36}$$

$$g(R) = \left(\frac{2R}{2R - 1.1}\right)^2\,, \tag{3.37}$$

$$\mu_{0.45} = 3.2 + 6e^{-0.17R} - 2.44e^{-0.06(2R)^{0.0645}}\,, \tag{3.38}$$

$$n = \left(0.8 + e^{-0.15R}\right)\left(\frac{1}{1 + 10^{-11}(2R)^{12}} - 1\right) + \frac{1}{1 + 10^{-11}(2R)^{12}} \tag{3.39}$$

Kirchhoff's law then holds at the capillary junctions to describe the mass distribution.

The model developed by Pries and Secomb [217, 218, 220, 221] for vessel adaptation and remodelling is the following:

$$\frac{1}{R}\frac{dR}{dt} = \log(\tau_w(Q) + \tau_{ref}) - k_p \log \tau_e(P) + k_m \log\left(\frac{Q_{ref}}{Q H_D} + 1\right) - k_s\,, \tag{3.40}$$

where the first logarithmic term reflects the effect of wall shear stress evaluated as:

$$\tau_w = \frac{4\mu_{app}|Q|}{\pi R^3}\,, \tag{3.41}$$

A small constant τ_{ref} is included in the argument of the logarithm to avoid singularities at low shear rates. The second term includes the effect of intravascular pressure (measured in millimetres of mercury):

$$\tau_e(P) = 100 - 86\exp\left\{-5000[\log(\log P)]^{5.4}\right\}\,. \tag{3.42}$$

The third term refers to the effect of metabolic hematocrit, and the last to the natural tendency of capillaries to shrink.

The final remodelled tumor-induced vasculature is used in [166, 167, 253] (see also [62] for a review) to assess the efficacy of the network to deliver a continuously infused drug or a bolus. It is found that only a small fraction of the injected drug reaches the tumour surface because it flows through the highly conductive dilated backbone, largely by-passing the tumour and recirculating back to the parent vessel. This results supports the idea that a nomalisation of the vascular network is necessary to optimise drug delivery as proposed by Jain and coworkers [109, 130, 131].

Recently, in references [215, 219, 222], Pries and coworkers focused on the problem caused by functional shunts. For two different vessels connecting the same two points of a vascular network, the shorter vessel is subject to higher shear stresses because the pressure differences between the ends of the vessels

are identical, but its length is shorter (assuming that the diameter of the two vessels is initially the same). Therefore, the shorter vessel is stimulated to increase its size and flow. The consequence of this mechanism is that longer pathways are bypassed, since they progressively bring less flow, so that they might be pruned eventually. From this observation, the authors conclude that there must be a signalling process that communicates upstream the status of the downstream vascular network. This might be provided by conducted responses that travel upstream via gap junctions along the walls of microvessels. They suggest conexin as a possible candidate, and hypothesize that the lack of such communication mechanisms might explain observed vascular pathologies (for instance, in tumour-related angiogenesis), leading to abnormal flows and increased heterogeneity in the distribution of oxygen.

This hypothesis has been included in a very recent article by Watson et al. [290], discussed in Section 2.3.3, which, however, deals with retinal angiogenesis. It would be very interesting to extend its application to tumour-induced vascular networks, since as already dissed above one of the results deduced in [166, 167, 253] is that drug infusion is inefficient due to the formation of shunts which by-pass the tumour.

Finally, for completeness, we mention that the modelling approach presented above has also been applied to wound healing by Machado et al. [152].

Intussusception is another mechanism of vessel remodelling, and occurs as a result of internal division of the vessel lumen. Although recognized as an important mechanism of vessel remodelling, intussusception has received much less attention than sprouting angiogenesis.

Szczerba and Székely [264, 267] developed a model that couples flow and vessel remodelling of a pre-existing capillary interstitium. The flow is described by Stokes flow and the vessel walls are discretized into cell-like elements. Discrete elements are then eliminated from the vessel lumen if the shear stress due to blood flow is above a given threshold, and added if it is below another threshold. Under these rules, the two capillary walls evolve to form pillars in regions of low shear stress, and move away in regions of high shear stress. This gives rise to capillary beds with a small characteristic size (determined by the size of the network elements), which only look realistic when compared to tissues that require substantial oxygenation.

In their original version of the model [264], the authors could not avoid artificial artero-venous anastomosis and the formation of shunts, which is consistent with the observations in the articles by Pries and Secomb [215, 219, 222]. In order to overcome this problem, the computational model was extended in [268] to include molecular signals affecting remodelling, and then further in [267], to consider the structural maturation of the vessel wall, in addition to control by stimulating or inhibiting chemical factors.

3.6 Coupling Angiogenesis and Tumour Growth

One of the first attempts (which nowadays can be considered naive) to couple the dynamics of angiogenesis to tumour growth can be found in [29, 76], where a free-boundary value problem was proposed to describe the evolution of angiogenic factors, capillary density, live tumour cells, dead tumour cells and nutrients. Growth inhibitory factors were also considered, but were not included in the simulations. The model was able to predict the formation of a necrotic

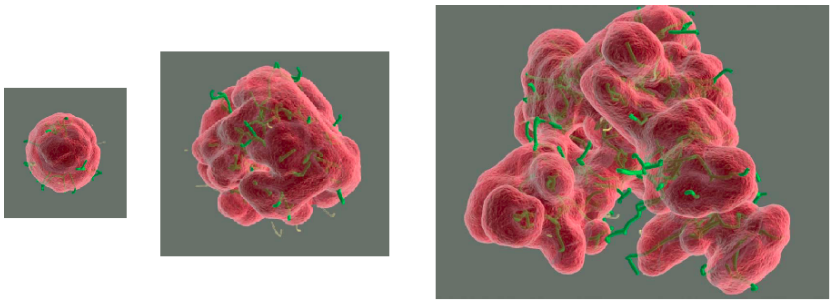

Figure 11: Angiogenesis coupled to a tumour growth model as modelled in ref. [96, 154, 302]. Figure courtesy of J. Lowengrub and P. Macklin.

region in the core of the tumour, a proliferating rim at the tumour surface and a quiescent region in the middle. It also predicted the angiogenesis process, with the proliferation of capillaries just outside the tumour surface and the penetration of capillary sprouts into the periphery of the tumour. The action of anti-angiogenic factors was also considered, which lead to the regression of the capillary network and eventually to the regression of the tumour size. However, this one-dimensional simulation could not account for the branching structure of the capillary network and the heterogeneous tumour growth along the network. Recently, Hogea and coworkers [122] applied a level-set method to perform a two-dimensional simulation for different spatial distributions of pre-existing capillaries, with the same morphological problem that also characterizes the other continuum models for wound healing described in Section 2.2.1.

Still starting from the tumour growth model proposed in [29, 76], a convected element method is used in Pindera et al. [209] to get more realistic vasculatures. The method consists of superimposing two domains: a base domain associated with the solid tumour and the surrounding host tissue, and a vasculature domain that is discretized by a 1D grid that evolves in a Lagrangian manner prescribed by the convected element method. The two separate domains communicate with each another through suitable source and sink terms. Vessel growth is described by a model based on that proposed by Levine et al. [145, 146]. Blood flow in the vessel network is also included, which delivers nutrients to the tumour and the surrounding tissue.

In articles [96, 154, 302], the discretized approach described in Section 2.3 was successfully coupled to a tumour growth model previously developed by Cristini et al. [70] (see also [69]). This approach has subsequently been applied to tumour cell invasion [97] and to the vascular growth of gliomas [28]. An example of the simulation results is shown in Figure 11.

The authors in [153] showed that the module describing tumour growth is characterized by a gross morphological instability. Depending on the microenvironmental conditions, this instability can lead to tumour invasion via individual cells, cell chains, strands, or detached clusters infiltrating into adjacent tissue; this produces the typical morphological patterns seen in the histopathology of different cancers. However, this intrinsic feature of the tumour growth model is strongly modified by the coupling to the vascular network, which continually remodels.

With regards to the local coupling between tumour and vessel growth, it

is found (in agreement with clinical observations) that the stress generated by massive cell duplication may shut down blood vessels. In fact, this is particularly important when the blood vessels are still immature, a feature which has not yet been considered in the model. This phenomenon will, of course, dramatically affect the flow, and will result in the formation of hypoxic regions and the instigation of the angiogenesis process.

It is also found that degradation of the ECM by tumour cells has a large effect on the development of the vascular network. For instance, when the degradation of ECM is strong, the newly formed vessels tend to encapsulate, rather than penetrate, the tumour. This has the benefit that the vessels are less effective in delivering nutrients to the tumour. However, from a therapeutic point of view, it means that it is more difficult for chemotherapeutic drugs to reach the core of the tumour mass and, in particular, the hypoxic regions that are difficult to target with radiotherapy.

With the same aim of coupling angiogenesis and tumour growth, Alarcon and co-workers [4, 5, 6, 7, 8, 41, 51, 199] used a cellular automata model. The model retains hybrid characteristics, since nutrients and chemical factors, mainly VEGF, evolve according to RD equations, which are suitably discretized using a finite difference scheme. Sub-cellular models of the cell cycle govern cell proliferation and apoptosis through the activation of p53. The underlying vasculature permeating the tissue has a hexagonal structure. Initially, the tissue contains some tumour cells that grow and develop into a vascularized tumour mass. Vascular network remodelling (without changing the structure of the network due to the sprouting of new vessels) is considered in [7, 51], where the size of the capillaries is adjusted in time according to the rules proposed by Pries and Secomb (defined in Eq. (3.40)). Following the ideas in [109, 130, 131], the model is further developed in [7] to focus on the normalisation of vessel networks, with a view to the optimisation of drug delivery. In [199], the vessel network evolves via the sprouting of tip cells (with a probability that increases with the local VEGF concentration), the formation of new capillary loops due to anastomosis, and pruning of vessel segments with low wall shear stress.

Perfahl et al. [206] extended the model proposed by Owen et al. [199] to three spatial dimensions. Each lattice site can be occupied by several cells that move according to a reinforced random walk. The ensemble of cells is superimposed onto a vascular network consisting of vessel segments connecting adjacent nodes on the lattice. They used an experimentally derived vascular network for their initial conditions, and tried to predict the outcome of the *in vivo* experiment. Nutrients and chemical factors perfuse in and out of the network. The vessel network evolves again via sprouting, anastomosis and pruning. An example of the simulation results is shown in Figure 12.

Gevertz and Torquato, [105], study angiogenesis and vascular growth of glioblastoma using a cellular automata model based on a Voronoi tessellation. Tumour cells are divided into proliferative cells, non-proliferative/hypoxic cells, and necrotic cells. The tissue is provided with a capillary network with a heterogeneous distribution based on an underlying triangular sub-structure (similar to references [292, 293, 294], which will be discussed below). The network is heterogeneous, in the sense that not all sides of the homogeneous triangular mesh are occupied by vessels. The network then evolves, with new sides of the triangular mesh being activated according to the production and diffusion of VEGF, Ang-1 and Ang-2, and according to the presence of the related receptors, VEGFr and

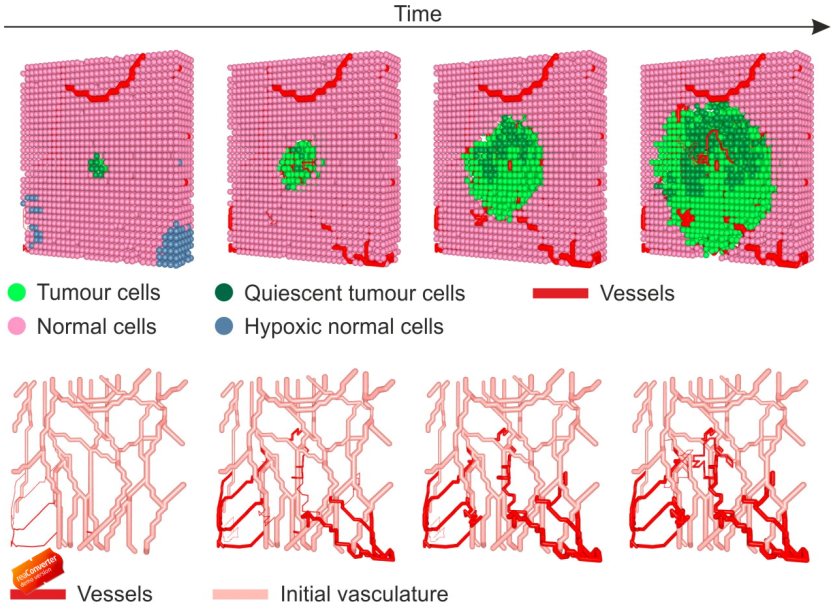

Figure 12: Angiogenesis model coupled to a tumour growth model as simulated in ref. [206]. Figure courtesy of H. Perfahl.

Tie-2.

The cellular automaton models proposed by Rieger and coworkers [24, 143, 292, 293, 294, 295] focus on the interaction between tumour cells, capillaries, and blood flow. With regards to the vessels, each site occupied by a vessel is characterized by its radius, its blood flow rate (if the element is part of a loop through which blood can flow), and its wall shear stress. As already seen in the previous section, these characteristics determine vessel remodelling, through dilation, regression, pruning and sprouting. An important characteristic of the tumour cell modelling is the time spent in an under-oxygenated state. In addition, excessive pressure from the tumour cells can cause vessel collapse.

They also incorporate vessel dilation within the tumour related to a change in the vascularization program based on the observations by Erber et al. [83]. In [83], it is suggested that the vascular patterning program is influenced by ephrin and ephrin receptors (EphB4/ephrinB2) which act as inhibitors of vessel branching and switch the vascularization program from sprouting angiogenesis to circumferential vessel growth (independent from the shear-induced dilation mentioned above). As a result, the radius of vessels (which were originally capillaries) within the tumour can increase up to three times. Since blood flow increases with the fourth power of the capillary radius, this has drastic consequences for the blood flow patterns within the tumor.

More in detail, in [24], the authors employ a hybrid probabilistic cellular automaton model to describe the transformation of a regular vasculature into a highly heterogeneous tumour capillary network. The model is defined on a square lattice (which is then extended into three dimensions in ref. [143]), where each site may be empty or occupied by a single tumour cell and/or by a vessel segment, characterized by a specific radius, blood flow rate, and shear stress.

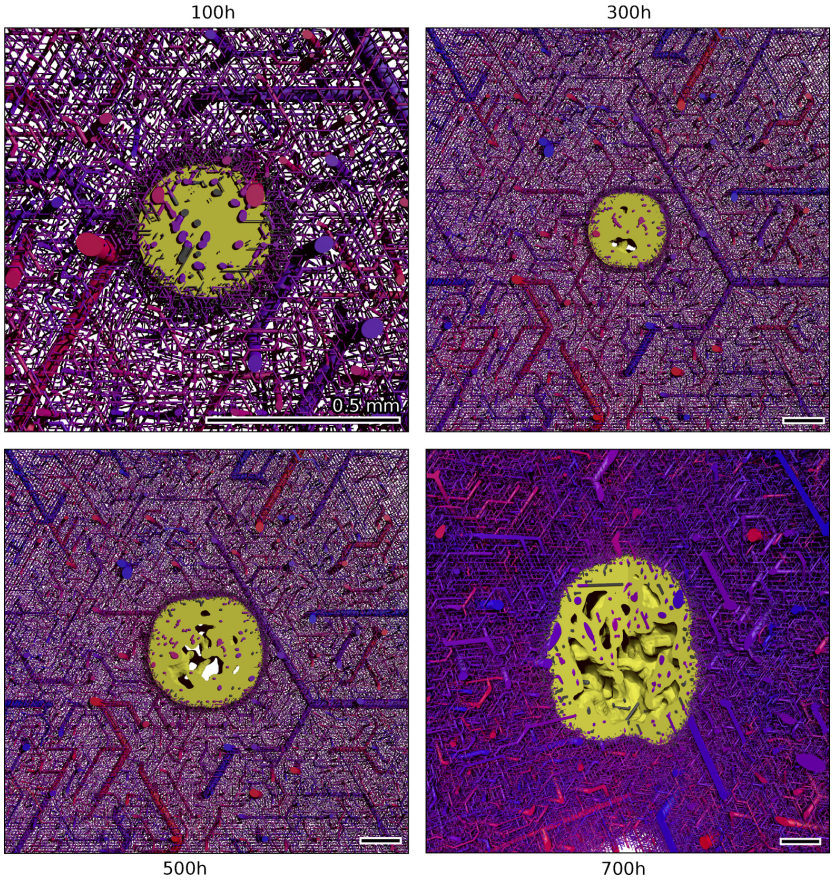

Figure 13: Snapshots from the simulation of a growing tumor at time 100, 300, 500 and 700 h. The first three pictures show 400 μm thick slices through the origin. The scale bar represents 0.5 mm at all times. The first figure is a close-up, illustrating the fine-structure of the arterio-venous initial network. The figure for the last time (700 h) shows a 3D view where the quarter of the virtual camera is cut out. The yellow region indicates the viable tumor mass and void spaces within the tumor are necrotic regions. The network is color-coded by blood pressure: red represents high pressure (arteries) and blue represents low pressure (veins). Figure courtesy of H. Rieger (see [143, 294, 295]).

The tumour and the vasculature evolve in separate layers, i.e. vessel elements can occupy sites where malignant cells are also present. Each lattice site also contains several microenvironmental variables, e.g. the oxygen transported by the vasculature and the pro-angiogenic growth factors synthesized by the malignant cells. The production of angiogenic factors is described by a function linearly decreasing in space, which approximates the exponentially decaying Green's function characteristic of diffusion problems with a point-source and a spatially constant decay rate.

As already observed in Section 2.5, the shear stress exerted by the blood flow upon the vessel walls is the principal stimulus for ECs. In particular, if the emerging vessels are approximated by cylindrical tubes of a given radius, the blood flow is determined by the pressure drop between the end points of each vascular segment, according to the Poiseuille law given by Eq. (3.34). The boundary conditions for the pressure are defined so as to obtain a homogeneous flow distribution in the vessels of the original regular network.

A tumour cell can proliferate only if it has at least one free neighbouring site and if it senses a sufficient concentration of oxygen. The probability of duplication depends on a pre-determined mitotic time. On the other hand, malignant individuals undergo apoptosis with probability 1/2, only if their oxygen concentration is below a given threshold for a sufficiently long time.

New vascular segments can be introduced between two circulated vessels only if:

1. The local amount of TAF is above a certain level;
2. No site in the migration path is occupied by tumour cells;
3. No neighbouring site of the migration path is occupied by other vessels;
4. The distance between the two parent segments is low enough.

If all the conditions above are satisfied, a new segment is added with a probability established by an estimated EC proliferation time. With the same probability, a vessel segment, surrounded by tumour cells and with a TAF concentration sufficiently large, may also increase its radius up to a maximum. A circulated capillary, which is surrounded by the tumour, collapses with a defined probability if the wall shear stress falls below a critical value, whereas a vessel segment, which is under-oxygenated and not circulated, is eliminated with probability equal to 1/2. The overall system evolves in time following a Monte Carlo algorithm. The microscopic variables are updated after each update in the configuration of the discrete elements (i.e. the tumour and the vasculature).

The resulting simulations are initialised with a regular mesh of vessels with a small tumour mass in the centre, and describe a compartmentalization of the tumour cluster into several regions (i.e. necrotic, quiescent, proliferating), which also differ in vessel density and diameter. The model also predicts that microvascular density does not necessarily determine the dynamics of tumour progression, which is instead influenced by the topology of the *original* network as well as by the metabolic demand of the individual tumour cells. In particular, the 3D realization performed in [143] shows that vessel collapse leads to a correlated percolation process, that is driven towards criticality by the mechanism of hydrodynamic vessel stabilization.

In [292], the same research group extends the above model, employing a 2D triangular lattice. They include the following additional effects:

- Oxygen sources are calculated implicitly (driven by concentration gradients between blood and tissue);
- Modifications are made to the rules for vessel collapse;
- The insertion of completely new perfused vessels is accounted for.

This extended approach also considers the effective viscosity of blood as described in Section 2.5.

One of the interesting outcomes of the model is the analysis of the time-evolution of the distribution of a drug, which has been injected into the blood stream, within the tumour mass, and the results are compared with those obtained from a model containing only vessel ingrowth.

A further extension of this model, which focusses on growth in an arterio-venous system, is presented in [293]. The most relevant improvement is that the vasculature is modelled as a network of connected ideal tubes that run along the bonds of the 2D triangular lattice. Individual vessels and tumour cells can therefore occupy the same space within the grid. The model further incorporates a hierarchically organized initial vasculature, which comprises arteries, veins, and capillaries, and it reproduces the standard processes of sprouting angiogenesis, vessel co-option, dilation and regression, as well as tumour cell proliferation and death.

The resulting simulations show that the emerging tumour vasculature is non-hierarchical and is compartmentalized into well-characterized zones. They display a complex geometry with necrotic zones and hot-spots of increased vessel density, as well as efficient transport of an injected drug.

Finally, in [294], the same group presents a 3D version of their vascular remodelling model with initially arterio-venous vessel network (see Figure 13), which comprises also a number of small changes with respect to [293]. They include the dynamics occurring at the cell level involving vessel wall degradation or maturation, and they represent the tumour mass by a continuous variable, with terms describing the flux and the proliferation/death rate.

Drasdo's well-known individual cell-based model (see, for instance, [225]) has also been coupled to an angiogenesis model in [82]. Here a tumour is embedded in a 3D cubic network of capillaries as shown in Figure 14. The tumour mass takes up the oxygen supplied by the pre-existing vasculature and proliferates. When their internal oxygen level drops below a certain threshold, cells become hypoxic and start secreting long-diffusing pro-angiogenic factors. These chemicals then activate the ECs to form vessel sprouts, which in turn chemotactically move towards the spheroid and eventually form new capillary loops. The ensemble of cells was described by an individual cell-based model that accounts for contact-inhibition of growth and nutrient-related growth and apoptosis.

A similar cubic vessel network is used by Shirinifard et al. [245], who propose a very complex 3D uncompartmentalized CPM following most of the rules detailed above. In addition, vascular and inactive neovascular ECs secrete a short-range chemoattractant towards which they are chemotactically attracted; they also elastically connect to neighbouring individuals until the intercellular distance becomes too high. The inactive neovascular ECs are able to differentiate into active neovascular ECs in response to high levels of long-diffusing

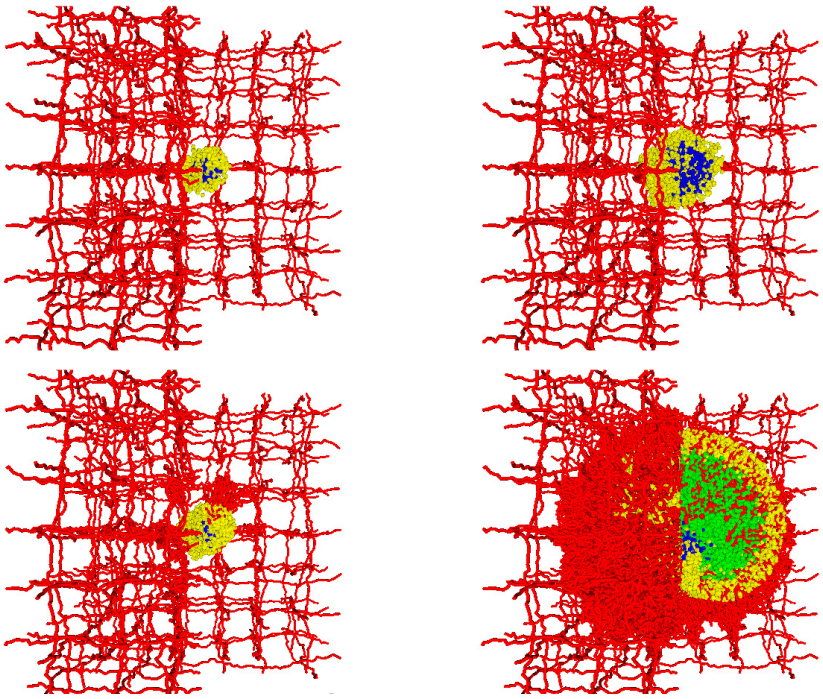

Figure 14: Tumour growth as simulated by the individual cell-based model presented in [82] in a static vessel network (left) and with angiogenesis (right). Figure courtesy of N. Jagiella (modified from [82]).

pro-angiogenic factors. Active neovascular ECs then move by chemotaxis up gradients of both long- and short-diffusing chemical substances, and proliferate.

The Hamiltonian regulating the evolution of the entire system is formed of the classical terms which describe the morphological changes of the different types of tumour and ECs (i.e. Eq. (2.26) applied to volumes and not to areas, since the model is 3D), and their mutual adhesions (i.e. Eq. (2.25)). Normal and hypoxic tumour cells, and active neovascular individuals, undergo mitosis when they reach a volume double their initial size. This is allowed by a low value of λ^{volume}, and by the growth of their target volume at a rate that depends on the level of oxygen and of the long-diffusing angiogenic factors, according to a Michaelis-Menten law. The authors also implement two different chemotactic terms for both the long- and the short-diffusing chemical substances, with concentrations denoted by c_l and c_s respectively:

$$\begin{aligned}\Delta H_{chemical} \quad &= \mu^{ch}\left[\frac{c_l(\mathbf{x}_{target})}{sc_0 + c_l(\mathbf{x}_{target})} - \frac{c_l(\mathbf{x}_{source})}{sc_0 + c_l(\mathbf{x}_{source})}\right] \\ &+\mu^{ch}\left(c_s(\mathbf{x}_{target}) - c_s(\mathbf{x}_{source})\right) . \end{aligned} \tag{3.43}$$

Finally, the authors add an energetic contribution to account for the tight junctions which maintain the integrity of blood vessels:

$$H_{elastic} = \lambda^{elastic}(l_{\sigma,\sigma'} - l_{target})^2. \tag{3.44}$$

Here l_{target} is the equilibrium length of the connection, and $l_{\sigma,\sigma'}$ is the actual distance between neighbouring cells σ and σ', which causes the rupture of the capillary if it becomes too long.

The evolution of the concentration of the long-range angiogenic factor, c_l, is described by an RD equation similar to (2.28); its secretion occurs only from the hypoxic tumour cells, whereas both decay and diffusion occur over the entire domain. The description of the evolution of the concentration of the short-range chemical, c_s, is simply the 3D extension of the model for the autocrine growth factor employed in [171, 172, 173, 174].

The proposed modeling environment is able to distinguish the main phases of tumour development. The cancer mass is first characterized by an avascular linear growth, during which it remains in a spherical morphology whilst increasing its volume. Then the tumour undergoes a vascular transition, as it recruits its own capillary network, thus overcoming diffusional limitations. The malignant mass first elongates into a cylinder, and then reorganizes into a paddle shape.

For sake of completeness, we also mention that a similar morphology has been found and studied by Astanin and co-workers [18, 19], and by Bertuzzi and co-workers [35, 36, 37, 40]. They used PDE models to describe the growth of cylindrical arrangements of tumour cells (called *tumour cords*) along pre-existing capillaries and capillary networks (see Figure 15), but they ignored angiogenesis. Both approaches use the framework of mixture theory (see [13, 52]), and the evolution of the volume fractions of the cell populations is determined via mass balance equations, coupled to RD models for the chemicals of interest. For instance, in [19], attention is focused on the metabolism of both tumour and host cells, and on the possibility that tumour cells have to switch from an aerobic to an anaerobic metabolism. The structure of the model for the volume fractions

of aerobic cells ϕ_o, anaerobic cells ϕ_g, and host cells ϕ_h, is given by the following set of governing equations (in dimensionless form):

$$\frac{\partial \phi_o}{\partial t} = \nabla \cdot [K\phi_o \nabla \Sigma(\phi_o + \phi_g)] + (\zeta_o)_+ \phi_o - \epsilon(-\zeta_o)_+ \phi_o - S_{o\to g}\,, \quad (3.45)$$

$$\frac{\partial \phi_g}{\partial t} = \nabla \cdot [K\phi_g \nabla \Sigma(\phi_o + \phi_g)] + (\zeta_g)_+ \phi_g - \epsilon(-\zeta_g)_+ \phi_g + S_{o\to g}\,, \quad (3.46)$$

$$\frac{\partial \phi_h}{\partial t} = \nabla \cdot [K\phi_h \nabla \Sigma(\phi_h)] - \epsilon\phi_h \left(\theta - (1-\phi_h) c_o c_g\right)_+\,, \quad (3.47)$$

where $\zeta_o = k_o c_o c_g - \theta$, $\zeta_g = k_1 k_o c_g - \theta$, and the term $S_{o\to g} = \nu\phi_o H(-\zeta_o)$ describes the aerobic-anaerobic switch. The first two equations hold within the tumour, and the last outside it. The function Σ expresses the response of cells to compression. Two RD equations for the concentrations of oxygen and glucose released from the blood vessels then close the system.

The models by Bertuzzi and coworkers [33, 35, 36, 37, 40] generally close the system of mass balance equations with a constrained mixture assumption (i.e. that all populations move with the same velocity), and a saturation assumption (i.e. that the sum of the volume fractions of all the cell populations involved is constant). The motion of the interstitial fluid with respect to the cell population is governed by Darcy's law.

In [32, 34, 38], the tumour cord model is applied to study the response to single-dose radiation treatments, and then extended in [39] to include the kinetics of the repair/misrepair process of radiation damage, and the influence of re-oxygenation on the response to two impulsive irradiations separated by a time interval (i.e. a split-dose response).

4 Lymphangiogenesis

The lymphatic system plays a key role in the human body. It forms the main tissue-drainage system, which helps to maintain tissue-fluid homeostasis [259]. Its primary function is to sustain and control a pressure gradient from the blood capillaries, through the interstitium, to the lymphatic vessels. This allows the clearance of extravasated fluids, tissue waste products, and plasma proteins, and it is also involved in fat metabolism and in graft rejection. The lymphatic system is also essential for immuno-surveillance in the body, since it provides one of the main routes for the immune cells. As a result, a malfunctional lymphatic system can lead or contribute to many diseases, such as lymphedema, fat metabolism, immune diseases, psoriasis, Melkersson-Rosenthal-Meischer syndrome, Kaposi sarcoma, lymphatic filariasis, Crohn's disease, and chronic inflammation in general [9, 135, 204].

The lymphatic network also plays an important role in the progression of cancer. In particular, the intravasation of lymph vessels by cancer cells leads to metastasis of cancer in the body, and there are also indications that tumour lymphangiogenesis is correlated with cancer metastasis (see, for instance, [1, 78, 160, 248, 260]). A malfunctional lymphatic system can lead to an increase in interstitial pressure, which results in swollen tissue and difficulties in drug delivery [130, 131]. In addition, a reduction in the pressure gradient between the blood and the lymphatic system leads to a much slower, mainly diffusive,

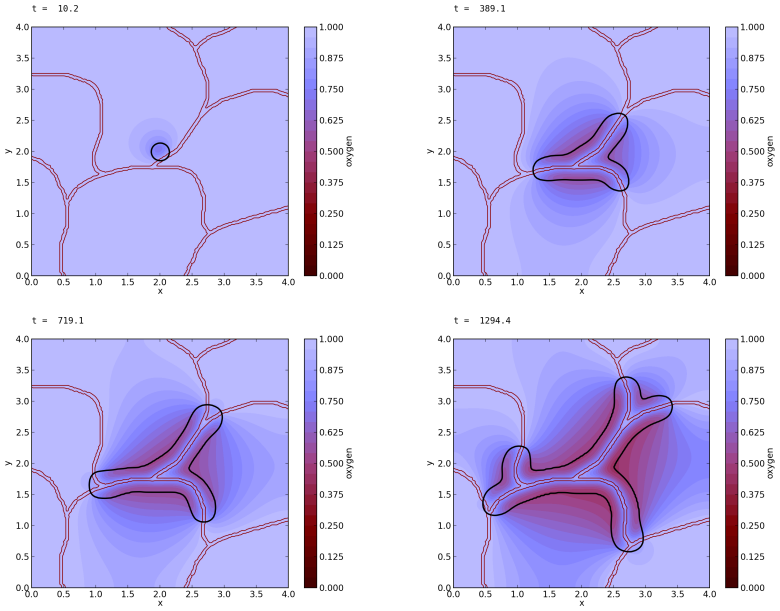

Figure 15: Growth of a tumour cord in a vascular network. Colours indicate the concentration of oxygen. The plots show how the increased metabolism of tumour cells leads to the formation of a hypoxic region away from the capillaries. Figure courtesy of S. Astanin.

movement of nutrients, and thus to an increased accumulation of waste products in the tissue.

The term lymphangiogenesis is used to refer to the development of lymphatic vessel networks both *de novo* and from pre-existing networks. However, in spite of the evident importance, lymphangiogenesis is much less studied than angiogenesis and vasculogenesis, and the morphological, spatial, and temporal features of lymphangiogenesis are poorly understood. A recent review of *in vitro* and *in vivo* experimental models for investigating lymphangiogenesis can be found in Bruyère and Noël [43]. Previously, research was hindered by the lack of markers for the lymphatic vessels, but this has been remedied in the last couple of decades by the identification of specific molecular markers, such as Prox1 (transcription factor), podoplanin (transmembrane glycoprotein), LYVE-1 (lymphatic vessel hyaluronan receptor 1) and VEGFR-3 (vascular endothelial growth factor receptor-3) [71].

The formation of lymphatic networks is coordinated primarily by the growth factors VEGF-C and VEGF-D, mediated through the receptor VEGFR-3 [21]. VEGF-C, in particular, appears to be the most essential factor in promoting lymphangiogenesis by generating a chemotactic response from the lymphatic endothelial cells (LECs). This process differs from angiogenesis and vasculogenesis of blood ECs, which is mainly induced by VEGF-A, and mediated through the receptor VEGFR-2; see [230, 269] for excellent illustrations of the molecular characteristics of blood and LECs, and [2, 134, 194] for further information on the molecular biology of lymphangiogenesis. Other influences on lymphatic net-

work development come from the molecular interactions between the LECs and the biophysical and molecular environment of their local ECM, which can affect migration, adhesion, proliferation, differentiation and organisation [133, 296].

Commencing with the observation that one of the main roles of the lymphatic system is to maintain interstitial fluid balance and protein convection, Swartz and co-workers [42, 92, 118, 119, 193] have investigated the effects of interstitial flow on lymphangiogenesis. In [42], they observed *in vivo* that interstitial fluid channels formed in a collagen implant before LEC organization, and that the subsequent lymphatic capillary network organization was initiated primarily in the direction of lymph flow. Subsequently, they have shown *in vitro* that blood and LEC morphogenesis is triggered differentially by very low rates of interstitial flow [193], and by the synergistic combination of interstitial flow and proteolytic release of ECM-bound VEGF, [118]. In the latter case, they accounted for the synergy by proposing, and demonstrating with the support of an advection-diffusion model, that the flow generates a downstream bias in the distribution of VEGF and a shift in the maximum concentration, that the cell will then follow downstream (see also [92], where this phenomenon is described as the generation of *autologous morphogen gradients*). The work was then extended to explore the effects of ECM composition on the EC reorganisation [119] by manufacturing matrices with different proportions of fibrin and collagen. They found that organisation of blood ECs and LECs preferred distinct matrix compositions, and that the structures produced were morphologically different.

Compared to angiogenesis and vasculogenesis, very little research has been directed at modelling the formation and remodelling of lymphatic vessels. In order to explain the collagen pre-patterning caused by interstitial fluid flow, before the migration of LECs to form networks, observed in [42], Roose and Fowler [228] propose a model developed in the framework of the theory of mixtures and using the theory of two phase rubber materials due to Flory et al. [93]. The model considers the interaction of the collagen gel with a solute, such as protons, which can remodel the gel. It consists of two coupled fourth order PDEs describing the evolution of the collagen volume fraction ϕ and the solute concentration c, that can be written as follows:

$$\begin{cases} \dfrac{\partial \phi}{\partial t} = \nabla \cdot \left\{ \phi^2 (1-\phi)^2 \left[F \nabla \phi - \kappa \nabla (\nabla^2 \phi) + G \nabla c \right] \right\} , \\ \dfrac{\partial c}{\partial t} = \nabla \cdot \left\{ -c \phi^2 (1-\phi)^2 \left[F \nabla \phi - \kappa \nabla (\nabla^2 \phi) + G \nabla c \right] \right\} \\ \qquad\qquad + \dfrac{1}{Pe} \nabla \cdot \left[D(\phi) \nabla c \right] , \end{cases} \tag{4.1}$$

where Pe is the Peclet number. Here $F = f_{\phi\phi} - c f_{\phi c}$ and $G = f_{\phi c} - c f_{cc}$, where the function f measures the influence of entropy, enthalpy and elastic energy on the organisation of the collagen gel, and is given by:

$$f = (1-\phi)\log(1-\phi) + \chi\phi(1-\phi) + \frac{1}{2N_x}\left(\phi_0 - \phi - \frac{1}{3}\phi \log\frac{\phi_0}{\phi}\right). \tag{4.2}$$

As the sign of the terms F and G is not determined, there might be an anti-diffusive term in the equation for the volume fraction (4.1), although it is regularized by the bi-Laplacian, as in the angiogenesis model in [275]. They studied

the linear stability of the homogeneous distribution, finding that patterning can be observed above a critical level of solute concentration. The time-scales of the fastest growing modes are consistent with experimental findings.

To investigate the onset of lymphangiogenesis in and around tumours due to tumour-secreted growth factors, Friedman and Lolas [205] propose a continuum model consisting of eight RD equations. These equations govern the evolution of the density of LECs and tumour cells, and the concentrations of ECM, VEGF-C, urokinase secreted by LECs and by tumour cells, and plasmin activated by LECs and tumour cells. The LECs and tumour cells migrate due to diffusion, chemotaxis and haptotaxis, and their proliferation is modelled by logistic growth. The LECs also proliferate due to VEGF-C-induced mitosis. The ECM is degraded proteolytically by plasmin, and re-establishes itself logistically. Tumour-activated plasmin plays an important role in the model, since it both proteolytically cleaves tumour-secreted VEGF-C and releases matrix-bound VEGF-C (in its role as an ECM-degrading protease). Simulations in 1D produce sharp peaks in the density of LECs in several distinct locations, that may be regarded as the formation of a network of lymphatic vessels. A limitation of the model is that it does not take into account any competition for space. In ref. [99], the authors study the model analytically to prove existence and uniqueness of the solution.

Finally, whilst they neglect any effects of lymphangiogenesis, we mention the recent article by Wu et al. [299], who investigate the effect of interstitial fluid pressure/flow (IFP/IFF) and the lymphatic network on vascularized tumour growth. Elevated IFP inside the tumour can block the delivery of nutrients or drugs, and may also affect the gradients of biochemical signals around the tumour. This work extends the model for angiogenesis and vascularized tumour growth in [154, 166, 167, 252, 302] already discussed in Sections 2.5 and 2.6, to include IFF and drainage through the lymphatic system. The IFF is modelled using a two-phase continuum model, where the phases are fluid and cells, with a source term representing the release of IFF from the vasculature, and a sink term representing the drainage of IFF into the lymphatic network, which also allows for tumour stress-induced collapse of lymphatic vessels. The lymphatic network is modelled by a continuous density field, and is degraded by a proteolytic enzyme. In agreement with experimental observations, the IFP is elevated inside the tumour, leading to large IFF directed towards the surrounding tissue. Their results also indicate that the root cause of the plateau in the IFP inside the tumour is the elevated interstitial hydraulic conductivity combined with poor lymphatic drainage.

5 Discussion

Focussing on the literature developed in the last ten years to describe the formation of vascular networks, we have identified several classes of models, from continuum to discrete and cell-based models. Each type of model, with its own advantages and limitations, has achieved significant results. Indeed, all of the proposed mathematical approaches have improved considerably in the last ten years, and have shown an increased ability to reproduce accurately selected phases, and to identify or confirm the underlying mechanisms of the vasculogenic process.

In spite of this, all of the models must be updated constantly to keep pace with new biological discoveries in the field, and all of them could be extended to include more effects. In the main body of the article, we have already indicated critical features of the different models and suggested some possible developments. Here, we simply restrict ourselves to a discussion of the general features of the modelling frameworks that could be improved.

Aside from the specific applications, each model class described above provides a distinct, and complementary, framework to describe the formation of vascular networks. However, it is evident that some of the experimental observations can be explained only by one particular type of model, and not by the others (or better by some types of models than by others). For instance, the continuum models discussed in Section 2.2.1 successfully describe the early stages of vasculogenesis, which are dominated by the chemotactic and persistent motion of the ECs. However, as discussed in Section 2.2.2, they needed to be suitably extended to describe the subsequent phases of the process, when the cells adhere more strongly to the substratum and mechanical interactions with the substratum become important. Even in this phase, future work will be required to include plastic effects related to the attachment and detachment mechanisms of focal adhesion points.

In this respect, although adhesion mechanics is one of the basic aspects of CPMs, to date they are not able to deal with mechanical effects, such as deformation of the substrate. However, in principle it should be feasible to include these effects, since CPMs are based on an energetic formulation and it is standard in continuum mechanics to define constitutive equations on the basis of energetic considerations, at least in the elastic or poroelastic case. Hence, it would be interesting to investigate the possibility of generalizing and calibrating the Hamiltonian to include an extra elastic energy term derived from a continuum mechanics model. However, it is not so clear how this could be done for other cell-based models, e.g. a cellular automata model.

As they are focussed on the cellular scale, generally speaking cell-based models possess a lot of flexibility in their ability to describe vasculogenesis. They allow a detailed description of the behaviour of single ECs during network formation and stabilization, and of their morphological evolution and adhesion mechanics. They also permit proper inclusion of intra-cellular processes, that are fundamental in determining the biophysical properties and behaviour of the cell. This essential feature, which is more difficult to include in continuum models, is of great interest to the biomedical community, in particular in view of the recent understanding of genetic processes and proteomics. Such characteristics, already included in some cellular automata models and in extended cellular Potts models (CPMs), allow a mesoscopic description of cell dynamics so that its behaviour can be linked successfully to the underlying sub-cellular machineries. For example, the model can include the activation or inactivation of intra-cellular protein cascades by chemical factors diffusing in the outer environment (conveniently described by continuum approximations, such as RD equations), or take into account of the expression and internalisation of receptors and adhesion molecules like cadherins and integrins.

Discrete and discretized models also permit the coupling of mesoscopic dynamics to the intra-cellular processes. Their main advantage, however, is that they are currently able to capture more explicitly the dynamics of vessel branching, anastomosis, pruning, and vessel diameter remodelling. In principle, some

of these processes could also be included into a CPM, but this remains to be done.

Generally speaking, a practical limitation of cell-based models is the fact that sometimes they are not so efficient at providing a general outlook on the system as a whole. In addition, they are computationally expensive. This becomes particularly evident when one needs to simulate large regions of tissue, whilst maintaining a good resolution at the cellular or even sub-cellular scale, or when one has to perform many simulations either because of the inherent stochasticity embedded in the models or because of the need to conduct a parameter sweep. On the other hand, continuum models are more suited and computationally cheaper to describe the behaviour of tissues from the macroscopic point of view, but it is more difficult to account for sub-cellular mechanisms. In this respect, it would be desirable to develop some coarse-graining techniques which relate a tissue-scale description to a cell-based model, so that it is possible to focus on the cellular or sub-cellular level where and when needed and homogenize where and when this level of detail is excessive. This feature is particularly important when coupling the vasculature dynamiwith the evolution of the whole tissue.

Acknowledgements

This publication was based on work supported in part by Award No KUK-C1-013-04, made by King Abdullah University of Science and Technology (KAUST).

References

[1] Achen, M.G., Stacker, S.A., 2006. *Tumor lymphangiogenesis and metastatic spread - new players begin to emerge.* Int. J. Cancer, 119, 1755–1760.

[2] Adams, R.H., Alitalo, K., 2007. *Molecular regulation of angiogenesis and lymphangiogenesis.* Nat. Rev. Mol. Cell. Biol., 8, 464–478.

[3] Addison-Smith, B., McElwain, D.L.S., Maini, P.K., 2008. *A simple mechanistic model of sprout spacing in tumour-associated angiogenesis.* J. Theor. Biol., 250, 1–15.

[4] Alarcon, T., Byrne, H.M., Maini, P.K., 2003. *A cellular automaton model for tumour growth in an inhomegeneous environment.* J. Theor. Biol., 225, 257–274.

[5] Alarcon, T., Byrne, H.M., Maini, P.K., 2005. *A multiple scale model of tumour growth.* Multiscale Model. Sim., 3, 440–475.

[6] Alarcon, T., Byrne, H.M., Maini, P.K., 2005. *A design principle for vascular beds: The role of complex blood rheology.* Microvasc. Res., 69, 156–172.

[7] Alarcon, T., Owen, M.R., Byrne, H.M., Maini, P.K., 2006. *Multiscale modelling of tumour growth and therapy: The influence of vessels normalisation and chemotherapy.* Comp. Math. Methods Med., 7, 85–119.

[8] Alarcon, T., 2009. *Modelling tumour-induced angiogenesis: A review of individual-based models and multiscale approaches.* In **The Mathematics of Cancer and Developmental Biology**. M.A. Herrero, F. Giraldez, Eds. Contemporary Mathematics, 492, 45–47.

[9] Alitalo, K., 2011. *The lymphatic vasculature in disease.* Nature Med., 17, 1371-1380.

[10] Ambler, C.A., Nowicki, J.L., Burke, A.C., Bautch, V.L., 2001. *Assembly of trunk and limb blood vessels involves extensive migration and vasculogenesis of somite-derived angioblasts.* Dev. Biol., 234, 352–364.

[11] Ambrosi, D., Bussolino, F., Preziosi, L., 2005. *A review of vasculogenesis models.* J. Theor. Med., 6, 1–19.

[12] Ambrosi, D., Gamba, A., Serini, G., 2004. *Cell directional persistence and chemotaxis in vascular morphogenesis.* Bull. Math. Biol., 66, 1851–1873.

[13] Ambrosi, D., Preziosi, L., 2009. *Cell adhesion mechanisms and stress relaxation in the mechanics of tumours.* Biomech. Model. Mechanobiol., 8, 397–413.

[14] Anderson, A.R.A., Chaplain, M.A.J., 1998. *Continuous and discrete mathematical models of tumor-induced angiogenesis.* Bull. Math. Biol., 60, 857–900.

[15] Anderson, A.R.A., Chaplain, M.A.J., 1998. *A mathematical model for capillary network formation in the absence of endothelial cell proliferation.* Appl. Math. Lett., 11, 109–114.

[16] Anderson, A.R.A., Chaplain, M.A.J., Rejniak, K.A., Eds. 2007. **Single-Cell-Based Models in Biology and Medicine**, Mathematics and Biosciences in Interaction (MBI) series, Birkhaüser-Verlag.

[17] Arnaoutova, I., Kleinman, H.K., 2010. *In vitro angiogenesis: Endothelial cell tube formation on gelled basement membrane extract.* Nat. Protoc., 5, 628–635.

[18] Astanin, S., Preziosi, L., 2009. *Mathematical modelling of the Warburg effect in tumour cords.* J. Theor. Biol., 258, 578–590.

[19] Astanin, S., Tosin, A., 2007. *Mathematical model of tumour cord growth along the source of nutrient.* Math. Model. Nat. Phenom., 2, 153–177.

[20] Aubert, M., Chaplain, M.A.J., McDougall, S.R., Devlin, A., Mitchell, C.A., 2011. *A continuous mathematical model of the developing murine retinal vasculature.* Bull. Math. Biol., 73, 2430-2451.

[21] Bahram, F., Claesson-Welsh, L., 2010. *VEGF-mediated signal transduction in lymphatic endothelial cells.* Pathophysiology, 17, 253–261.

[22] Balding, D., McElwain, D.L.S., 1985. *A mathematical model of tumor-induced capillary growth.* J. Theor. Biol., 114, 53–73.

[23] Baluk, P., Morikawa, S., Haskell, A., Mancuso, M., McDonald, D.M., 2003. *Abnormalities of basement membrane on blood vessels and endothelial sprouts in tumors.* Am. J. Pathol., 163, 1801–1815.

[24] Bartha, K., Rieger, H., 2006. *Vascular network remodeling via vessel cooption, regression and growth in tumors.* J. Theor. Biol., 241, 903–918.

[25] Bauer, A.L., Jackson, T.L., Jiang, Y., 2007. *A cell-based model exhibiting branching and anastomosis during tumor-induced angiogenesis.* Biophys. J., 92, 3105–3121.

[26] Bauer, A.L., Jackson, T.L., Jiang, Y., 2009. *Topography of extracellular matrix mediates vascular morphogenesis and migration speeds in angiogenesis.* PLOS Comp. Biol., e1000445.

[27] Bayley, P., Ahlstrom, P., Martin, S.R., Forsen S., 1984. *The kinetics of calcium binding to calmodulin: Quin 2 and ANS stopped-flow fluorescence studies.* Biochem. Biophys. Res. Commun., 120, 185–191.

[28] Bearer, E.L., Lowengrub, J.S., Chuang, Y.L., Frieboes, H.B., Jin, F., Wise, S.M., Ferrari, M., Agus, D.B., Cristini, V., 2009. *Multiparameter computational modeling of tumor invasion.* Cancer Res., 69, 4493–4501.

[29] Bellomo, N., De Angelis, E., Preziosi, L., 2004. *Multiscale modelling and mathematical problems related to tumor evolution and medical therapy.* J. Theor. Med., 5, 111–136.

[30] Bentley, K., Gerhardt, H., Bates, P. A., 2008. *Agent-based simulation of notch-mediated tip cell selection in angiogenic sprout initialisation.* J. Theor. Biol., 250, 25–36.

[31] Berridge, M.J., Bootman, M.D., Roderick, H.L., 2003. *Calcium signalling: Dynamics, homeostasis and remodelling.* Nature Rev. Mol. Cell Biol., 4, 517–529.

[32] Bertuzzi, A., DOnofrio, A., Fasano, A., Gandolfi, A., 2003. *Regression and regrowth of tumour cords following single-dose anticancer treatment.* Bull. Math. Biol., 65, 903–931.

[33] Bertuzzi, A., Fasano, A., Filidoro L., Gandolfi, A., Sinisgalli, C., 2005. *Dynamics of tumour cords following changes in oxygen availability: A model including a delayed exit from quiescence*, Math. Comp. Model., 41, 1119–1135.

[34] Bertuzzi, A., Fasano, A., Gandolfi, A., 2004. *A free boundary problem with unilateral constraints describing the evolution of a tumour cord under the influence of cell killing agents.* SIAM J. Math. Anal., 36, 882–915.

[35] Bertuzzi, A., Fasano, A., Gandolfi, A., 2005. *A mathematical model for tumor cords incorporating the flow of interstitial fluid.* Math. Mod. Meth. Appl. Sci., 15, 1735–1777.

[36] Bertuzzi, A., Fasano, A., Gandolfi, A., Marangi D., 2002. *Cell kinetics in tumour cords studied by a model with variable cell cycle length*, Math. Biosci., 177&178, 103–125.

[37] Bertuzzi, A., Fasano, A., Gandolfi, A., Sinisgalli, C., 2007. *Interstitial pressure and extracellular fluid motion in tumor cords.* Math. Biosci. Eng., 2, 445–460.

[38] Bertuzzi, A., Fasano, A., Gandolfi, A., Sinisgalli, C., 2007. *Cell resensitization after delivery of a cycle-specific anticancer drug and effect of dose splitting: Learning from tumour cords.* J. Theor. Biol., 244, 388–399.

[39] Bertuzzi, A., Fasano, A., Gandolfi, A., Sinisgalli, C., 2008. *Reoxygenation and split-dose response to radiation in a tumour model with Krogh-type vascular geometry.* Bull. Math. Biol., 70, 992–1012.

[40] Bertuzzi, A., Gandolfi, A., 2000. *Cell kinetics in a tumour cord*, J. Theor. Biol., 204, 587–599.

[41] Betteridge, P., Owen, M.R., Alarcon, T., Maini, P.K., Byrne, H.M., 2006. *The impact of cell crowding and cell movement on vascular tumour growth.* Netw. Heter. Media., 1, 515–535.

[42] Boardman, K.C., Swartz, M.A., 2003. *Interstitial flow as a guide for lymphangiogenesis.* Circ. Res., 92, 801–808.

[43] Bruyère, F., Noël, A., 2010. *Lymphangiogenesis: In vitro and in vivo models.* FASEB J., 24, 8–21.

[44] Bussolati, B., Deregibus, M. C., Camussi, G., 2010. *Characterization of molecular and functional alterations of tumor endothelial cells to design anti-angiogenic strategies.* Curr. Vasc. Pharmacology, 8, 220–232.

[45] Bussolati, B., Deambrosis, I., Russo, S., Deregibus, M.C., Camussi, G., 2003. *Altered angiogenesis and survival in human tumor-derived endothelial cells.* FASEB J., 17, 1159–1161.

[46] Bussolati, B., Grange, C., Camussi, G., 2011. *Tumor exploits alternative strategies to achieve vascularization.* FASEB J., 25, 2874–2882.

[47] Bussolino, F., Arese, M., Audero, E., Giraudo, E., Marchio, S., Mitola, S., Primo, L., Serino, G., 2003. *Biological aspects in tumor angiogenesis.* In **Cancer Modeling and Simulation**, Preziosi, L., ed., Mathematical Biology and Medicine Sciences, Chapman and Hall/CRC, 1–16.

[48] Byrne, H.M., Chaplain M.A.J., 1995. *Mathematical models for tumour angiogenesis: Numerical simulations and nonlinear wave solutions.* Bull. Math. Biol., 57, 46–86.

[49] Byrne, H.M., Chaplain, M.A.J., 1996. *Explicit solutions of a simplified model of capillary sprout growth during tumor angiogenesis.* Appl. Math. Lett., 9, 69-74.

[50] Byrne, H.M., Chaplain, M.A.J., Evans, D.L., Hopkinson, I., 2000. *Mathematical modelling of angiogenesis in wound healing: Comparison of theory and experiment.* J. Theor. Med., 2, 175–197.

[51] Byrne, H.M., Owen, M.R., Alarcon, T., Murphy, J., Maini, P.K., 2006. *Modelling the response of vascular tumours to anticancer therapies: A multiscale approach.* Math. Mod. Meth. App. Sci., 16, 1–25.

[52] Byrne, H.M., Preziosi, L., 2004. *Modeling solid tumour growth using the theory of mixtures.* Math. Med. Biol., 20, 341–366.

[53] Cai, Y., Gulnark, K., Zhang, H., Cao, J., Xu, S., Long, Q., 2009. *Numerical simulation of tumor-induced angiogenesis influenced by the extra-cellular matrix mechanical environment.* Acta Mech. Sin. 25, 889–895.

[54] Capasso, V., Morale, D., 2009. *Stochastic modelling of tumour-induced angiogenesis.* J. Math. Biol., 58, 219-233

[55] Capasso, V., Morale, D., Facchetti, G., 2011 *The role of stochasticity in a model of retinal angiogenesis.* IMA J. Appl. Math., 77, 729–747.

[56] Carmeliet, P., Jain, R. K., 2000. *Angiogenesis in cancer and other diseases.* Nature, 407, 249–257.

[57] Carmeliet, P., 2005. *Angiogenesis in life, disease and medicine.* Nature, 438, 932–936.

[58] Caspi, O., Lesman, A., Basevitch, Y., Gepstein, A., Arbel, G., Habib, I.H., Gepstein, L., Levenberg, S., 2007. *Tissue engineering of vascularized cardiac muscle from human embryonic stem cells.* Circ. Res., 100, 263–272.

[59] Chaplain, M.A.J., 2000. *Mathematical modelling of angiogenesis.* J. Neuro-Onc., 50, 37-51.

[60] Chaplain, M.A.J., Anderson, A.R.A., 1996. *Mathematical modelling, simulation and prediction of tumour-induced angiogenesis.* Invasion & Metastasis, 16, 222-234.

[61] Chaplain, M.A.J., Giles, S.M., Sleeman, B.D., Jarvis, R.J., 1995. *A mathematical model for tumour angiogenesis.* J. Math. Biol., 33, 744-770.

[62] Chaplain, M.A.J., McDougall, S.R., Anderson, A.R.A., 2006. *Mathematical modeling of tumor-induced angiogenesis.* Annu. Rev. Biomed. Eng., 8, 233-257.

[63] Chaplain, M.A.J., Stuart, A.M., 1993. *A model mechanism for the chemotactic response of endothelial cells to tumour angiogenesis factor.* IMA J. Math. Appl. Med. Biol., 10, 149-168.

[64] Chatelain, C., Balois, T., Ciarletta, P., Ben Amar, M., 2011. *Emergence of microstructural patterns in skin cancer: A phase separation analysis in a binary mixture.* New J. Phys., 13, 115013.

[65] Chauviere, A., Hillen, T., Preziosi, L., 2007. *Modeling cell movement in anisotropic and heterogeneous tissues.* Netw. Het. Media, 2, 333–357.

[66] Chen, T.T., Luque, A., Lee, S., Anderson, S. M., Segura, T., Iruela-Arispe, M.L., 2010. *Anchorage of VEGF to the extracellular matrix conveys differential signaling responses to endothelial cells.* J. Cell Biol., 188, 595–609.

[67] Chilibeck, P.D., Paterson, D.H., Cunningham, D.A., Taylor, A.W., Noble, E.G., 1997. *Muscle capillarization O2 diffusion distance, and VO2 kinetics in old and young individuals.* J. Appl. Physiol., 82, 63–69.

[68] Coniglio, A., de Candia, A., Di Talia, S., Gamba, A., 2004. *Percolation and Burgers' dynamics in a model of capillary formation.* Phys. Rev. E, 69, 051910.

[69] Cristini, V., J. Lowengrub, J., Eds., 2010. **Multiscale Modeling of Cancer: An Integrated Experimental and Mathematical Modeling Approach**. Cambridge University Press.

[70] Cristini, V., Lowengrub, J.S., Nie, Q., 2003. *Nonlinear simulation of tumor growth.* J. Math. Biol., 46, 191–224.

[71] Cueni, L.N., Detmar, M., 2006. *New insights into the molecular control of the lymphatic vascular system and its role in disease.* J. Invest. Dermatol., 126, 2167–2177.

[72] Czirok, A., Little, C. D., 2012. *Pattern Formation During Vasculogenesis.* Birth Defects Research (Part C), 96, 153 - 162.

[73] Das, A., Lauffenburger, D., Asada, H., Kamm, R. D., 2010. *A hybrid continuumdiscrete modelling approach to predict and control angiogenesis: Analysis of combinatorial growth factor and matrix effects on vessel-sprouting morphology.* Phil. Trans. R. Soc. A, 368, 2937–2960.

[74] Davidson, F.A., Anderson, A.R.A., Chaplain, M.A.J., 2000. *Steady-state solution of a generic model for the formation of capillary networks.* Appl. Math. Lett., 13, 127–132.

[75] Deakin, A.S., 1976. *Model for initial vascular patterns in melanoma transplants.* Growth, 40, 191–201.

[76] De Angelis, E., Preziosi, L., 2000. *Advection-diffusion models for solid tumour evolution in vivo and related free boundary problem.* Math. Mod. Meth. Appl. Sci., 10, 379–407.

[77] De Bock, K., Cauwenberghs, S., Carmeliet, P., 2011. *Vessel abnormalization: Another hallmark of cancer? Molecular mechanisms and therapeutic implications.* Curr. Opin. Genet. Dev., 21, 73 –79.

[78] Detmar, M., 2009. *Tumor and lymph node lymphangiogenesis.* In **From Local Invasion to Metastatic Cancer**, S.P.L. Leong ed., Current Clinical Oncology Vol. 6, Springer, 255–261.

[79] Dike, L.E., Chen, C.S., Mrksich, M., Tien, J., Whitesides, G.M., Ingber, D.E., 1999. *Geometric control of switching between growth, apoptosis, and differentiation during angiogenesis using micropatterned substrates. In vitro.* Cell Dev. Biol. Anim., 35, 441–448.

[80] DiMilla, P.A., Stone, J.A., Quinn, J.A., Albelda, S.M., Lauffenburger, D.A., 1993. *Maximal migration of human smooth-muscle cells on fibronectin and type-IV collagen occurs at an intermediate attachment strength.* J. Cell Biol., 122, 729–737.

[81] Drake, C. J., LaRue, A., Ferrara, N., Little, C. D., 2000. *VEGF regulates cell behavior during vasculogenesis.* Dev. Biol., 224, 178–188.

[82] Drasdo, D., Jagiella, N., Ramis-Conde, I., Vignon-Clementel, I., Weens, W., 2009. *Modeling steps from a benign tumor to an invasive cancer: Examples of intrinsically multiscale problems.* In **From Single Scale-based Models to Multiscale Modeling**, A. Chauviere, L. Preziosi, C. Verdier, Eds., CRC/Academic Press, 379–416.

[83] Erber, R., Eichelsbacher, U., Powajbo, V., Korn, T., Djonov, V., Lin, J., Hammes, H.P., Grobholz, R., Ullrich, A., Vajkoczy, P., 2006. *EphB4 controls blood vascular morphogenesis during postnatal angiogenesis.* EMBO J., 25, 628–641

[84] Ferrara, N., 2002. *VEGF and the quest for tumour angiogenesis factors.* Nat. Rev. Cancer, 2, 795–803.

[85] Ferrara, N., Gerber, H.P., LeCouter, J., 2003. *The biology of VEGF and its receptors.* Nature Med., 9, 669–676.

[86] Filbet, F., Laurençot, P., Perthame, B., 2004. *Derivation of hyperbolic models for chemosensitive movement.* J. Math. Biol., 50, 189–207.

[87] Fiorio Pla, A., Grange, C., Antoniotti, S., Tomatis, C., Merlino, A., Bussolati, B., Munaron, L., 2008. *Arachidonic acid-induced Ca2+ entry is involved in early steps of tumor angiogenesis.* Mol. Cancer Res., 6, 535–545.

[88] Fiorio Pla, A., Munaron, L., 2001. *Calcium influx, arachidonic acid, and control of endothelial cell proliferation.* Cell Calcium, 30, 235–244.

[89] Fiorio Pla, A., Genova, T., Pupo, E., Tomatis, C., Genazzani, A., Zaninetti, R., Munaron, L., 2010. *Multiple roles of protein kinase a on arachidonic acidmediated Ca2+ entry and tumor-derived human endothelial cells migration.* Mol. Cancer Res., 8, 1466–1476.

[90] Flegg, J.A., McElwain, D.L.S., Byrne, H.M., Turner, I.W., 2009. *A three species model to simulate application of hyperbaric oxygen therapy to chronic wounds.* PLoS Comput. Biol., 5, e1000451.

[91] Flegg, J.A., Byrne, H.M., McElwain, D.L.S., 2010. *Mathematical model of hyperbaric oxygen therapy applied to chronic diabetic wounds.* Bull. Math. Biol. 72, 1867–1891.

[92] Fleury, M.E., Boardman, K.C., Swartz, M.A., 2006. *Autologous morphogen gradients by subtle interstitial flow and matrix interactions.* Biophys. J., 91, 113–121.

[93] Flory, J.P., 1953. **Principles of Polymer Chemistry**. Cornell University Press.

[94] Folkman, J., Haudenschild, C., 1980. *Angiogenesis in vitro.* Nature, 288, 551–556.

[95] Fong, G., Zhang, L., Bryce, D., Peng, J., 1999. *Increased hemangioblast commitment, not vascular disorganization, is the primary defect in flt-1 knock-out mice.* Development, 126, 3015–3025.

[96] Frieboes, H., Jin, F., Chuang, Y.-L., Wise, S.M., Lowengrub, J.S., Cristini, V., 2010. *Three-dimensional multispecies nonlinear tumor growth II: Tumor invasion and angiogenesis.* J. Theor. Biol., 264, 1254–1278.

[97] Frieboes, H.B., Lowengrub, J.S., Wise, S.M., Zheng, X., Macklin, P., Bearer, E.L., Cristini, V., 2007. *Computer simulation of glioma growth and morphology.* NeuroImage, 37, S59–S70.

[98] Friedl, P., 2004. *Prespecification and plasticity: Shifting mechanisms of cell migration.* Curr. Opin. Cell. Biol., 16, 14–23.

[99] Friedman, A., Lolas, G., 2005. *Analysis of a mathematical model of tumor lymphangiogenesis.* Math. Mod. Meth. Appl. Sci., 15, 95-107.

[100] Fruttiger, M., 2002. *Development of the mouse retinal vasculature: Angiogenesis versus vasculogenesis.* Investig. Ophthalmol. Vis. Sci., 43, 522-527.

[101] Fukumura, D., Duda, D. G., Munn, L. L., Jain, R. K., 2010. *Tumor microvasculature and microenvironment: Novel insights through intravital imaging in pre-clinical models.* Microcirculation, 17, 206–225.

[102] Gaffney, E., Pugh, K., Maini, P., Arnold, F., 2002. *Investigating a simple model of cutaneous wound healing angiogenesis.* J. Math. Biol. 45, 337-374.

[103] Gamba, A., Ambrosi, D., Coniglio, A., de Candia, A., di Talia, S., Giraudo, E., Serini, G., Preziosi, L., Bussolino, F., 2003. *Percolation, morphogenesis, and Burgers dynamics in blood vessel formation.* Phys. Rev. Lett., 90, 101–118.

[104] Gariano, R.F., 2003. *Cellular mechanisms in retinal vascular development.* Prog. Retin. Eye Res., 22, 295-306.

[105] Gevertz, J.L., Torquato, S., 2006. *Modeling the effects of vasculature evolution on early brain tumor growth.* J. Theor. Biol., 243, 517–531.

[106] Glazier, J.A., Balter, A., Merks, R.M.H., Poplawski, N.J., Swat, M., 2007. *The Glazier-Graner-Hogeweg model: Extension, future direction, and opportunitites for further study.* In **Single-Cell-Based Models in Biology and Medicine**, A.R.A. Anderson, M.A.J. Chaplain, K.A. Rejniak eds., Mathematics and Biosciences in Interactions, Birkhaüser, 157–167.

[107] Glazier, J.A., Balter, A., Poplawski, N.J., 2007. *Magnetization to morphogenesis: A brief history of the Glazier-Graner-Hogeweg model.* In **Single-Cell-Based Models in Biology and Medicine**, A.R.A. Anderson, M.A.J. Chaplain, K.A. Rejniak eds., Mathematics and Biosciences in Interactions, Birkhaüser, 79–106.

[108] Glazier, J. A., Graner, F., 1993. *Simulation of the differential adhesion driven rearrangement of biological cells.* Phys. Rev. E, 47, 2128–2154.

[109] Goel, S., Duda, D.G., Xu, L., Munn, L.L., Boucher, Y., Fukumura, D., Jain, R.K., 2011. *Normalization of the vasculature for treatment of cancer and other diseases.* Physiol. Rev., 91, 1071–1121.

[110] Goto, Y., Miura, M., Iijima, T., 1996. *Extrusion mechanisms of intracellular Ca2+ in human aortic endothelial cells.* Eur. J. Pharmacol., 314, 185–192.

[111] Graner, F., Glazier, J.A., 1992. *Simulation of biological cell sorting using a two dimensional extended Potts model.* Phys. Rev. Lett., 69, 2013–2017.

[112] Grange, C., Bussolati, B., Bruno, S., Fonsato, V., Sapino, A., Camussi, G., 2006. *Isolation and characterization of human breast tumor-derived endothelial cells.* Oncol. Rep., 15, 381–386.

[113] Grant, D., Tashiro, K., Segui-Real, B., Yamada, Y., Martin, G., Kleinman, H., 1989. *Two different laminin domains mediate the differentiation of human endothelial cells into capillary-like structures in vitro.* Cell, 58, 933–943.

[114] Griffith, L.G., Naughton, G., 2002. *Tissue engineering: Current challenges and expanding opportunities.* Science, 295, 1009–1014.

[115] Guangqi, E., Cao, Y., Bhattacharya, S., Dutta, S., Wang, E., Mukhopadhyay, D., 2012. *Endogenous vascular endothelial growth factor-A (VEGF-A) maintains endothelial cell homeostasis by regulating VEGF receptor-2 transcription.* J. Biol. Chem., 287, 3029-3041.

[116] Guyton, A., Hall, J. 2000. **Textbook of Medical Physiology.** W.B. Saunders, St. Louis.

[117] Harrington, H.A., Maier, M., Naidoo, L., Whitaker, N., Kevrekidis, P.G., 2007. *A hybrid model for tumor-induced angiogenesis in the cornea in the presence of inhibitors.* Math. Comp. Model., 46, 513–524.

[118] Helm, C.L., Fleury, M.E., Zisch, A.H., Boschetti, F., Swartz, M.A., 2005. *Synergy between interstitial flow and VEGF directs capillary morphogenesis in vitro through a gradient amplification mechanism.* Proc. Natl. Acad. Sci. U.S.A., 102, 15779–15784.

[119] Helm, C.L., Zisch, A., Swartz, M.A., 2007. *Engineered blood and lymphatic capillaries in 3-D VEGF-fibrin-collagen matrices with interstitial flow.* Biotechnol. Bioeng., 96, 167–176.

[120] Helmlinger, G., Endo, M., Ferrara, N., Hlatky, L., Jain, R., 2000. *Formation of endothelial cell networks.* Nature, 405, 139–141.

[121] Hillen, T., Painter, K.J., 2009. *A user's guide to PDE models for chemotaxis.* J. Math. Biol., 58, 183–217.

[122] Hogea, C.S., Murray, B.T., Sethian, J.A., 2006. *Simulating complex tumor dynamics from avascular to vascular growth using a general level-set method.* J. Math. Biol., 53, 86–134.

[123] Holmes, M., Sleeman, B.D., 2000. *A mathematical model of tumor angiogenesis incorporating cellular traction and viscoelastic effects.* J. Theor. Biol., 202, 95–112.

[124] Hryshko, L.V., Philipson, K.D., 1997. *Sodium-calcium exchange: Recent advances.* Basic Res. Cardiol., 92, 45–51.

[125] Huang, S., Brangwynne, C. P., Parker, K. K., Ingber, D. E., 2005. *Symmetry-breaking in mammalian cell cohort migration during tissue pattern formation: Role of random-walk persistence.* Cell Motil. Cytoskeleton, 61, 201–213.

[126] Hudon, V., Berthod, F., Black, A.F., Damour, O., Germain, L., Auger, F.A., 2003. *A tissue-engineered endothelialized dermis to study the modulation of angiogenic and angiostatic molecules on capillary-like tube formation in vitro.* Br. J. Dermatol., 148, 1094–1104.

[127] Jabbarzadeh, E., Abrams, C.F., 2007. *Strategies to enhance capillary formation inside biomaterials: A computational study.* Tissue Engng., 13, 2073–2086.

[128] Jackson, T., Ed., 2012. **Modeling Tumor Vasculature: Molecular, Cellular, and Tissue Level Aspects and Implications**. Springer.

[129] Jackson, T., Zheng, X., 2010. *A cell-based model of endothelial cell migration, proliferation and maturation during corneal angiogenesis.* Bull. Math. Biol., 72, 830868.

[130] Jain, R.K., 2001. *Normalizing tumor vasculature with anti-angiogenic therapy: A new paradigm for combination therapy.* Nature Med., 7, 987–989.

[131] Jain, R.K., 2005. *Normalization of tumor vasculature: An emerging concept in antiangiogenic therapy.* Science, 307, 58–62.

[132] Jain, R.K., Au, P., Tam , J., Duda, D.G., Fukumura, D., 2005. *Engineering vascularized tissue.* Nat. Biotechnol., 23, 821-823.

[133] Ji, R.-C., 2006. *Lymphatic endothelial cells, lymphangiogenesis, and extracellular matrix.* Lymphat. Res. Biol., 4, 83–100.

[134] Karpanen, T., Alitalo, K., 2008. *Molecular biology and pathology of lymphangiogenesis.* Annu. Rev. Pathol., 3, 367–397.

[135] Karpanen, T., Alitalo, K., 2001. *Lymphatic vessels as targets of tumor therapy?* J. Exp. Med., 194, F37–42.

[136] Kimura, H., Esumi, H., 2003. *Reciprocal regulation between nitric oxide and vascular endothelial growth factor in angiogenesis.* Acta Biochim. Pol., 50, 49–59.

[137] Klingauf, J., Neher, E., 1997. *Modeling buffered Ca^{2+} diffusion near the membrane: Implications for secretion in neuroendocrine cells.* Biophys. J., 72, 674–690.

[138] Köhn-Luque, A., de Back, W., Starruss, J., Mattiotti, A., Deutsch, A., Prez-Pomares, J.M., Herrero, M.A., 2011. *Early embryonic vascular patterning by matrix-mediated paracrine signalling: A mathematical model study.* PLoS One, 6, e24175.

[139] Kowalczyk, R., 2005. *Preventing blow-up in a chemotaxis model.* J. Math. Anal. Appl., 305, 566–588.

[140] Krogh, A., 1919. *The number and distribution of capillaries in muscle with calculations of the oxygen pressure head necessary for supplying the tissue.* J. Physiol., 52, 409–415.

[141] Kubota, Y., Kleinman, H., Martin, G., Lawley, T., 1988. *Role of laminin and basement membrane in the morphological differentiation of human endothelial cells into capillary-like structures.* J. Cell Biol., 107, 1589–1598.

[142] Lanza, V., Ambrosi, D., Preziosi, L., 2006. *Exogenous control of vascular network formation in vitro: A mathematical model.* Netw. Heter. Media, 1, 621–637.

[143] Lee, D. S., Bartha, K., Rieger, H., 2006. *Flow correlated percolation during vascular remodeling in growing tumors.* Phys. Rev. Lett., 96 (5), 058104.

[144] Levenberg, S., Rouwkema, J., Macdonald, M., Garfein, E.S., Kohane, D.S., Darland, D.C., Marini, R., van Blitterswijk, C.A., Mulligan, R.C., D'Amore P.A., Langer, R., 2005. *Engineering vascularized skeletal muscle tissue.* Nature Biotechnol., 23, 879–884.

[145] Levine, H.A., Pamuk, S., Sleeman B.D., Nilsen-Hamilton, M., 2001. *Mathematical modeling of capillary formation and development in tumor angiogenesis: Penetration into the stroma.* Bull. Math. Biol., 63, 801–863.

[146] Levine, H.A., Sleeman, B.D., Nilsen-Hamilton, M., 2000. *A mathematical model for the roles of pericytes and macrophages in the initiation of angiogenesis. I. The role of protease inhibitors in preventing angiogenesis.* Math Biosci., 168, 77-115.

[147] Levine, H., Sleeman, B., Nilsen-Hamilton, M., 2001. *Mathematical modeling of the onset of capillary formation initiating angiogenesis.* J. Math. Biol., 42, 195–238.

[148] Levine, H.A., Tucker, A.L., Nilsen-Hamilton, M.A., 2002. *Mathematical model for the role of cell signal transduction in the initiation and inhibition of angiogenesis.* Growth Factors, 20, 155-175.

[149] Liu, G., Qutub, A.A., Vempati, P., Mac Gabhann, F., Popel, A.S., 2011. *Module-based multiscale simulation of angiogenesis in skeletal muscle*, BMC Theor. Biol. Med. Model., 8, 6.

[150] Lloyd, B.A., Szczerba, D., Szkely, G., 2007. *A coupled finite element model of tumor growth and vascularization.* In **Medical Image Computing and Computer-Assisted Intervention MICCAI 2007**, Lecture Notes in Computer Science, 874–881.

[151] Lowengrub, J.S., Frieboes, H.B., Jin, F., Chuang, Y.L., Li, X., Macklin, P., Cristini, V., 2010. *Nonlinear modelling of cancer: Bridging the gap between cells and tumours.* Nonlinearity, 23, R1–R9.

[152] Machado, M.J.C., Watson, M.G., Devlin, A.H., Chaplain, M.A.J., McDougall, S.R., Mitchell, C.A., 2011. *Dynamics of angiogenesis during wound healing: A coupled in vivo and in silico study.* Microcirculation, 18, 183–197.

[153] Macklin, P., Lowengrub, J.S., 2007. *Nonlinear simulation of the effect of microenvironment on tumor growth.* J. Theor. Biol., 245, 677–704.

[154] Macklin, P., McDougall, S., Anderson, A.R.A., Chaplain, M.A.J., Cristini, V., Lowengrub, J., 2009. *Multiscale modeling and nonlinear simulation of vascular tumour growth.* J. Math. Biol., 58, 765–798.

[155] Maggelakis, S.A., 2003. *A mathematical model of tissue replacement during epidermal wound healing.* Appl. Math. Mod., 27, 189–196.

[156] Maggelakis, S.A., 2003. *Modeling the role of angiogenesis in epidermal wound healing.* Discr. Cont. Dyn. Sys., 4, 267–273.

[157] Maggelakis, S.A., Savakis, A.E., 1996. *A mathematical model of growth factor induced capillary growth in the retina.* Math. Comp. Model., 24, 33–41.

[158] Maggelakis, S.A., Savakis, A.E., 1999. *A mathematical model of retinal neovascularization.* Math. Comp. Model., 29, 91–97.

[159] Mahoney, A. W., Smith, B. G., Flann, N. S., Podgorski, G. J., 2008. *Discovering novel cancer therapies: A computational modeling and search approach.* IEEE Conf. on Computational Intelligence in Bioinformatics and Bioengineering, 233 - 240.

[160] Mandriota, S.J., Jussila, L., Jeltsch, M., Compagni, A., Baetens, D., Prevo, R., Banerji, S., Huarte, J., Montesano, R., Jackson, D.G., Orci, L., Alitalo, K., Christofori, G., Pepper, M.S., *Vascular endothelial growth factor-C-mediated lymphangiogenesis promotes tumour metastasis.* EMBO J., 20, 672–682.

[161] Manoussaki, D., 2004. *A mechanochemical model of vasculogenesis and angiogenesis.* Math. Model. Num. Anal., 37, 581–599.

[162] Manoussaki, D., Lubkin, S.R., Vernon, R.B., Murray, J.D., 1996. *A mechanical model for the formation of vascular networks in vitro.* Acta Biotheor., 44, 271–282.

[163] Mantzaris, N.V., Webb, S., Othmer, H.G., 2004. *Mathematical modeling of tumor-induced angiogenesis.* J. Math. Biol., 49, 111–187.

[164] Marée, A. F. M., Grieneisen, V. A., Hogeweg, P., 2007. *The cellular Potts model and biophysical properties of cells, tissues and morphogenesis.* In **Single-Cell-Based Models in Biology and Medicine**, A.R.A. Anderson, M.A.J. Chaplain, K.A. Rejniak, eds., Mathematics and Biosciences in Interactions, Birkhaüser, 107–136.

[165] Markus, M., Bohm, D., Schmick, M., 1999. *Simulation of vessel morphogenesis using cellular automata.* Math. Biosci., 156, 191–206.

[166] McDougall, S.R., Anderson, A.R.A., Chaplain, M.A.J., 2006. *Mathematical modeling of dynamic adaptive tumour-induced angiogenesis: Clinical applications and therapeutic targeting strategies.* J. Theor. Biol., 241, 564–589.

[167] McDougall, S.R., Anderson, A.R.A., Chaplain, M.A.J., Sherratt, J., 2002. *Mathematical modelling of flow through vascular networks: Implications for tumour-induced angiogenesis and chemotherapy strategies.* Bull. Math. Biol., 64, 673–702.

[168] McDougall, S.R., Chaplain, M.A.J., Stephanou, A., Anderson, A.R.A., 2010. *Modelling the impact of pericyte migration and coverage of vessels on the efficacy of vascular disrupting agents.* Math. Model. Nat. Phenom., 5, 163–202.

[169] McDougall, S.R., Watson, M.G., Devlin, A.H., Mitchell, C.A., Chaplain, M.A.J., 2012. *A hybrid discrete-continuum mathematical model of pattern prediction in the developing retinal vasculature.* Bull. Math. Biol., 74, 2272–2314.

[170] Merks, R.M.H., Brodsky, S.V., Goligorksy, M.S., Newman, S.A., Glazier, J.A., 2006. *Cell elongation is key to in silico replication of in vitro vasculogenesis and subsequent remodeling.* Dev. Biol., 289, 44–54.

[171] Merks, R. M. H., Glazier, J. A., 2006. *Dynamic mechanisms of blood vessel growth.* Inst. Phys. Publ., 19, C1–C10.

[172] Merks, R.M.H., Glazier, J.A., Brodsky, S.V., Goligorksy, M.S., Newman, S.A., 2006. *Cell elongation is key to in silico replication of in vitro vasculogenesis and subsequent remodeling.* Develop. Biol., 289, 44–54.

[173] Merks, R.M.H., Perryn, E.D., Shirinifard, A., Glazier, J.A., 2008. *Contact-inhibited chemotactic motility: Role in de novo and sprouting blood vessel growth.* PLOS Comp. Biol., 4, e1000163.

[174] Merks, R.M.H., Newman, S.A., Glazier, J.A., 2004. *Cell-oriented modeling of in vitro capillary development.* Lect. Notes Comput. Sc., 3305, 425–434.

[175] Milde, F., Bergdorf, M., Koumoutsakos. P., 2008. *A hybrid model for three-dimensional simulations of sprouting angiogenesis.* Biophys. J., 95, 3146–3160.

[176] Moon, J.J., West, J.L., 2008. *Vascularization of engineered tissues: Approaches to promote angiogenesis in biomaterials.* Curr. Top. Med. Chem., 8, 300–310.

[177] Mottola, A., Antoniotti, S., Lovisolo, D., Munaron, L., 2005. *Regulation of noncapacitative calcium entry by arachidonic acid and nitric oxide in endothelial cells.* FASEB J., 19, 2075–2077.

[178] Muller, Y., Christinger, H., Keyt, B. and de Vos, A., 1997. *The crystal structure of vascular endothelial growth factor (VEGF) refined to 1.93 Å resolution: Multiple copy flexibility and receptor binding.* Structure, 5, 1325–1338.

[179] Munaron, L., 2002. *Calcium signalling and control of cell proliferation by tyrosine kinase receptors (review).* Int. J. Mol. Med., 10, 671–676.

[180] Munaron, L., 2006. *Intracellular calcium, endothelial cells and angiogenesis.* Recent Patents Anticancer Drug Discov., 1, 105–119.

[181] Munaron, L., 2009. *A tridimensional model of proangiogenic calcium signals in endothelial cells.* The Open Biol. J., 2, 114–129.

[182] Munaron, L., Antoniotti, S., Distasi, C., Lovisolo, D., 1997. *Arachidonic acid mediates calcium influx induced by basic fibroblast growth factor in Balb-c 3T3 fibroblasts.* Cell Calcium, 22, 179–188.

[183] Munaron, L., Fiorio Pla, A., 2000. *Calcium influx induced by activation of tyrosine kinase receptors in cultured bovine aortic endothelial cells.* J. Cell Physiol., 185, 454–463.

[184] Munaron, L., Fiorio Pla, A., 2000. *Endothelial calcium machinery and angiogenesis: Understanding physiology to interfere with pathology.* Curr. Medic. Chem., 16, 4691–4703.

[185] Murray, J.D., Oster, G.F., 1984. *Cell traction models for generation of pattern and form in morphogenesis.* J. Math. Biol., 19, 265–279.

[186] Murray, J.D., Oster, G.F., 1984. *Generation of biological pattern and form.* J. Math. Appl. Med. Biol., 1, 51–75.

[187] Murray, J.D., Oster, G.F., Harris, A.K., 1983. *A mechanical model for mesenchymal morphogenesis.* J. Math. Biol., 17, 125–129.

[188] Murray, J.D., Manoussaki, D., Lubkin, S.R., Vernon, R.B., 1998. *A mechanical theory of in vitro vascular network formation.* In **Vascular Morphogenesis: In Vivo, In Vitro and In Mente**, C. Little, V. Mironov and H. Sage, Eds., Birkhäuser, Boston.

[189] Murray, J.D., Swanson, K.R., 1999. *On the mechanochemical theory of biological pattern formation with applications to wound healing and angiogenesis.* In **On Growth and Form: Spatio-temporal Pattern Formation in Biology**, M.A.J. Chaplain, G.D. Singh, J.C. McLachlan, Eds., J. Wiley and Sons.

[190] Murray, J.D., 2003. *On the mechanical theory of biological pattern formation with application to vasculogenesis.* Comp. Rend. Biol., 326, 2239–2252.

[191] Namy, P., Ohayon, J., Traqui, P., 2004. *Critical conditions for pattern formation and in vitro tubulogenesis driven by cellular traction fields.* J. Theor. Biol., 227, 103–120.

[192] Neufeld, G., Cohen, T., Gengrinovitch, S., Poltorak, Z., 1999. *Vascular endothelial growth factor (VEGF) and its receptors.* Faseb J., 13, 9–22.

[193] Ng, C.P., Helm, C.-L.E., Swartz, M.A., 2004. *Interstitial flow differentially stimulates blood and endothelial cell morhpogenesis in vitro.* Microvas. Res., 68, 258–264.

[194] Norrmén, C., Tammela, T., Petrova, T.V., Alitalo, K., 2011. *Biological basis of therapeutic lymphangiogenesis.* Circulation, 123, 1335-1351.

[195] Olsen, L., Sherratt, J.A., Maini, P.K., Arnold, F., 1997. *A mathematical model for the capillary endothelial cell extracellular matrix interactions in wound healing angiogenesis.* IMA J. Math. Appl. Med. Biol., 14, 261–282.

[196] Orme, M.E., Chaplain, M.A.J., 1997. *Two-dimensional models of tumour angiogenesis and anti-angiogenesis strategies.* IMA J. Math. Appl. Med. Biol., 14, 189-205.

[197] Oster, G. F., Murray, J. D., Harris, A. K., 1983. *Mechanical aspects of mesenchymal morphogenesis. Cell traction models for generation of pattern and form in morphogenesis.* J. Embryol. Exp. Morph., 78, 83–125.

[198] Othmer, H., Stevens, A., 1997. *Aggregation, blowup and collapse: The ABC's of generalized taxis.* SIAM J. Appl. Math., 57, 1044–1081.

[199] Owen, M.R., Alarcon, T., Maini, P.K., Byrne, H.M., 2009. *Angiogenesis and vascular remodelling in normal and cancerous tissues.* J. Math. Biol., 58, 689–721.

[200] Palecek, S.P., Loftus, J.C., Ginsberg, M.H., Lauffenburger, D.A., Horwitz, A.F., 1997. *Integrin-ligand binding properties govern cell migration speed through cell-substratum adhesiveness.* Nature, 385, 537–540.

[201] Parker, B.S., Argani, P., Cook, B.P., Liangfeng, H., Chartrand, S.D., Zhang, M., Saha, S., Bardelli, A., Jiang, Y., St Martin, T.B., Nacht, M., Teicher, B.A., Klinger, K.W., Sukumar, S., Madden, S.L., 2004. *Alterations in vascular gene expression in invasive breast carcinoma.* Cancer Res., 64, 7857–7866.

[202] Parsa, H., Upadhyay, R., Sia, S.K., 2011. *Uncovering the behaviors of individual cells within a multicellular microvascular community.* Proc. Natl. Acad. Sci. U.S.A., 108, 5133–5138.

[203] Peirce, S.M., 2008. *Computational and mathematical modeling of angiogenesis.* Microcirculation, 15, 739-751.

[204] Pepper, M.S., 2001. *Lymphangiogenesis and tumor metastasis: Myth or reality?* Clin. Cancer Res., 7, 462–468.

[205] Pepper, M.S., Lolas, G., 2008. *The lymphatic vascular system in lymphangiogenesis, invasion and metastasis: A mathematical approach.* In **Selected Topics in Cancer Modeling: Genesis, Evolution, Immune Competition, and Therapy**, E. De Angelis, M.A.J. Chaplain, N. Bellomo, Eds., Birkhäuser, 255–276.

[206] Perfahl, H., Byrne, H.M., Chen, T., Estrella, V., Alarcon, T., Lapin, A., Gatenby, R.A., Gillies, R.J., Lloyd, M.C., Maini, P.K., Reuss, M., Owen, M.R., 2011. *Multiscale modelling of vascular tumour growth in 3D: The roles of domain size and boundary conditions.* PLoS One, 6, e14790.

[207] Pettet, G., Byrne, H.M., McElwain, D.L.S., Norbury, J., 1996. *A model of wound-healing angiogenesis*, Math. Bio. Sci., 136, 35–63.

[208] Pettet, G., Chaplain, M.A.J., McElwain, D.L.S., Byrne, H.M., 1996. *On the role of angiogenesis in wound healing*, Proc. R. Soc. Lond. B, 263, 1487–1493.

[209] Pindera, M.Z., Ding, H., Chen, Z., 2008. *Convected element method for simulation of angiogenesis.* J. Math. Biol., 57, 467–495.

[210] Plank M.J., Sleeman, B.D., 2003. *A reinforced random walk model of tumour angiogenesis and anti-angiogenic strategies.* Math. Med. Biol., 20, 135–181.

[211] Plank M.J., Sleeman, B.D., 2004. *Lattice and non-lattice models of tumour angiogenesis.* Bull. Math. Biol., 66, 1785–1819.

[212] Plank M.J., Sleeman, B.D., Jones, P.F., 2004. *A mathematical model of tumour angiogenesis, regulated by vascular endothelial growth factor and the angiopoietins.* J. Theor. Biol., 229, 435–454.

[213] Pluen, A., Netti, P.A., Jain, R.K., Berk, D.A., 1999. *Diffusion of macromolecules in agarose gels: Comparison of linear and globular configurations.* Biophys. J., 77, 542–552.

[214] Preziosi, L., Ambrosi, D., Verdier, C., 2010. *An elasto-visco-plastic model of cell aggregates.* J. Theor. Biol., 262, 35–47.

[215] Pries, A.R., Höpfner, M., le Noble, F., Dewhirst, M.W., Secomb, T.W., 2011. *The shunt problem: Control of functional shunting in normal and tumour vasculature.* Nature Rev. Cancer, 10, 587–593.

[216] Pries, A.R., Secomb, T.W., Gaehtgens, P., 1996. *Biophysical aspects of blood flow in the microvasculature.* Cardiovasc. Res., 32, 654–667.

[217] Pries, A.R., Reglin, B., Secomb, T.W., 2001. *Structural adaptation of microvascular networks: Functional roles of adaptive responses.* Am. J. Physiol. Heart Circ. Physiol., 281, H1015–H1025.

[218] Pries, A.R., Reglin, B., Secomb, T.W., 2001. *Structural adaptation of vascular networks role of the pressure response.* Hypertension, 38, 1476–1479.

[219] Pries, A.R., Reglin, B., Secomb, T.W., 2011. *Modeling of angioadaptation: Insight for vascular development.* Int. J. Dev. Biol., 55, 399–405.

[220] Pries, A.R., Secomb, T.W., Gaehtgens, P., 1998. *Structural adaptation and stability of microvascular networks: Theory and simulations.* Am. J. Physiol., 275, H349–H360.

[221] Pries, A.R., Secomb, T.W., 2005. *Control of blood vessel structure: Insights from theoretical models.* Am. J. Physiol. Heart Circ. Physiol., 288, 1010–1015.

[222] Pries, A.R., Secomb, T.W., 2008. *Modeling structural adaptation of microcirculation.* Microcirculation, 15, 753–764.

[223] Qutub, A.A., Mac Gabhann, F., Karagiannis, E.D., Vempati, P., Popel, A.S., 2009. *Multiscale models of angiogenesis.* IEEE Eng. Med. Biol. Mag., 28, 14–31. Erratum in: IEEE Eng. Med. Biol. Mag., 28, 65.

[224] Qutub, A.A., Popel, A.S., 2009. *Elongation, proliferation and migration differentiate endothelial cell phenotypes and determine capillary sprouting.* BMC Syst. Biol., 3, 13.

[225] Radszuweit, M., Block, M., Hengstler, J.G., Schöll, E., Drasdo, D., 2009. *Comparing the growth kinetics of cell populations in two and three dimensions.* Phys. Rev. E, 79, 051907.

[226] Risau, W., Flamme, I., 1995. *Vasculogenesis.* Annu. Rev. Cell Dev. Biol., 11, 73–91.

[227] Risau, W., 1997. *Mechanisms of angiogenesis.* Nature, 386, 671–674.

[228] Roose, T., Fowler, A.C., 2008. *Network development in biological gels: Role in lymphatic vessel development.* Bull. Math. Biol., 70, 1772-1789.

[229] Ruhrberg, C., Gerhardt, H., Golding, M., Watson, R., Ioannidou, S., Fujisawa, H., Betsholtz, C., Shima, D., 2002. *Spatially restricted patterning cues provided by heparin-binding VEGF-A control blood vessel branching morphogenesis.* Gen. Devel., 16, 2684–2698.

[230] Saharinen, P., Tammela, T., Karkkainen, M.J., Alitalo, K., 2004. *Lymphatic vasculature: Development, molecular regulation and role in tumor metastasis and inflammation* Trends Immunol., 25, 387–395.

[231] Sambeth, R., Bamgaertner, A., 2001. *Autocatalytic polymerization generates persistent random walk of crawling cells.* Phys. Rev. Lett., 86, 5196–5199.

[232] Sansone, B.C., Scalerandi, M., Condat, C.A., 2001. *Emergence of taxis and synergy in angiogenesis.* Phys. Rev. Lett., 87, 128102.

[233] Savill, N. J., Hogeweg, P., 1997. *Modelling morphogenesis: from single cells to crawling slugs.* J. Theor. Biol., 184, 118–124.

[234] Schmidt, A., Brixius, K., Bloch, W., 2007. *Endothelial precursor cell migration during vasculogenesis.* Circ. Res., 101, 125–136.

[235] Schugart, R., Friedman, A., Zhao, R., Sen, C., 2008. *Wound angiogenesis as a function of tissue oxygen tension: A mathematical model.* Proc. Nat. Acad. Sci. USA, 105, 2628–2633.

[236] Scianna, M., Merks, R.M.H., Preziosi, L., Medico, E., 2009. *Individual cell-based models of cell scatter of ARO and MLP-29 cells in response to hepatocyte growth factor.* J. Theor. Biol., 260, 151–160.

[237] Scianna, M., Munaron, L., 2011. *Multiscale model of tumor-derived capillary-like network formation.* Netw. Heterog. Media, 6, 597–624.

[238] Scianna, M., Munaron, L., Preziosi, L., 2011. *A multiscale hybrid approach for vasculogenesis and related potential blocking therapies.* Prog. Biophys. Mol. Biol., 106, 450–462.

[239] Scianna, M., Preziosi, L., 2012. *Multiscale developments of cellular Potts models*, Multiscale Model. Simul., 10, 342–382.

[240] Scianna, M., Preziosi, L., 2013. **Cellular Potts Models: Multiscale Developments and Biological Applications**, Chapman & Hall/CRC Press.

[241] Scianna, M., Preziosi, L., 2013. *Modeling the influence of nucleus elasticity on cell invasion in fiber networks and microchannels.* J. Theor. Biol., 317, 394–406.

[242] Scianna, M., Preziosi, L., Wolf, K., 2013. *A Cellular Potts Model simulating cell migration on and in matrix environments.* Math. Biosci. Engng., 10, 235–261.

[243] Seaman, S., Stevens, J., Yang, M. Y., Logsdon, D., Graff-Cherry, C., St Croix, B., 2007. *Genes that distinguish physiological and pathological angiogenesis.* Cancer Cell, 11, 539–554.

[244] Serini, G., Ambrosi, D., Giraudo, E., Gamba, A., Preziosi, L., Bussolino, F., 2003. *Modeling the early stages of vascular network assembly.* EMBO J., 22, 1771–1779.

[245] Shirinifard, A., Gens, J. S., Zaitlen, B., L., Poplawski, N. J., Swat, M., Glazier, J. A., 2009. *3D multi-cell simulation of tumor growth and angiogenesis.* PLoS ONE, 4, e7190.

[246] Sleeman, B.D., Anderson, A.R.A., Chaplain, M.A.J., 1999. *A mathematical analysis of a model for capillary network formation in the absence of endothelial cell proliferation.* Appl. Math. Lett., 12, 121–127.

[247] Sleeman, B.D., Wallis, I.P., 2002. *Tumour induced angiogenesis as a reinforced random walk: Modelling capillary network formation without endothelial cell proliferation.* Math. Comp. Model., 36, 339–358.

[248] Stacker, S.A., Achen, M.G., Jussila, L., Baldwin, M.E., Alitalo, K., 2002. *Lymphangiogenesis and cancer metastasis.* Nat. Rev. Cancer, 2, 573–583.

[249] Stamper, I.J,, Byrne, H.M., Owen, M.R., Maini, P.K., 2007. *Modelling the role of angiogenesis and vasculogenesis in solid tumour growth.* Bull. Math. Biol., 69, 27372772.

[250] Steinberg, M. S., 1963. *Reconstruction of tissues by dissociated cells. Some morphogenetic tissue movements and the sorting out of embryonic cells may have a common explanation.* Science, 141, 401–408.

[251] Steinberg, M. S., 1970. *Does differential adhesion govern self-assembly processes in histogenesis? Equilibrium configurations and the emergence of a hierarchy among populations of embryonic cells.* J. Exp. Zool., 173, 395–433.

[252] Stephanou, A., McDougall, S.R., Anderson, A.R.A., Chaplain, M.A.J., 2005. *Mathematical modelling of flow in 2d and 3d vascular networks: Applications to anti-angiogenic and chemotherapeutic drug strategies.* Math. Comput. Model., 41, 1137–1156.

[253] Stephanou, A., McDougall, S.R., Anderson, A.R.A., Chaplain, M.A.J., 2006. *Mathematical modeling of the influence of blood rheological properties upon adaptive tumour-induced angiogenesis.* Math. Comput. Model., 44, 96–123.

[254] Straume, O., Salvesen, H. B., Akslen, L. A., 1999. *Angiogenesis is prognostically important in vertical growth phase melanomas.* Int. J. Oncol., 15, 595–599.

[255] Stroock, A.D., Fischbach, C., 2010. *Microfluidic culture models of tumor angiogenesis.* Tissue Eng. A., 16, 2143–2146.

[256] Sun, S., Wheeler, M.F., Obeyesekere, M., Patrick, C. Jr., 2005. *Multiscale angiogenesis modeling using mixed finite element methods.* Multiscale Model. Simul., 4, 1137–1167.

[257] Sun, S., Wheeler, M.F., Obeyesekere, M., Patrick, C. Jr., 2005. *A deterministic model of growth factor-induced angiogenesis.* Bull. Math. Biol., 67, 313–337.

[258] Sun, S., Wheeler, M.F., Obeyesekere, M., Patrick, C. Jr., 2005. *Nonlinear behaviors of capillary formation in a deterministic angiogenesis model.* Nonlin. Anal.: Theory, Meth. Appl., 63, e2237-e2246.

[259] Swartz, M.A., 2001. *The physiology of the lymphatic system.* Adv. Drug Deliver. Rev., 50, 3–20.

[260] Swartz, M.A., Skobe, M., 2001. *Lymphatic function, lymphangiogenesis, and cancer metastasis.* Microsc. Res. Techniq., 55, 92–99.

[261] Szabo, A., Perryn, E. D., Czirok, A., 2007.*Network formation of tissue cells via preferential attraction to elongated structures.* Phys. Rev. Lett., 98, 038102.

[262] Szabo, A., Mehes, E., Kosa, E., Czirok, A., 2008. *Multicellular sprouting in vitro.* Biophys. J., 95, 2702–2710.

[263] Szabo, A., Czirok, A., 2010. *The role of cell-cell adhesion in the formation of multicellular sprouts.* Math. Model. Nat. Phenom., 5, 106–122.

[264] Szczerba, D., Kurz, H., Székely, G., 2009. *A computational model of intussusceptive microvascular growth and remodeling.* J. Theor. Biol., 261, 570–583.

[265] Szczerba, D., Székely, G., 2002. *Macroscopic modeling of vascular systems.* In **Medical Image Computing and Computer-Assisted Intervention MICCAI 2002**, Lecture Notes in Computer Science, 284–292.

[266] Szczerba, D., Székely, G., 2005. *Simulating vascular systems in arbitrary anatomies.* In **Medical Image Computing and Computer-Assisted Intervention MICCAI 2005**, Lecture Notes in Computer Science, 641–648.

[267] Szczerba, D., Székely, G., 2005. *Computational model of flow-tissue interactions in intussusceptive angiogenesis.* J. Theor. Biol., 234, 87–97.

[268] Szczerba, D., Székely, G., Kurz, H., 2006. *A multiphysics model of capillary growth and remodeling.* In **Computational Science, ICCS 2006**. Lecture Notes in Computer Science, Springer.

[269] Tammela, T., Alitalo, K., 2010. *Lymphangiogenesis: Molecular mechanisms and future promise.* Cell, 140, 460–476.

[270] Thackham, J.A., McElwain, D.L.S., Long, R.J., 2008. *The use of hyperbaric oxygen therapy to treat chronic wounds: A review.* Wound Rep. Regen., 16, 321–330.

[271] Tomatis, C., Fiorio Pla, A., Munaron, L., 2007. *Cytosolic calcium microdomains by arachidonic acid and nitric oxide in endothelial cells.* Cell Calcium, 41, 261–269.

[272] Tong, S., Yuan, F., 2001. *Numerical simulations of angiogenesis in the cornea.* Microvasc. Res., 61, 14–27.

[273] Tosin, A., Ambrosi, D., Preziosi, L., 2006. *Mechanics and chemotaxis in the morphogenesis of vascular networks.* Bull. Math. Biol., 68, 1819–1836.

[274] Tranqui, L., Traqui, P., 2000. *Mechanical signalling and angiogenesis. The integration of cell-extracellular matrix couplings.* C.R. Acad. Sci. Paris, Science de la Vie, 323, 31–47.

[275] Travasso, R.D.M., Corvera Poire, E., Castro, M., Rodriguez-Manzaneque, J.C., Hernandez-Machado, A., 2011. *Tumor angiogenesis and vascular patterning: A mathematical model.* PLOS One, 6, e19989.

[276] Tremblay, P.L., Hudon, V., Berthod, F., Germain, L., Auger, F.A., 2005. *Inosculation of tissue-engineered capillaries with the host's vasculature in a reconstructed skin transplanted on mice.* Am. J. Transplant, 5, 1002–1010.

[277] Vailhé, B., Vittet, D., Feige, J. J., 2001. *In vitro models of vasculogenesis and angiogenesis.* Lab. Investig., 81, 439–452.

[278] Valant, P.A., Adjei, P.N., Haynes, D.H., 1992. *Rapid Ca2+ extrusion via the Na+/Ca2+ exchanger of the human platelet.* J. Membr. Biol., 130, 63–82.

[279] Valero, C., Javierre, E., Garca-Aznar, J.M., Gmez-Benito, M.J., *Numerical modelling of the angiogenesis process in wound contraction.* Biomech. Model. Mechanobiol., DOI: 10.1007/s10237-012-0403-x.

[280] Verbridge, S.S., Choi, N.W., Zheng, Y., Brooks, D.J., Stroock, A.D., Fischbach, C., 2010. *Oxygen-controlled three-dimensional cultures to analyze tumor angiogenesis.* Tissue Eng. A, 16, 2133–2141.

[281] Vermolen, F.J., Javierre, E., 2009. *A suite of continuum models for different aspects in wound healing.* In **Bioengineering Research of Chronic Wounds, Studies in Mechanobiology, Tissue Engineering and Biomaterials**, Springer-Verlag, 127–168.

[282] Vermolen, F.J., Javierre, E., 2010. *Computer simulations from a finite-element model for wound contraction and closure*, J. Tissue Viabil., 19, 43–53.

[283] Vermolen, F.J., Javierre, E., 2012. *A finite-element model for healing of cutaneous wounds combining contraction, angiogenesis and closure*, J. Math. Biol., 65, 967–996.

[284] Vernon, R., Angello, J., Iruela-Arispe, M.-L., Lane, T., Sage, E.-H., 1992. *Reorganization of basement membrane matrices by cellular traction promotes the formation of cellular networks in vitro.* Lab. Invest., 66, 536–546.

[285] Vernon, R., Lara S. L., Drake C. J., Iruela-Arispe M.-L., Angello J., Little C. D. and Sage E.-H., 1995. *Organized type 1 collagen influences of endothelial patterns during spontaneous angiogenesis in vitro: Planar cultures as models of vascular development.* In Vitro Vasc. Develop. Biol., 31, 120–131.

[286] Vernon, R., Sage, E.-H., 1995. *Between molecules and morphology. extracellular matrix and creation of vascular form.* Amer. J. Path., 1447, 873–883.

[287] Vitanis, V., 2004. **Vascularization of Tumour Growth Models**. Diploma Thesis, University of Thessaloniki and Swiss Federal Institute of Technology (ETHZ).

[288] Walter, M., Cook, W., Ealick, S., Nagabhushan, T., Trotta, P., Bugg, C., 1992. *Three-dimensional structure of recombinant human granulocyte-macrophage colony-stimulating factor*, J. Mol. Biol., 224, 1075–1085.

[289] Watson, E.L., Jacobson, K.L., Singh, J.C., Di Julio, D.H., 2004. *Arachidonic acid regulates two Ca2+ entry pathways via nitric oxide.* Cell Signal., 16, 157–165.

[290] Watson, M.G., McDougall, S.R., Chaplain, M.A., Devlin, A.H., Mitchell, C.A., 2012. *Dynamics of angiogenesis during murine retinal development: A coupled in vivo and in silico study.* J. R. Soc. Interface, 9, 2351–2364.

[291] Webb, D.J., Horwitz, A.F., 2003. *New dimensions in cell migration.* Nature Cell Biol., 5, 690–692.

[292] Welter, M., Bartha, K., Rieger, H., 2008. *Emergent vascular network inhomogenities and resulting blood flow patterns in a growing tumor.* J. Theor. Biol., 250, 257–280.

[293] Welter, M., Bartha, K., Rieger, H., 2009. *Vascular remodelling of an arterio-venous blood vessel network during solid tumor growth.* J. Theor. Biol., 259, 405–422.

[294] Welter, M., Rieger, H., 2010. *Physical determinants of vascular network remodeling during tumor growth.* Europ. Phys. J. E, 33, 149–163.

[295] Welter, M., Rieger, H., 2012. *Blood vessel network remodelling during tumor growth.* In **Modeling Tumor vasculature: Molecular, Cellular, and Tissue Level Aspects and Implications**. T. Jackson, Ed., 335–360, Springer.

[296] Wiig, H., Keskin, D., Kalluri, R., 2010. *Interaction between the extracellular matrix and lymphatics: Consequences for lymphangiogenesis and lymphatic function.* Matrix Biol., 29, 645–656.

[297] Wise, S.M., Lowengrub, J.S., Frieboes, H.B., Cristini, V., 2008. *Three-dimensional multispecies nonlinear tumor growth: I. Model and numerical method.* J. Theor. Biol., 253, 524–543.

[298] Wolf, K., Mazo, I., Leung, H., Engelke, K., von Andrian, U. H., Deryugina, E. I., Strongin, A. Y., Bröcker, E.-B., Friedl, P., 2003. *Compensation mechanism in tumor cell migration: mesenchymal–ameboid transition after blocking of pericellular proteolysis.* J. Cell. Biol., 160, 267–277.

[299] Wu, M., Frieboes, H.B., McDougall S.R., Chaplain, M.A.J., Cristini, V., Lowengrub, J. 2012. *The effect of interstitial pressure on tumor growth: Coupling with the blood and lymphatic vascular systems.* J. Theor. Biol., 320, 131–151.

[300] Xue, C., Friedman, A., Sen, C.K., 2009. *A mathematical model of ischemic cutaneous wounds.* Proc. Nat. Acad. Sci. U.S.A., 106, 16782-16787.

[301] Zhao, G., Wu, J., Xu, S., Collins, M.W., Long, Q., Koenig, C.S., Jiang, Y., Wang, J., Padhani, A.R., 2007. *Numerical simulation of blood flow and interstitial fluid pressure in solid tumor microcirculation based on tumor induced angiogenesis.* Mech. Sin., 23, 477–483.

[302] Zheng, X., Wise, S.M., Cristini, V., 2005. *Nonlinear simulation of tumor necrosis, neovascularization and tissue invasion via an adaptive finite-element/level-set method.* Bull. Math. Biol., 67, 211–259.

[303] Zheng, Y., Chen, J., Craven, M., Choi, N.W., Totorica, S., Diaz-Santana, A., Kermani, P., Hempstead, B., Fischbach-Teschl, C., Lopez, J.A., Stroock, A.D., 2012. *In vitro microvessels for the study of angiogenesis and thrombosis.* Proc. Natl. Acad. Sci. U.S.A., 109, 9342–9347.